Accuracy Assesment of direct sensor orientation in UAV Photogrammetry

Jonathan Stam

december 2010

0.1 abstract

With the advent of Unmanned Aerial Vehicles, it becomes possible to use these vehicles to acquire photogrammetric images in a more cheap and flexible way compared with conventional photogrammetry from a full-sized airplane. A big factor in costs and resources in conventional photogrammetry is signalling and measuring ground control points, which are necessary to determine the location and attitude of the photos. Eliminating the need for ground control points would make the photogrammetric process much less costly and labour intensive.
A UAV contains navigational sensors (a GPS receiver and a Inertial Measurement Unit) for it's own navigation. The output of these sensors can also be used for the orientation of the photographs. However, the accuracy of these sensors, especially low cost off-the-shelf sensors, is limited.
This thesis concentrates on determining the accuracy of low-cost navigational sensors and the effect of inaccuracies in these sensors on the result of the photogrammetric product: a Digital Terrain Model. Using a UAV developed by the company Heering UAS, founded by Pieter Wijkstra, the effects of inaccuracies in the GPS receiver and the IMU in the UAV on the outcoming Digital Elevation model has been tested. First the theoretical effects of inaccuracies of navigation sensors on the final product is investigated, using the photogrammetric collinearity equations. To validate the theoretical results, a number of tests has been carried out using an available platform with an off-the-shelf camera and dito navigation sensors.
A first test, using flight data and photos taken at the unfinished A4 highway site just south of Delft, shows the sensitivity of the final model to errors in the navigational sensors. This test did not give enough data though to give enough insight in the effects of navigational sensor errors. Therefore a second test was carried out using a larger photoblock flown at the dyke of the river Lek at Ammerstol. This test showed that the errors in the terrain model caused by errors in the on-board GPS receiver follow the results of the theoretical simulation. However, because at the time, the UAV did not contain a reliable IMU, the effect of IMU errors could not be tested. So a third test was conducted, using an off-the-shelf IMU combined with a high accuracy GPS receiver to asses the effect of errors in the IMU on the resulting terrain model.
The results show that off-the-shelf navigation sensors are not accurate enough to produce a reliable end result. Therefore eliminating ground control points would result in a final product which is not accurate enough. Using the available navigation sensors it is possible to reduce the amount of ground control points.

0.2 Acknowledgements

Graduation is not an easy task. The graduate is expected to deliver a scientifically sound research on an advanced topic. Not only requires this advanced knowledge of the topic to be researched, but also motivation, discipline, structure and also patience. Due to various reasons, these qualities do not come naturally to me. The completion of this graduation research can be seen as a small miracle, regarding my background.
However, the completion of this thesis has not been possible without the continuous support of several people. First of all, I want to thank my direct supervisors Kourosh Kosh Elham of the section Optical and Acoustic Remote Sensing (OARS) and Pieter Wijkstra of the Aerospace Software and Technologies Institute (ASTI) for giving me the possibility to perform this research, for their collaboration, support and comments during my research and the writing of the thesis.
Furthermore I want to thank professor Massimo Menenti, dr. Sandra Verhagen and prof. Peter van Oosterom for reading the thesis, therefore making my graduation possible.
During my research there were a number of people helping out with measurements and/or commenting on results. When testing the accuracy of the Ublox I was helped by Christophe de Wagter from ASTI who provided the receiver and explained how to get it to work. Christiaan Tiberius and Hans van der Marel helped out by providing me with coordinates of the RD-benchmark and commenting on the results. Testing of the IMU had not been possible without the help of Sylvie Soudarissanane, Alex Busch and Jochem Lesparre who explained the working of the TotalStation and assisted me during the measurements of the ground control points on the parking lot.
Last but certainly not least, I want to thank the people close to me, such as my parents, for their continuous support and patience while I was conducting my research and writing my thesis.

Contents

Chapter 1

Introduction

1.1 Motivation

The last couple of years, Unmanned Aerial Vehicles (UAVs) have been developed and introduced in a large number of applications. One of these applications is aerial photogrammetry. Because a UAV usually flies at a low altitude, aerial photographs taken from a UAV often have a large scale and therefore contain a lot of detail. Using these large scale photographs it is possible to determine a Digital Elevation Model with a high resolution. These high resolution Digital Elevation Models are used for applications needing a high level of detail. For example, currently the northern dyke along the Lek river between Rotterdam and Schoonhoven is being strengthened. High resolution DTMs show small and local height differences and can therefore help to monitor the changes in the shape and height of the dyke during the strengthening. To be able to use DTMs to monitor the changes of the dyke, several high accuracy DTMs should be made during the strenghtening process, so they can be compared with each other. Therefore a platform should be used which can determine a high resolution DTM in a relatively cheap and flexible way. The idea of using a UAV to capture photogrammetric images for the purpose of creation of high resolution DTMs originates from here: to be able to generate high resolution DTMs in a flexible and inexpensive way. Flexibility and cost factors justify the use of navigation sensors (GPS receiver and an Inertial Measurement Unit, IMU) aboard the UAV for the orientation of the photos, because setting up and measuring ground control points is a lengthy and expensive process. This thesis concentrates on assessing the accuracy of the navigation sensors and the effect of the accuracy of these sensors on the accuracy of the final product.

1.2 Problem description

In conventional photogrammetric projects, the location and orientation of the camera, the exterior orientation, is determined by measuring a group of terrain points both in the photos and in the terrain. These points are clearly signalized and thus recognizable in the photos. By determining the coordinates of those points both in the terrain system and in the photo, the transformation between the terrain coordinate system and the photo coordinate system can be found. The parameters describing this transformation are the exterior orientation parameters.
Instead of using the normal photogrammetric process of determining the object coordinates X_0, Y_0, Z_0 and rotation angles of the camera ω, ϕ, κ using ground control points (known as Aerial triangulation), the GPS and Inertial measurements from the airplane itself can be used for this exterior orientation of the photographs. As mentioned earlier, this saves placing ground control points in the terrain and measuring them both on the ground and in the photographs. Heipke et al [2002] and Cramer et al [2000] show that this works, but at the cost of lower accuracy. As explained in the previous section, the final product is a high resolution DTM. Because using a UAV for photogrammetric flights and orientation without the use of ground control points is a very flexible way to obtain information, these high resolution DTMs can be used to monitor small height differences in the terrain over a certain amount of time. However, to obtain this it is necessary to distinguish these small height changes over measurement inaccuracies. Therefore the accuracy of the final product should be high (in the order of centimeters). The accuracy is directly dependent on the accuracy of the exterior orientation of the pictures. This exterior orientation is determined by the object coordinates and rotation angles of the camera projection centre. So the accuracy of the exterior orientation and thus of the object measurements within the pictures is dependent on the accuracy of these parameters.
Because the unmanned airplane of Heering UAS flies at 50 meters altitude with a low velocity, a project would need far too much ground control points when the standard technique is used. Using a lot of ground control points means that they should be signalled in the field, measured and maintained, which is very labour-intensive (and thus expensive). To make the system cheap and flexible a UAV is used with low cost measuring equipment. However, low cost GPS and IMU systems are less accurate than their high-end (and thus expensive) counterparts. This loss of accuracy will work through in the accuracy on the ground, i.e. the accuracy of the resulting Digital Terrain Model.

Heipke et al [2002] shows that the approach of using the outputs of the navigational sensors as exterior orientation parameters works when high accurate commercial systems are used, the accuracy is usually lower than when Aerial Triangulation is used. This research will focus on evaluating the accuracy of the final product when low-cost "off the shelf" sensors are used.

1.3 Objectives and research questions

As described above, the main objective of this research is to evaluate the accuracy of digital terrain models, derived from aerial imagery taken from an unmanned aerial vehicle without using ground control points, but instead using low-cost GPS and IMU sensors aboard the UAV. Therefore it is needed to know the influence of the accuracy of these sensors on the outcoming model. Furthermore, there are more factors compromizing the accuracy of the outcoming model, these have to be researched and quantified. These objectives lead to the following research questions:

- Main Question: What is the accuracy of object measurements using low cost GPS and IMU sensors and standard cameras for exterior orientation on an unmanned aerial vehicle?

To answer this main question, the following sub-question needs to be answered:

- Which factors limit the accuracy of the terrain model?
- What is the effect of these factors on the accuracy of the terrain model?
- To what extend is it possible to create a Digital Elevation Model using direct sensor orientation?
- How does the resulting terrain model compare with accurate models?
- How should the used techniques be enhanced to obtain the desired accuracy for the DEM?

1.4 Related work

Both the idea of UAV photogrammetry and the use of direct sensor information for the exterior orientation of the photographs is not new. The advance

of GPS and the simplification of IMU systems has made direct sensor measurement of exterior orientation parameters a serious alternative to conventional aerial triangulation since the end of the 1990's. Aerial photography from unmanned aerial vehicles is not new either, although the usage was limited to hobby projects taking aerial photographs from kites or balloons until the mid 2000's, when the advance of powered and professional UAV's made professional UAV photogrammetry possible.

1.4.1 UAV photogrammetry

The use of UAV's dedicated for aerial photogrammetry is quite new. A couple of papers have been written on the subject, mostly describing a particular UAV platform, it's main applications and examples of flights.
Everaerts [2008] describes the advent of Unmanned Aerial Vehicles and their use in Photogrammetry and Remote Sensing applications. UAV's have been around for several years, but were used mainly by the military for shooting practice. They were later used as platforms for reconnaisance and offensive actions. The last couple of years, the UAV made it's entry in the civil world. These systems are notably different than their military counterparts.
Although the usage of UAVs in civil products is quite new, over the years a lot of systems have been developed. This is made possible due to the fact that these are relatively low-cost systems. Due to navigational equipments becoming smaller, the payload of the aircrafts are reduced, making it possible to use small model aircrafts for all kinds of tasks for which accurate navigation is required. Furthermore the basis for a UAV is the aircraft itself, which can be made from a standard model aircraft. A list of UAV projects is maintained by the International Unmanned Vehicle Systems Information Source (www.uvs-info.com). The following table shows the increase in number of UAV projects

Year	2004	2005	2006	2007
Civil/Commercial	33	55	47	61
Military	362	397	413	491
Dual Purpose	39	44	77	117
Research	43	35	31	46
Developmental		219	217	269

Table 1.1: Evolution of numbers of UAV projects (Van Blyenburgh [2007])

Several examples of UAV's for photogrammetry and remote sensing purposes have been developed over the years. Haarbrink [2008] describes a UAV pho-

togrammetry platform, based on helicopters. It is made by the company Geocopter B.V. from the Netherlands. In this paper some of the advantages of UAV photogrammetry compared with conventional photogrammetry from a full sized aircraft is discussed (such as more possible flying days). A general description of the platform setup (e.g. flight and navigational controls, GPS/IMU integration and ground control segment) of both platforms is given. Furthermore some examples of the acquisition of photographs are given. Geocopter photographed a small part of a Dutch motorway and made a flight at the Geofort, an old fortress in the Netherlands which is being used as an educational centre on Geo-Information. Geocopter used Match-T developed by the company Inpho to process the acquired photographs. On the whole, Haarbrink [2008] is an introductionary paper showing the possibilities of UAV Photogrammetry and Digital Terrain Model extraction from photographs taken from UAVs.

[Eisenbeiss 2008], is a doctoral thesis from the university of Zurich, describes the development and testing of an unmanned helicopter aimed at photogrammetric acquisition. The thesis states that the technique is rather new and claims to have defined the term "UAV Photogrammetry". This doctoral thesis describes the possibilities, problems, advantages and disadvantages of several different UAV systems in depth. Several platforms are described and tested. An overview of possible types of UAV is given in table 1.1. Do note that [Eisenbeiss 2008] regards static aerial platforms such as balloons and kites also as "unmanned aerial vehicles". If this term is correct for this kind of platforms remains to be seen. On the one hand these platforms are not motored and can't therefore be moving "on their own". On the other hand is the term "aerostat" a bit misleading because these platforms can be guided by ropes or lines from the ground and are very sensitive to wind effects.

	Fixed Wing	Rotary Wing
unpowered	Glider	
powered	propellor aircraft Jet aircraft	Helicopter Multiple rotor

Table 1.2: Different UAV categories [derived from Eisenbeiss 2008]

Of the systems given in table 1.1 the powered fixed wing aircraft performs best on stability, range, safety and practicability. Because jet engines are very expensive, most powered fixed wing UAV's are powered by propellors.

However, jet engined UAV's do exist, but these are usually military applications.

Testing the different UAV's for photogrammetric purposes gave the authors of Eisenbeiss [2008] high resolution imagery of the campus of Zurich university. Dedicated software for photogrammetric processes has been used to try to orient the images, including PhotoModeler and Leica Photogrammetric Suite, which has also been used in my research. The processing in these software packages resulted in coherent image blocks, which followed the blocks as they were flown. This therefore showed that UAV photogrammetry can be seen as a serious alternative to conventional photogrammetry. The thesis closes with a description of possible application fields including archeology, disaster management and environmental and agricultural applications.
Colomina et al [2009] describes the uVISION project. The goal of this project is to develop a system for the generation of high quality, spatially referenced geoinformation at an affordable cost. To achieve this, they developed small low altitude unmanned helicopters. Real-time navigation and sensor precise orientation functions are used for the navigation of the aircraft and the orientation of the photos.
Gruen et al [2009] describes an application of the Zurich helicopter described in Eisenbeiss [2008] in a archeological project in Bhutan. The goal of this project was to map the ruins of a large citadel covered by the jungle in a river valley. To be able to map the citadel, extensive surveying works were carried out. The photogrammetric flights were part of these surveying works.
Another research aimed at archaelogical study is described in Chiabrando et al [2010]. Tests with a UAV and an RPV (Remote Piloted Vehicle) have been carried out in the Piedmont region in Italy. The paper deals with the pros and cons of UAVs and RPVs in the context of supporting of arheological studies. A comparison has been made between a helicopter and a fixed wing plane.
Patias et al [2009] describe the use of UAVs for the production of high resolution OrthoImages in the framework of archeological excavations on the Greek island of Keros. For this project also a helicopter is used. The OrthoImages are determined by collecting aerial photographs. Also DTMs are created, but for this laserscanners are used.

1.4.2 Direct sensor orientation

The idea of using GPS and INS measurements from the aircraft which is used as a platform for the aerial photographs has been described in many papers. Cramer et al [2000] describes in detail how the direct sensor measure-

ment technique is compared with conventional aerial photogrammetry using ground control points. The objective of the research described in Cramer et al [2000] is to test the accuracy performance of a specific GPS/INS sensor. To do this several test flights have been carried out in a well surveyed area in the vicinity of Stuttgart in Germany. Several GPS receivers were used for the reference station, using different baselines (more on differential GPS in section 3.1), so that the influence of the baseline length on the accuracy could be assessed. Furthermore these test flights were carried out on two different altitudes, so that the influence of different scale factors could be determined. The results were processed in two ways:

1. The direct sensor measurements were compared with the exterior orientation parameters which followed from a standard aerial triangulation

2. Using the direct sensor measurements as fixed exterior orientations, the coordinates of checkpoints are determined and compared with the known coordinates.

The results of these tests were very promising. The comparison of exterior orientation parameters determined from direct sensor measurements and standard triangulation showed differences of a couple of decimeters for the position of the cameras. The rotation angles differed a couple of millidegrees. Notable was that the differences were lower for the lower altitutde flights. The baseline length didn't seem to matter.
The comparison between the coordinates of the checkpoints determined from the photographs and those observed in the field showed differences of up to 20 cm, regardless of flying height and baseline length.

Heipke et al [2002] is a report of an extended test undertaken by the European Organization for Experimental Photogrammetric Research (OEEPE). This test was a collaboration of different institutes around Europe specialized in Photogrammetry. The test setup was more or less the same as described in Cramer et al [2000], however two systems from two different companies were tested. The tests contained two phases. In the first phase ground control points were used for calibration of the system while the second phase was purely based on direct sensor measurements. In the second phase, points known in ground coordinates were only used as checkpoints. The observed - computed checkpoint differences were mostly under 30 cm for all tested systems.

The tests described in the papers mentioned above show that direct sensor measurement is possible and shows much potential. However, all tests were

performed using full-sized aircraft filled with professional and state of the art photogrammetric equipment, high end (and therefore highly accurate) GPS receivers and advanced commercial inertial measurement systems. How direct sensor measurement of the exterior orientation parameters will cope in a home built model aircraft with an off-the-shelf mirror reflex camera, a standard GPS receiver and a budget IMU will fare remains to be seen. However, the tests described in the paper show that comparison between two different methods of orientation can give insightful information on the accuracy of the system. Therefore the same principle of determining the exterior orientation parameters from direct sensor measurements and aerial triangulation and comparing the outcomes will be the basis of this research.

1.5 Outline

The test analysis described in [Cramer et al 2000] gave a good impression of the possibilities of direct sensor orientation in conventional photogrammetry. However, a similar test using UAV photogrammetry has not been conducted yet. Therefore this research will more or less follow the analysis method described in [Cramer et al 2000]. However, expected error influence of single navigation sensors are determined and compared with the practical test outcomes

To back up the research, first of all a description of photogrammetry in general is given, the techniques of UAV photogrammetry and direct sensor measurement are described and compared with conventional aerial photogrammetry. This all is described in chapter 2. Chapter 3 describes the techniques behind the GPS and INS sensors aboard the aircraft. A general description of their workings is given and factors compromizing their accuracy are summed up. Furthermore Kalman Filtering, a technique used for combining the measurements of the two measurement sensors, is shortly described.

The measurement errors in the GPS and INS sensors aboard the aircraft have an influence on the outcoming terrain model. Using the standard mathematical background of photogrammetric measurements, a theoretical assesment is made of these influences. This theoretical assesment and it's outcome is described in chapter 4. Chapter 5 describes the influence of non-sharp photograph's on the outcoming terrain model.

The results of the theoretical assesment described in chapter 4 are compared with results from two actual test flights, these comparisons are made and described in the chapters 6 and 7. Chapter 8 rounds the thesis up with the main conclusions and recommendations.

Chapter 2

Background

2.1 General principles of Photogrammetry

Photogrammetry is the technique that uses photographs for mapmaking and surveying, according to the Encyclopedia Britannica. The technique has been thought possible since the advent of photography halfway the 19th century, but it was not until the advance of flight that photogrammetry was used for surveying large areas of terrain. When it became possible for man to fly, cameras could be taken aboard airplanes and large area's of terrain could be photographed straight down from a flying plane. This was the advance of aerial photogrammetry. During the First and Second World Wars aerial photogrammetry was mainly used for military purposes. The civil usage of aerial photogrammetry took a flight after the Second World War.

Using photographs for surveying purposes yields that the location of terrain objects are determined by pinpointing them in the photographs. By using straight down aerial photographs a map can easily be made by just pinpointing terrain objects in one photograph. However, from a single photograph it is not possible to determine height information. To determine height information, it is necessary that an object is observed from two different locations under an angle. This angle is called the parallax angle. This follows the same principle why mankind sees depth, see figure 2.1.

The left eye gives a 2D image of the row of pins slightly from the left, the right eye gives a 2D image of the row of pins slightly from the right. The two eyes observe the pins from a small angle, the parallax angle. Therefore the brain has enough information to project a 3D image of the row of pins. More or less the same principle applies for photographs.
The size of the parallax angle is rather important. If the parallax angle is

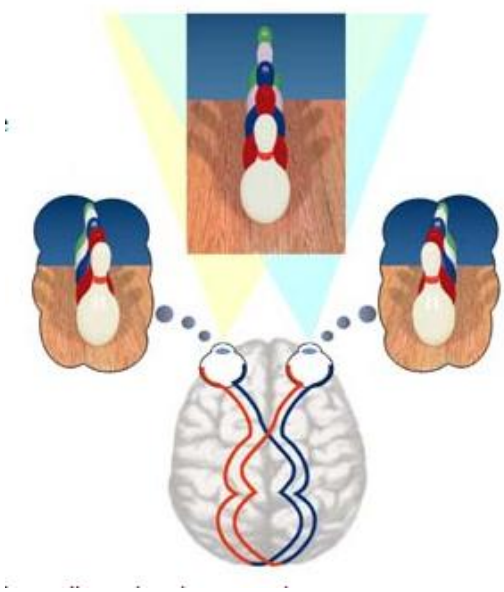

Figure 2.1: How mankind sees depth

too small, inaccuracies in the 3rd dimension can occur.

To be able to determine height information from aerial photographs, objects thus have to be present in at least two photographs taken from different locations. This requires careful flight planning. Normally a flight undertaken to capture photographs for the purpose of photogrammetry is planned in such a way that photographs are taken in strips, where the photo's in the strip overlap each other with 60% and the strips overlap each other with 30%, the latter is called the sidelap.

2.1.1 Mathematical background

To determine the location of a terrain object from the photographs, a series of mathematical operations has to be performed. A detailed description of all mathematical formulae and equations contributing the photogrammetric process can be found in Vosselman [1999]. This section will suffice with the most important equations defining the orientations of the photographs.
First of all, the scale factor and the camera coordinate system, the interior orientation, need to be defined. Then this camera coordinate system needs to be related to the terrain coordinate system. This relation is the exterior orientation, defined by 6 exterior orientation parameters. These 6 parameters are then used to determine the terrain coordinates of objects from the

photographs.

Scale and interior orientation

First of all, the terrain object has to be pinpointed in the photograph. This means measuring it's coordinates in the camera coordinate system. The centre of this coordinate system is the midpoint of the camera lens. Therefore the coordinates of a terrain point in the photo (also known as photo coordinates) are determined from the point where through the camera lens midpoint intersects the photo film perpendicularry. This point is called the principal point, which has coordinates x_0, y_0. This is usually slightly off the photo midpoint. The x and y photo coordinates of a terrain object are now determined in relation to this principal point. The photo film (or photo chip in case of a digital camera) is placed at focal length from the lens. Therefore the z photo-coordinates of the object points in the photo's is equal to the camera constant f. Determining the x_0,y_0 and f values for a camera used for photogrammetric measurements is therefore very important. The used camera need to be calibrated. The result of this camera calibration gives us the interior orientation of the camera. For a flat terrain, where H is the same for all points, the focal length of the camera and the flying height determines the scale or scale number of the photographs, via the equation $s = \frac{f}{H}$, see also figure 2.2

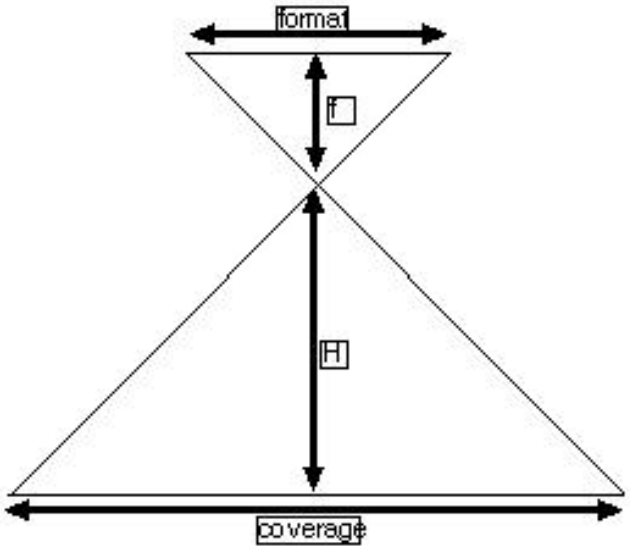

Figure 2.2: Photogrammetry scale

Furthermore, the interior orientation parameters include lens distortion parameters, which defines how an image is distorted by the camera lens. In the case of digital cameras, the pixel size is also an interior orientation parameter, because the pixel size defines the resolution of the photos.

Collinearity equations and exterior orientation

When the photo coordinates of terrain points are measured, they need to be transformed to terrain coordinates. A set of equations, known as the collinearity equations describe the relation between photo coordinates and terrain coordinates.

$$\begin{aligned} x_c &= -f\frac{r_{11}(X-X_c^0)+r_{21}(Y-Y_c^0)+r_{31}(Z-Z_c^0)}{r_{13}(X-X_c^0)+r_{23}(Y-Y_c^0)+r_{33}(Z-Z_c^0)} \\ y_c &= -f\frac{r_{12}(X-X_c^0)+r_{22}(Y-Y_c^0)+r_{32}(Z-Z_c^0)}{r_{13}(X-X_c^0)+r_{23}(Y-Y_c^0)+r_{33}(Z-Z_c^0)} \end{aligned} \tag{2.1}$$

The elements in equation 2.1 have the following meaning:

parameter	meaning
x_c	x-photo coordinate of object in photo c
y_c	y-photo coordinate of object in photo c
f	focal length of the camera
X, Y, Z	terrain coords of object
X_c^0, Y_c^0, Z_c^0	terrain coords of camera during capture of photo c

Table 2.1: Collinearity equation elements

The elements r_{ij} in the collinearity equations point to a standard three dimensional rotation matrix

$$R = \begin{bmatrix} r_{11} & r_{12} & r_{13} \\ r_{21} & r_{22} & r_{23} \\ r_{31} & r_{32} & r_{33} \end{bmatrix} \tag{2.2}$$

These elements are calculated from the angles of three rotations around the axes of the coordinate system. The rotation around the X-axis is the roll or ω angle, The rotation around the Y-axis is the pitch or ϕ angle and the rotation around the Z-axis is the heading or κ angle

As explained earlier, the terrain point in question should be visible in at least 2 photos. When the collinearity equations are reviewed, it can be seen that the unknowns are the terrain coordinates X, Y, Z of the object point. The observations are the photo coordinates x, y of the object point. The

other parameters in the equations determine the position and attitude of the camera at time of capturing the photograph. Determining these parameters is the exterior orientation of the photographs, therefore the position and attitude parameters of the camera are known as the exterior orientation parameters.
When the exterior orientation parameters are known, a certain object point will be measured in at least two different photos, giving the photo coordinates x_1, y_1, x_2, y_2. Thus we have 4 observations and 3 unknowns. Therefore the unknown terrain coordinates of the point can be found using a standard least squares estimation on the basis of the given orientation parameters. This is done by constructing a line from the photo point of photo 1 through the projection centre to the terrain. The same is done from photo 2. The terrain point is then the intersection of the two constructed lines.

In conventional photogrammetry, the exterior orientation is done by creating points, the so-called Ground Control Points (GCP's) in the terrain, which are clearly visible in the pictures. The coordinates of these points are determined by terrestrial measurements (either GPS measurements or by classical surveying using a theodolite or a total station). These known points are then measured in the photographs. Using both the terrain coordinates and the photo coordinates of the ground control points the exterior orientation parameters are determined. In the collinearity equations the photo coordinates are again the measurements but this time the exterior orientation parameters are the unknowns. The coordinates of the Ground Control Points are seen as fixed parameters. With 6 unknowns, at least 3 ground control points are needed to determine the exterior orientation parameters of 1 photograph. This would mean that for large blocks of photographs for every photo at least 3 ground control points are needed. However, when so-called tiepoints are used, the amount of ground control points can be greatly reduced. Tiepoints are points which can be identified in two or more photographs, but their ground coordinates are unknown. With a sufficient amount of tiepoints spread over the block area, the exterior orientation parameters of all the photographs in the block can be determined. This process is called the aerial triangulation.

2.1.2 Photogrammetric process and equipments

The process of photogrammetry can be summarized in three stages: The planning stage, the actual flight and the processing of the photographs.

Planning phase

A photogrammetry project requires careful process planning and execution. First of all, it has to be decided how much detail and accuracy is needed for the final product. This dictates the choice of scale (and therefore focal length and flying height) which is going to be used. The size and shape of the area which is to be photographed need to be taken into account. Because fuel is expensive, the shortest flight route covering the whole area with enough overlap has to be determined. The planning of flying route and height gives the flight plan.
Accuracy requirements determines how the exterior orientation takes place and how much accuracy is needed for the navigational sensors. Careful placement, measurement and maintaining of Ground Control Points has to be done. These ground control points should be visible in the photographs. Furthermore their terrain coordinates need to be known with very high accuracy. Selection of GCP locations, measurements and maintaining them is all part of the signalization plan.

Photogrammetric flight

During the flight, the pilot needs to make sure that he exactly follows the flight plan specified in the previous phase. On larger systems there is an operator who at the right time takes the photographs. This operator has full control over the Camera platform and therefore has to make sure he uses the correct rotations. However the photo capture is done automatically more and more.

Processing phase

When the photo flight has been done, the resulting photographs have to be processed. This yields determination of the interior and exterior orientation parameters and deriving terrain information from the photographs. In the time of film photography, this was done using specialized equipments, such as stereoscopes and optical and mechanical stereoplotters, which enabled an operator to view a 3D image of the terrain using one photo pair. With a small device called a parallax meter, height differences in this 3D model could be determined. However, with the rise of digital photography, the stereoscope and the parallax meter have been relegated to the museum and in its place are strong software packages capable of triangulating large blocks of photos. High end professional photogrammetric software uses special monitors, which enable the operator to see a 3D view of the photographed terrain, using special glasses and a specialized mouse to replace the parallax meter.

However nowadays software packages such as PhotoModeler Scanner and Leica Photogrammetry Suite are able to automatically derive 3D models from photoblocks.

Equipments

Conventional aerial photogrammetry uses full sized aircrafts. Advanced camera's are used which are placed on a so-called gyro platform which is a platform which can rotate around its axes. Therefore the camera keeps looking straight down when the aircraft attitude changes. Furthermore, most stations use a device for Forward Motion Compensation (FMC). This is a system which compensates for unsharpness in the photographs caused by the aircraft moving while the shutter of the camera is open. Furthermore the aircraft contains high accuracy GPS equipment aboard to determine the location of the plane. Specialized photogrammetric cameras, with a large format and focal lengths and specialized lenses are used. An example of a photogrammetric camera platform is given in figure 2.3

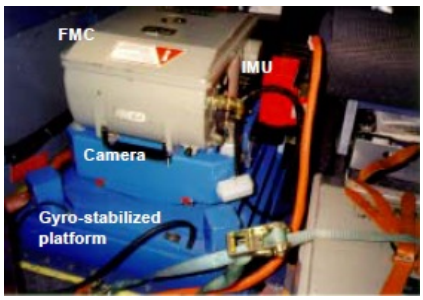

Figure 2.3: Conventional Photogrammetry Platform [Heipke et al 2002]

2.2 UAV Photogrammetry

A UAV (Unmanned Aerial Vehicle) is an aircraft without a pilot, as the name suggests. However, that does not mean automatically that the aircraft flies fully "on it's own". They are radio controlled either manually or via a predefined flight path. UAV systems have significant advantages due to the fact that they don't have a pilot: Weight and complexity are reduced, extending the endurance of the system. Furthermore, they are very suitable for "dull, dirty and dangerous" missions (UAS Roadmap [2005]), i.e. missions which require multiple repetitions of the same acquisition (which is considered dull, and therefore is best automated), or missions which would

normally send people to spots which are undesirable (such as a mud field) or outright dangerous (like an active volcano). Therefore data acquisition by a UAV in these areas has clear benefits.
Low altitude UAV systems have the added advantage of reduced cost. Instead of using the best available equipments, which are both expensive and heavy, equipments which are "just-good-enough" are being used.
As stated before, an Unmanned Aerial Vehicle does not fly out of itself. Therefore a system is needed to get the vehicle in the air. This is called the Unmanned Aerial System (UAS), and consits of the Airborne UAV, a Ground Control Station and a Data Processing Centre. The UAV is the object in the air taking the photographs. It is guided by the Ground Control Station. Here the mission is planned, carried out and the obtained data (in case of aerial photogrammetry, the photographs) is sent to the Data Processing Centre, where it is processed and made into the final product.
With the ongoing development of radiocontrolled vehicles, application of radiocontrolled aircraft in the field of photogrammetry couldn't stay behind. Eisenbeiss [2008] explains the technique of UAV photogrammetry in depth. The basic principle is more or less the same as conventional aerial photogrammetry. However instead of using a full sized piloted aircraft, an unmanned aircraft is used that is flown either by radiocontrol or flies autonomously using onboard sensors and a predefined flight path to find it's course. UAV's used for photogrammetry are usually quite small (smaller than the person operating the aircraft from afar). The equipment which can be carried aboard the UAV is therefore limited. On the airplanes Heering UAS uses there is space for a camera and some small standard sensors for attitude control and navigation. Larger equipment such as gyroplatforms and Forward Motion Compensators are too big and heavy to be installed to the aircraft and therefore cannot be used. In digital cameras Forward Motion compensation is done electronically, using Time Delay Integration. A Time Delay Integration algorithm which integrates the received lines of light over a number of pixels. Therefore the photographed object is "followed" while the camera shutter is open, effectively reducing blur. However, only specialized digital cameras contain TDI, therefore using TDI is very expensive.
Modern photocameras have the ability to automatically take photographs with a predefined interval. Therefore the photographs are also taken automatically.

2.2.1 Advantages of UAV Photogrammetry

Compared with conventional aerial photogrammetry, UAV photogrammetry has certain advantages. First of all, because a model airplane is used, the

method is more flexible. The aircraft can be launched from anywhere and thus doesn't need a runway to start. Also, the flying height is lower than that used in conventional photogrammetry. Therefore the aircraft usually stays below clouds, which make it possible to fly during cloudy days. This increases the amount of days on which can be flown significantly.
Using UAV photogrammetry instead of conventional photogrammetry also gives a significant cost reduction. Obviously an Unmanned Aerial Vehicle does not require a pilot to fly the plane. Furthermore, during conventional photogrammetry flights, a camera operator is aboard the aircraft who rotates the camera so that the geometry between pictures is accurate enough. This camera operator is absent in UAV Photogrammetry. Therefore less personnel is needed in UAV Photogrammetry, which saves money. Furthermore, the aircraft navigation and orientation is measured and maintained by low-cost "off-the-shelf" sensors instead of the expensive specialized products used in conventional photogrammetry. The aircrafts are propulsed by rotors powered by small electric engines. Therefore batteries are needed but there is no need for aircraft fuel, which is very expensive. Therefore the lack of need for fuel saves costs significantly.
The lower flying height of the UAV results in a high scale for the photographs, the resolution of the photographs is therefore much higher than the results of conventional photogrammetry. A higher resolution results in more detail of the Digital Elevation Model derived fromt the photographs. Furthermore, a higher resolution would make it possible to pinpoint features in the photos more precisely, thus improving accuracy. Furthermore, small UAV's do not need to be launched from an airport and fly low enough not to fall under air traffic regulations. Therefore the deployment of UAV photogrammetry is much more flexible. Also the low flying altitude makes it possible to use a larger scale than in conventional photogrammetry, showing more detail in the photos.

2.2.2 Challenges of UAV photogrammetry

Compared with conventional photogrammetry, UAV photogrammetry has certain obvious differences. First of all, the used equipment is often simpler and thus cheaper than that used in conventional photogrammetry. The simple and thus low-cost equipments do set some challenges though. First of all, the simpler equipment is not as accurate as the advanced equipments dedicated to photogrammetric measurements in a full sized aircraft. This causes inaccuracies in the position and attitude measurements of the airplane. Furthermore, the used camera is an off-the-shelf mirror reflex camera instead of a dedicated photogrammetric camera. Extra inaccuracies due to

larger lense distortions can be the result of using this camera. Off-the-shelf camera's also have a smaller sensor size. Therefore the resulting picture is smaller and the ground coverage of one photo is smaller than in conventional photogrammetry, making it harder to maintain a certain overlap. The absence of dedicated photogrammetric equipments also limit the accuracy of the outcoming product.
The camera is fixed rigidly to the aircraft, instead of resting on a gyroplatform. Therefore the camera follows all rotations the aircraft makes. The propellor of the aircraft (or especially the rotors of a helicopter) causes vibrations in the aircraft. These vibrations are propagated to the camera. Therefore the camera vibrates when a photo is taken, causing the photos to be unsharp. Furthermore the aircraft is in motion the moment the photo is taken, causing forward motion blur. UAVs are light, making them difficult to control, especially when there is wind. This causes uncertainty in following a predefined flight path, making it difficult to maintain enough overlap between photos and weaving about of the aircraft causes more blur in the photos.
During conventional photogrammetric flights an operator rotates the camera platform so that the orientation of the photo's to each other is correct and a decent block can be made easily. This is not possible in UAV photogrammetry, therefore photo's in a photoblock can have large angles. Photogrammetric software can't always cope with these large angles. Experience from this research learned that especially Leica Photogrammetric Suite is prone to failure when the photo's in a block are not oriented nicely to each other.

2.3 Direct sensor orientation

As mentioned above, in conventional photogrammetry the exterior orientation of the photo's is determined by using Ground Control Points known in terrain coordinates. This involves measuring and maintaining the ground control points in the field, which is very labour intensive. This is in fact the most expensive part of conventional photogrammetry, so reducing or eliminating the need for ground control points would help reduce costs significantly. Furthermore, the ground control points need to be pinpointed in each and every photograph of the block to determine the exterior orientation. This is also very labour intensive. To prevent this labour-intensive work of setting up and maintaining Ground Control Points, direct sensor orientation is used. Instead of determining the exterior orientation from Ground Control Points, the GPS and inertial navigation sensors of the airplane are used to determine the exterior orientation parameters directly. This is a relatively new

technique. Cramer [2000] describes tests carried out on direct sensor measurements. Using different GPS receivers and internal navigation systems, photoblocks has been flown with a full sized aircraft. The GPS/INS output is then used for the 6 exterior orientation parameters. These parameters are then used to determine the coordinates of checkpoints on the ground, whose terrain coordinates have been determined using other measurement techniques.
This technique requires high accuracy position and attitude determination of the aircraft. In full sized aircrafts this is no problem, aboard most aircrafts there is enough space for high-end GPS receivers and inertial navigation equipment. However aboard a small unmanned vehicle (especially the size Heering UAS is designing and planning to use), this kind of equipment simply does not fit. Therefore a solution must be found to use direct sensor measurements on UAV photogrammetry with high accuracy.

2.4 Error budget of UAV Photogrammetry using Direct Sensor Orientation

The accuracy of the final product, i.e. the terrain model derived from the photographs, is dependent on several error factors. When determining the influence of these error factors on the accuracy of the outcoming product, a distinction between systematic and random errors has to be made. Systematic errors are errors with a constant factor. Therefore all measurements have the same error, and this can be solved for by calibrating the measurement platform. Random errors are errors due to external factors, whose behaviour can't be predicted beforehand and therefore is impossible to correct for.
There are several factors influencing the outcoming products of UAV Photogrammetry, such as errors in the GPS and IMU sensors, camera interior errors and GPS/IMU integration errors. This thesis focuses on the use of direct sensor measurements in UAV photogrammetry, therefore the main interest lies with the effect of inaccuracies in the sensor measurements on the accuracy of the outcoming product, therefore this thesis will deal with the following error sources:

- GPS inaccuracies
- IMU inaccuracies and wind effects
- forward movement blur in the pictures (due to the aircraft moving during the opening time of the camera lens, the pictures are slightly blurred).

- Time delay between registering GPS/IMU measurement and capture of photograph.

2.4.1 GPS errors

The GPS measurements are being used to determine the terrain coordinates of the camera projection centre. The GPS measurements do have error sources of their own though, for an overview of GPS errors and accuracy, see paragraph 3.1.2. As said before, the systematic GPS errors can be corrected by calibration. This calibration is also important to determine the offset between the GPS receiver and the projection centre of the camera, more on this in paragraph 3.3. After solving for the systematic errors, the GPS receiver still won't continually give the "right" position. Random errors due to various error sources continue to compromise the GPS outcome. Because the GPS outcomes are used to determine the coordinates of the projection centre of the camera, these random errors will propagate as inaccuracies in the position of the camera centre, which are 3 of the 6 exterior orientation parameters. Therefore errors in the GPS receiver have a significant effect on the accuracy of the outcoming product.

2.4.2 IMU errors

The Inertial Measurement Unit (IMU) measures attitute of the airplane, i.e. the rotation angles of the plane around the axes of a 3D right-handed coordinate syste. Three of the six exterior orientation parameters are the rotation angles of the camera. These rotation angles can be determined from the rotation angle of the aircraft and thus of the IMU measurements. Again, the IMU measurements are prone to both systematical and random errors. The systematical errors can be solved for by calibration. A calibration is also necessary to determine the angular differences between IMU rotation and camera rotation due to the design of the platform, see paragraph 3.3 for more details. Again the random errors in the IMU measurements will propagate into inaccuracies in the exterior orientation parameters. Therefore errors in the IMU measurements contribute significantly to the accuracy of the outcomig product.
General low-cost UAVs have a low weight and fly at a relatively low airspeed velocity. Therefore the airplane is bound to experience wind effects. The airspeed is effected by headwind (plane slows down) or tailwind (plane speeds up). Furthermore crosswinds can cause the plane to weave about instead of flying in a straight line. This influences both the GPS measurements (systematic and/or random fluctuations from expected flight path and flight

speed) and the Inertial measurements (extra rotational angles). Furthermore wind effects can cause crab angles (the aircraft flying a bit sideways), reducing the effective overlap between the photos. The true location of the aircraft can be determined from the GPS measurements if the receiver is accurate enough, therefore wind will have little effect on position determination. However it has been theorized that strong winds can cause the IMU to become unstable, making attitude determination in strong winds difficult. This theory has never been tested yet though. The aircraft is not durable enough to fly in strong winds, therefore testing an IMU on stability in strong winds is beyond the scope of this thesis.

2.4.3 Forward motion blur

When a photo is taken, the shutter of the camera opens for a very short time (about 1/1000th of a second) and then closes again. The light which falls on the camera film (or chip in case of a digital camera) is catched, which makes the actual photo. During this small time the aircraft keeps flying. Therefore the terrain will slide underneath the camera while the shutter is open. This causes forward motion blur. Forward motion blur will cause small distortions in the pictures, making it harder to pinpoint object points, thus reducing the measurement accuracy. This forward motion blur is dependent on shutter speed and aircraft speed and can therefore be estimated beforehand, making it possible to estimate the contribution of motion blur to the total accuracy of the final product.

2.4.4 Measurement timing

The GPS receiver records it's measurements with a certain frequency. Whenever a photo is taken, this photo is time stamped and given the GPS coordinates of the nearest GPS recording. This introduces a small time offset between the actual GPS measurement and the taking of the photograph. The location of the aircraft when the photo is taken can be interpolated using the GPS records, but such an interpolation is an estimation of the GPS-location and is therefore not entirely accurate.

Chapter 3

Navigation sensors for UAV Photogrammetry

3.1 Global Positioning system

3.1.1 Description of GPS

The Global Positioning System is a relatively new navigational system using dedicated satellites developed by the American army. The first satellite was launched in february 1978 (Van der Marel [2009]). In 1982 the first civil receivers became available. The system is operational for a broad public since 1994. Over the years the system has been expanded and renewed. Currently there are 24 satellites avaible. These satellites have an orbit height of 20200 km, an inclination of 55 degrees and are spread over 6 orbital planes. See figure 3.1.

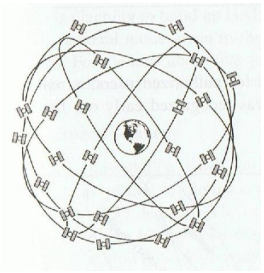

Figure 3.1: GPS constellation with 24 satellites (Seeber [2003])

The whole system consist of 3 segments, being the space segment, the user segment and the control segment (Husti [2000]). The space segment are the satellites, the user segment are the receivers and the control segment

consisting of 5 monitoring stations spread around the world which track the satellites and determines clock and orbit parameters of the satellites to keep the system running and to protect the accuracy of the system. At the moment the system is modernized.

The fundamental principle behind GPS is based on the measurement of so-called pseudoranges between the receiver and the satellites. The satellites send out a signal to the receiver containing amongst others the time of transmission and the location of the satellite. By determining the time difference between transmission and reception of the signal, the distance (the range) between the satellite and receiver is determined. By constructing lines between the observed satellites and the receiver the position of the receiver can be determined. To determine the location of the receiver, we need at the very least 3 satellites. This can be explained both mathematically and geometrically. The location of the receiver is expressed in coordinates, of which 3 need to be determined (lat,lon and height or X,Y,Z, depending on the used reference frame). Thus there are 3 unknowns, therefore observation theory shows that we need at the very least 3 observations to determine a result (Teunissen [2000]) . However, the clock in the receiver and the clock in the satellite are not synchronized, this causes an unknown clock error which has to be resolved. Therefore at least 4 observations and thus 4 satellites are needed to determine the location of a receiver. That is why the term pseudorange is used (Seeber [2003]). See also Figure 3.2

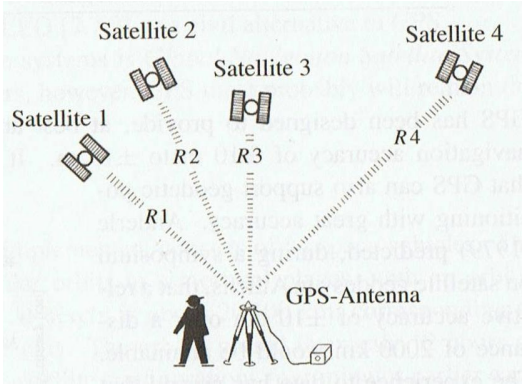

Figure 3.2: Basic principle of positioning with GPS, (Seeber [2003])

The satellites send their signals on two frequency bands, L1 and L2. These contain 2 signal codes, the Coarse/Acquisition (CA) code on L1 and the Precision (P) code on L1 and L2. To prevent saboteurs jamming the signal, the P-code is encrypted with a classified Y-code. This is called anti-spoofing. The P-code can only be read by higher end GPS receivers, which are capable

of reading both frequencies. The CA-code is the most basic GPS signal and can be read by the most basic receiver. The top-end receivers can also read the carrier phase on which the GPS signals are transmitted. These carrier phase measurements usually gives the highest precision.
The modernization scheme of GPS will add a third carrier wave (L5) and will add new civil signals on the L2 and L5 band. This modernization plan will therefore see a major improvement in accuracy for civil users.

Although the principle behind GPS measurements is very basic there are a number of different ways to determine a position using GPS. The main difference is between single point positioning techniques and differential GPS

Single Point Positioning

Single point positioning is the technique of determining a position with one receiver. The basic principle behind this is explained in the previous paragraph. To determine the time difference between satellite and receiver, the received code is compared with replica running in the receiver, the received signal will run behind compared with the signal replica. This "running behind" determines the time difference (see figure 3.3). The signal codes are binary. Therefore the time difference between sending and receiving is determined by counting the difference between code entries (ones or zeroes), called chips. The amount of chips the received signal is running behind the replica can then be multiplied with the chip rate, the amount of chips that are generated per second.

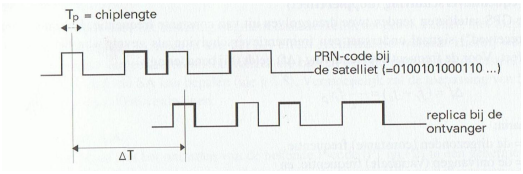

Figure 3.3: Basic principle of positioning with GPS, (Seeber [2003])

When a dual frequency GPS receiver is used, both the L1 and the L2 bands can be read. Therefore the more accurate P-code can be used. Furthermore it is possible to determine linear combinations between the 2 bands, making it possible to detect (and therefore eliminate) different kinds of errors. Furthermore these receivers are capable of reading the carrier phase. This makes determining the time difference more accurate, giving a more accurate position (see figure 3.4) These techniques increases accuracy but is seldom used in stand-alone applications.

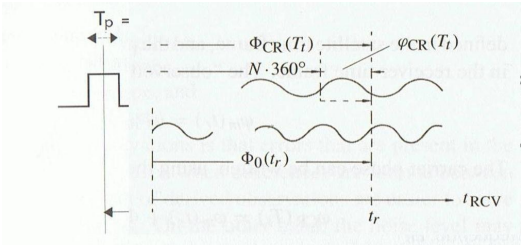

Figure 3.4: Carrier Phase measurements (Seeber [2003])

Differential GPS

When a second GPS receiver is used, it is possible to perform Differential GPS measurements. One GPS receiver, the reference station, is set up at a point which is known in coordinates and keeps measuring. The other GPS receiver, the rover, roams around the area to be measured and determines the coordinates of different points. Instead of coordinates directly from the GPS satellites, the baseline between the two receivers is calculated, see also figure 3.5

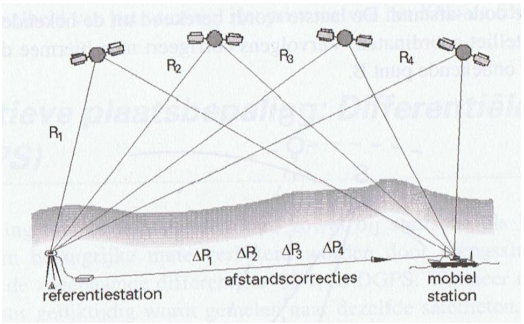

Figure 3.5: Baseline determination with Differential GPS (Husti [2000])

The main advantage of this technique is that error influencing factors which are more or less the same for both the reference station and the rover, such as atmospheric delays (see section 3.1.2 for a more detailed description), cancel out against each other. This causes a major improvement in the accuracy.
The best accuracy is obtained when differential GPS using phase measurements is used. However, for this technique two high-end Geodetic GPS receivers are necessary. Furthermore an awkward parameter is introduced in the observation equations, the Phase Ambiguity. Solving this Phase Ambiguity is not trivial. There are methods to work around this Phase Ambiguity. The description of this and the used observation equations is beyond the scope of this thesis though.

3.1.2 GPS accuracy

As explained in section 3.1, the GPS measurements are based on determining time differences between transmission and reception of the signal sent out by the satellites. The accuracy of the determined coordinates is therefore dependent on the accuracy of the determined time differences. It is assumed that the signal travels in a straight line and at the speed of light. The satellite and receiver clocks are not synchronized, but this is resolved by determining the satellite clock error, as discussed in section 3.1.
The signal can be delayed by all kinds of phenomena, the straight line assumption may not be true and there can be factors in both the satellite and the receiver reducing the accuracy. The main error contributions and their resulting range error is given in table 3.1.

Error Source	RMS Range Error
Satellite	
- Orbit	1 - 2 m
- Clock	1 - 2 m
Signal Propagation	
- ionosphere (2 frequencies)	cm - dm
- ionosphere (model, best)	1 - 2 m
- ionosphere (model, average)	5 - 10 m
- ionosphere (model, worst)	10 - 50 m
- troposphere	dm
- multipath	1 - 2 m
Receiver - observation noise	0.2 - 1 m
- hardware delays	dm - m
- antenna phase center	mm - cm

Table 3.1: GPS error budget (Seeber [2003])

Satellite orbits and clocks

To be able to determine the location of the receiver, the position of the satellite and time of transmission of the signal should be known. Information about the satellite orbit and time of transmission is sent in the GPS signal. The receiver is able to use this information to determine the location of the satellite at time of transmission of the signal. However both the satellite orbits and the satellite time transmitted in the signal contain errors. This will cause the receiver to determine a wrong position for the satellite and therefore a wrong calculation of it's coordinates. The error in the time of

transmission causes an error in the time difference estimation and thus in the range determination. This also influences the accuracy of the determined coordinates.

As explained in section 3.1, the control segment of the system tracks the satellites and the satellite clocks. Therefore they can determine precise orbits and clock errors. Information about these precise orbits and clock errors are assembled and made available by the International GNSS Service (IGS). After a measuring campaign, the user can download precise orbits and clock errors from the IGS and enhance his measurements. This requires post processing though, so this technique is not available when real time measurements are needed.

Ionospheric and Tropospheric delays

The signal has to travel about 20000 km between the satellite and the receiver. Assumed is that the signal travels through vacuum and therefore has the speed of light. Although this is true for the majority of the distance, once the signal enters the earth's atmosphere, the signal is delayed by ionospheric and tropospheric effects. The Ionosphere is the upper part of the atmosphere, ranging from 85 to 600 km altitude. Without going into too much detail, the GPS signal is delayed due to ionization of the atmosphere. The amount of delay the signal gets is more or less even over greater distances. Therefore the Ionospheric delay can:

1) Be modelled when using single point positioning.
2) Be solved for by using a dual frequency GPS receiver
3) Be eliminated by using differential GPS

The Troposphere is the lower part of the atmosphere, namely the part where the weather takes place. Therefore the signal gets delayed by substances in the troposphere (mainly water vapour). The distribution of this and therefore the distribution of the delays can differ from place to place. Therefore tropospheric effects are harder to deal with. Using differential GPS with short baselines can help. Otherwise models are used to reduce the influence of tropospheric delays.

Multipath effects

When measuring near tall objects, like trees and buildings, chances are that the GPS signal bounces off these objects before reaching the receiver (see figure 3.6). This causes the estimated range to be larger than it actually is and therefore causes an error in the estimated coordinates. One way to

reduce this problem is by using an antenna that only receives signals from above (so the bottom is isolized). When a dual frequency receiver is used, multipath effects can be detected.

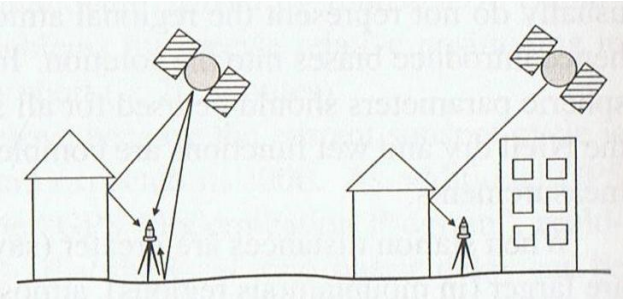

Figure 3.6: Multipath effects (Seeber [2003])

Receiver errors

The GPS signal itself is very weak. The antenna of the GPS receiver picks up all kinds of distortions such as electromagnetic currents from power lines and electric engines. This causes noise in the receiver. Under normal circumstances the signal-to-noise ratio is very bad. The signal can be amplified though, making the signal-noise-ratio better. However, during measurements, electro-magnetic fields from power lines, electromagnetic engines and the like can cause inaccuracies. This is specified as receiver noise. The inaccuracy values due to receiver noise are about 3 meters for C/A-code measurements, 30 cm for P-code measurements and about 2 mm for carrier wave measurements.

The antenna of the GPS receiver can be another error source. There are different types of antenna's, see figure 3.7. The GPS receiver determines the position of the antenna centre, there is however a difference between the mechanical centre, i.e. the physical midpoint of the antenna and the electronic centre, i.e. the point in the antenna the signals are aimed at and collected. Therefore the GPS-receiver determines the electronic centre of the antenna. The determination of the electronic centre is another source for inaccuracies. The resulting error size is depending on the antenna type.

Satellite Geometry

Besides the factors influencing the accuracy given in table 3.1, the accuracy of the position of the receiver is also dependent on the Geometry of the satellites

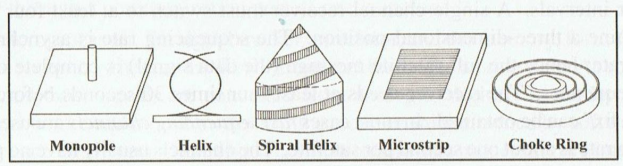

Figure 3.7: Different forms of GPS-receiver antenna's (Seeber [2003])

used for the measurements. Obviously, the more satellites there are in view, the better the accuracy is. However, the distribution of the used satellites over the sky and the looking angles between the receiver and the satellite also influence the accuracy. These factors are used to determine the Position Dilution of Precision (PDOP) value. This value describes the robustness of the satellite geometry. In figure 3.8 a good and a bad satellite constellation is shown. The PDOP value is thus a value which describes if the satellite constellation is good or bad.

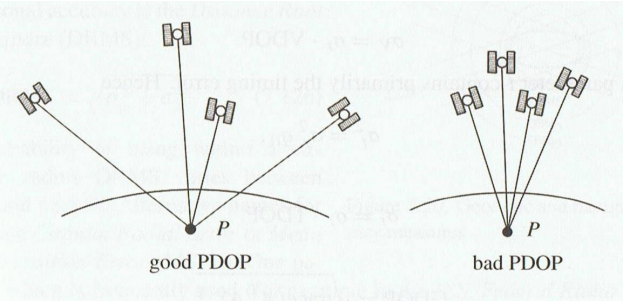

Figure 3.8: Satellite geometry and PDOP (Seeber [2003])

3.1.3 GPS in photogrammetry

In convential aerial photogrammetry, GPS measurements are used to determine the coordinates of Ground Control Points and check points. Furthermore, they are used to determine A-priori values for the exterior orientation parameters. When determining the exterior orientation using Ground Control Points, the collinearity equations (equation 2.2) are used, but with the Exterior orientation parameters as unknowns, the photo coordinates as observations and the terrain coordinates of the ground control poins as fixed values. This introduces a non-linear problem, which has to be solved in an iterative scheme using the linearized observation equations. This requires A-priori values for the unknowns (Teunissen [2000]). The Ground Control Points need to be determined with very high accuracy, so usually differential

GPS techniques using relatively small baselines are used to determine these. The accuracy of the A-priori values for the exterior orientation parameters is less important. Therefore these can be determined using a single GPS-receiver aboard the aircraft. Most aircraft have GPS-receivers on board to aid the navigation of the airplane, usually the coordinate output of these GPS-receivers is good enough to act as A-priori values for the iteratization.

The Ground Control Points need to be measured with an accuracy in the order of centimeters. To achieve this, differential GPS using carrier phase measurements should be used, because centimeter accuracy is easily achievable using this method.
When direct sensor measurements is used, the definite exterior orientation parameters have to be determined from the sensors aboard the aircraft. To determine an accurate terrain model, the exterior orientation parameters need to be known very accurately.

Cramer [2000] describes an extensive test of direct sensor measurements using a full size (piloted) aircraft. The test results described in this paper are very promising (check point RMS values of 1 to 2 dm). In the paper it was specified that highly sophisticated GPS/inertial measurement systems were used to determine the exterior orientation parameters, unfortunately no specifications were given. Furthermore, the system they used was already fully integrated, which greatly improves the accuracy. The paper doesn't say anything about the accuracy of the used GPS receiver. A comparison between the direct sensor measurement and an Aerial Triangulation has been made. The differences in the coordinates of the camera centre were lying between 10 and 20 cm. Unclear is however if the GPS-receiver itself has the same accuracy or if this accuracy was obtained after integrating and filtering the GPS measurements with the inertial measurements.

Schwarz [2004] gives an overview of the development of direct sensor measurements in both aerial photogrammetry and terrain based mobile mapping systems over the years. This paper also describes an integration between GPS measurements and inertial measurements. However, in this paper it is specified that high accuracy differential GPS (using dual frequency GPS receivers) is used. Therefore, to determine high accuracy coordinates of the camera centres, high accuracy GPS measurements are needed, before integrating them with inertial measurements.

GPS photogrammetry

GPS Photogrammmetry is a technique which includes GPS measurements from the aircraft to the aerial triangulation. So, instead of using the GPS results directly as exterior orientation parameters, the GPS measurements are used in the triangulation adjustment which determines the exterior orientation parameters. In this case, the measured "control points" are at the location of the camera centres. In theory this technique would not require ground control points for the triangulation adjustment. The coordinates of the camera centres and the rotation angles of the camera could be deduced from the GPS measurements of the on-board receiver and tiepoints which describe the geometry between the photos. However, this would demand that a GPS solution is continuously found throughout the flight. GPS integrity is however not guaranteed. For several reasons, the GPS signal can be blocked. The GPS receiver doesn't receive a signal and a location can't be computed. If such a loss of lock occurs, the aircraft obviously keeps on flying and photos are kept being taken. These photographs are then without coordinates of the camera centres. To prevent this from happening, an Inertial Measurement Unit is used, which keeps on measuring the movements of the aircraft if a GPS loss of lock occurs. The GPS and IMU measurements are combined using a Kalman filter (see paragraph 3.3) to give an accurate estimation for the camera centre coordinates, even if the GPS measurements are flawed. As described above, the accuracy of the GPS solution is dependent on a number of factors. Therefore the accuracy is not always guaranteed. In practice a limited number of Ground Control Points is used to improve accuracy.

3.2 Inertial measurement unit

To be able to derive a DEM from the aerial photographs, it is not enough to know the location of the camera at the moment the picture was taken. It is also necessary to know which way the camera looked. Therefore it is necessary to determine the rotation angles of the camera. When conventional photogrammetry techniques are used, these rotation angles are determined together with the coordinates of the camera centre using ground control points, as explained in paragraph 2.1.2. However, when direct sensor measurements are used the rotation angles of the camera need to be measured during the flight. This yields that the attitude (roll, pitch and yaw angles) need to be determined.

3.2.1 Inertial Measurements

To determine the attitude of airplanes, an inertial measurement system or inertial navigation system is used. Woodman [2007] gives a description of the main components of an inertial navigation system, describes how they work and gives some accuracy specifications. A typical intertial navigation system contains gyroscopes and accelerometers to determine the angular and linear velocities of the object the system is attached to. A classical inertial measurement system contains three accelerometers, which are used to determine the acceleration in X, Y and Z directions. The velocities are then determined from a starting value (or the result of the previous measurement), by integrating acceleration.
To determine the angular velocities, a common system contains three gyroscopes, each one of them detecting the angular velocity around one of the three axes (X, Y or Z) of a standard coordinate system. Two main types of inertial measurement systems exist, being the stable platform and the strapdown platform. The stable platform has its measurement sensors on a platform which is always level to the reference frame. Therefore the platform can be rotated around the axes it is fitted to, so when the aircraft makes a turn (and the aircraft rolls and/or pitches), the platform stays level (see also figure 3.9)

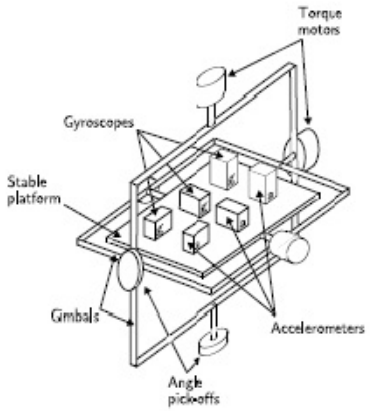

Figure 3.9: A stable platform IMU (Woodman [2007])

The strapdown platform is fixed rigidly to the system and therefore to the moving object. Therefore the whole platform rotates with the moving object. The main advantage of the strapdown platform is that is it easier to create and can be incorporated in smaller systems. The disadvantage is determining the output values takes more computation costs. However, computational possibilities have been increasing recent years and therefore computational

costs becomes less of an issue. Therefore the strapdown systems have become the dominant type of inertial navigation systems.

Gyroscopes

The rotation angles/angular accelerations are determined by gyroscopes. Over the years a lot of different gyroscope techniques are developed. A description of all these techniques is beyond the scope of this thesis. It suffices to mention the main types. A classical (mechanical) gyroscope consists of a spinning wheel mounted to two so called gimbals, which are rings which can rotate freely around their axes in two different directions (see also figure 3.10). A spinning wheel will resist changes in the orientation. Therefore, if the platform the gyroscope is mounted on makes an angle, the spinning wheel wants to keep it's orientation and because the gimbals can rotate freely, the gimbals will rotate according to the orientation change. From the mounting points of the gimbals the rotation angles can now be read off.

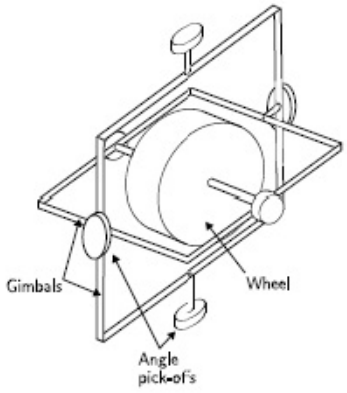

Figure 3.10: A conventional mechanical gyroscope (Woodman [2007])

The main disadvantages of these systems is that they are large, contain lots of moving parts and they require a few minutes to warm up. The moving parts cause friction, causing the spinning wheel not being able to rotate freely (and thus keep its orientation), which causes the output to drift over time.
A second type of gyroscope uses the interference of light to measure angular velocity. Two rays of light are sent into a circular optical fibre. When the sensor rotates, the distance of the path the light takes through the optic fibre changes (see figure 3.11). This is called the Sagnac effect. This causes a phase shift in the two light beams. When the beams are combined, this phase shift causes interference. Therefore the combined light intensity of the two rays can be measured to determine the angular velocity.

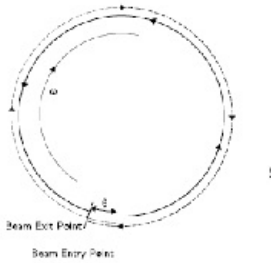

Figure 3.11: The Sagnac effect. The dashed line is beam travelling in the direction of rotation. The solid line is beam travelling against the rotation. θ is the angle through which the gyro turns. (Woodman [2007])

The main advantages are that optical gyroscopes don't have moving parts and require a few seconds to start up. The main disadvantage is that the accuracy depends on the size of the optic fibre circle: the larger the better. Therefore, high accuracy optical gyroscopes need large devices.
Small and relatively cheap gyroscopes are being developed at the moment, based on MEMS (Micro-machined ElectroMechanical Systems) technology. Such a gyroscope contains a mass element which vibrates along a so called drive axis. When the platform rotates, this causes a disturbance in the vibration. This disturbance is measured along an axis perpendicular to the drive axis, the sense axis (see figure 3.12) To determine the rotation along all three axes of a coordinate system, three MEMS-gyroscopes are needed. Despite this, they are smaller, lighter, cheaper and have a shorter start up time than mechanical and optical gyroscopes. However, the accuracy is far less when compared to these bigger gyroscopes.

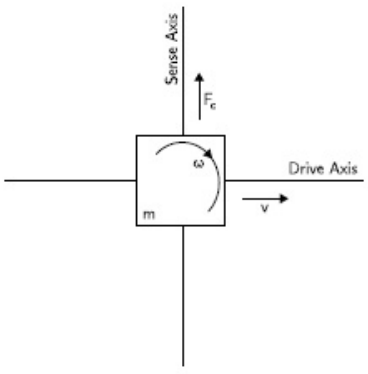

Figure 3.12: Workings of a MEMS vibrating mass gyroscope (Woodman [2007])

Accelerometers

Accelerometers are used to determine the linear acceleration of the platform. They come in two main forms, being mechanical accelerometers and solid state accelerometers.

Mechanical accelerometers contain a proof mass attached to springs in the input axis, proportional to the input axis a displacement pickoff is placed on which the displacement due to a force acting on the platform can be read. This can be calculated into acceleration using the second law of Newton. See Figure 3.13.

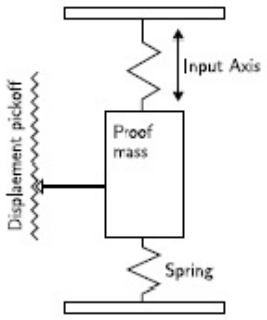

Figure 3.13: Mechanical accelerometer (Woodman [2007])

There are various different kinds of solid state accelerometers, but the basic principle is that a beam is resonated at a certain frequency. A free moving mass is attached at one side of the beam, on the other side the beam is place rigidly to the platform. When a force works on the platform along the input axis the beam bends, causing the frequency of the beam vibration to change. By measuring this frequency the acceleration can be measured, see Figure 3.14.

3.2.2 IMU accuracy factors

As described above an IMU consist of three gyroscopes and three accelerometers. These two measurement instruments both have their own factors which influence the accuracy of the measurements. The accuracy of these measurements influences the accuracy of the outcoming location and attitute determination. As described above there are many different techniques for constructing Gyroscopes and Accelerometers, however platforms based on MEMS technology are usually the cheapest and most easy to build in

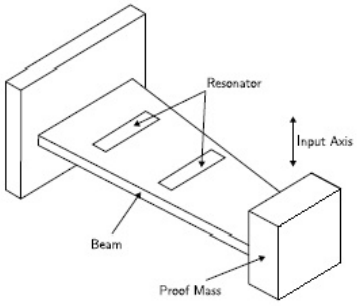

Figure 3.14: Solid State accelerometer (Woodman [2007])

unmanned vehicles, therefore the focus of this section is on the factors influencing the measurement accuracy of MEMS inertial measurement units. According to Woodman [2007] the factors influencing both the gyroscopes and the accelerometers are more or less the same, however their influence on the outcoming measurements is different. Woodman [2007] specifiecs the following accuracy factors:

- Constant Bias
- White Noise
- Bias Instability
- Temperature Effects
- Calibration errors

Constant Bias

Both measurement instruments in the IMU are subject to a constant bias. This is the average output from the device when it is not undergoing any movement, so the offset of the output from the true value. For Gyroscopes a constant bias error causes an error in the rotation angles that grows linearly with time. This is known as gyroscope drift. This gyroscope drift can easily be detected and solved for by letting the device measure for a specific amount of time, when it is not in motion. The drift should follow from this. This drift can then be substracted from actual measurements.
A constant bias of the accelerometer causes an error in the position estimate which grows quadratically with time. Estimating this constant bias could be done the same way as determining the gyroscope bias. However, this is complicated by gravity. Therefore, the precise orientation of the device to the

gravity field must be done. In practice this is done by mounting the device on a turntable, whose orientation can be controlled extremely accurately.

White Noise

All kinds of distortions in the measurement environment causes the gyroscope and accelerometer measurements to contain random noise, just as every other measurement sensor. This white noise causes the measurements to walk randomly around a mean, which can be regarded as the true value. However for both the gyroscopes and the accelerometers this white noise is not constant. For gyroscopes it grows proportionally over the square root of time. For accelerometers it grows proportionally to $t^{3/2}$.

Bias Instability

Due to noise in the electronic systems of the devices, the biases of the gyroscopes and accelerometers are not completely stable. Therefore the biases show a random walk. Integrating this random walk over time gives the influence of the bias instability over the measurements. A stable constant bias causes a first order random walk for gyroscope measurements and a second order random walk for accelerometers. Integrating this over time, it can be deducted that Bias Instability causes a second order random walk for gyroscopes and a third order random walk for accelerometers.

Temperature effects

For both the gyroscopes and the accelerometers, changes in the temperature of the device environment cause changes in the biases, which are not included in bias stability measurements. Therefore, temperature changes the biases of the instruments and causes an error of the same kind as constant bias. However, the relation between bias and temperature change is often highly nonlinear and depends on the specific device. Therefore it is very hard to model for temperature effects.

Calibration errors

Errors in scale factors, alignments and output linearities are known as calibration errors. These appear as a bias error which only are visible when the device is undergoing movement (so rotation for gyroscopes and acceleration for accelerometers). This causes drifts in the measurements during the movements.

3.3 Rotation systems and calibration

The GPS receiver and the IMU unit are not located exactly at the place of the projection centre of the camera, but it is the location and the attitude of this projection centre which must be determined. Therefore a calibration need to be performed, see figure 3.15

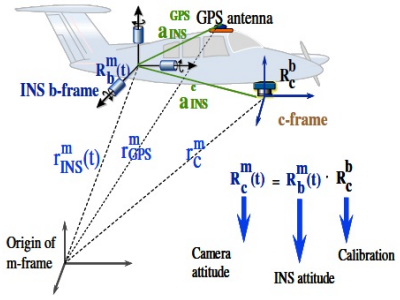

Figure 3.15: Dicrect Georeferencing principle (Schwarz [2004])

The location of the camera centre in this figure is given by the vector r_m^c, which is the vector between the origin of the m-frame defining the terrain coordinates and the c-frame, which is the camera frame, which defines the photo coordinates. Therefore, to determine the position of the projection centre of the camera, this vector must be retrieved. The GPS measurements gives the vector r_{gps}^m, the vector between the origin of the m-frame and the GPS antenna. To determine the location of the camera centre, the vector between the GPS antenna and the camera must be determined.
The same applies for the rotation vectors. The element $R_b^m(t)$ is the rotation matrix determining the IMU attitude relative to the m-frame, which is the terrain coordinate system at time of measurement t. The element $R_c^m(t)$ is the rotation matrix determining the camera attitute relative to the m-frame. The element R_c^b is the rotation matrix determining the rotation differences between the IMU and the camera. This rotation matrix for the angular differences must be found to be able to determine the rotation angles of the camera
The determination of both the vector between the GPS antenna and the camera centre and the rotation matrix R_b^c between the IMU and the camera is the calibration of the platform. Approximate calibration figures can be determined in the design of the system, but for very accurate results a calibration flight should be carried out. On a flat terrain, a number of ground control points must be set out and measured accurately. The platform flies over this area taking photographs. With the help of the ground control points, a tri-

angulation can be made. The outcoming exterior orientation parameters can then be compared with the GPS and IMU measurements. The differences are then the calibration parameters. This calibration will only work when the GPS and IMU measurements don't contain systematical errors.

3.4 Time delay and Kalman Filtering

3.4.1 Time delay between photo capture and GPS and IMU measurement

The rate of GPS and IMU measurements and the photo capture is not the same. Therefore the uncombined sensor measurements are all taken at specific time moments. Suppose for example that the IMU measurement rate is 1 measurement each 0.1 second, the GPS measurement rate is 1 measurement each 0.33 second and the photo capture is each 4 seconds. The measurement moments along the timeline are then as shown in figure 3.16.

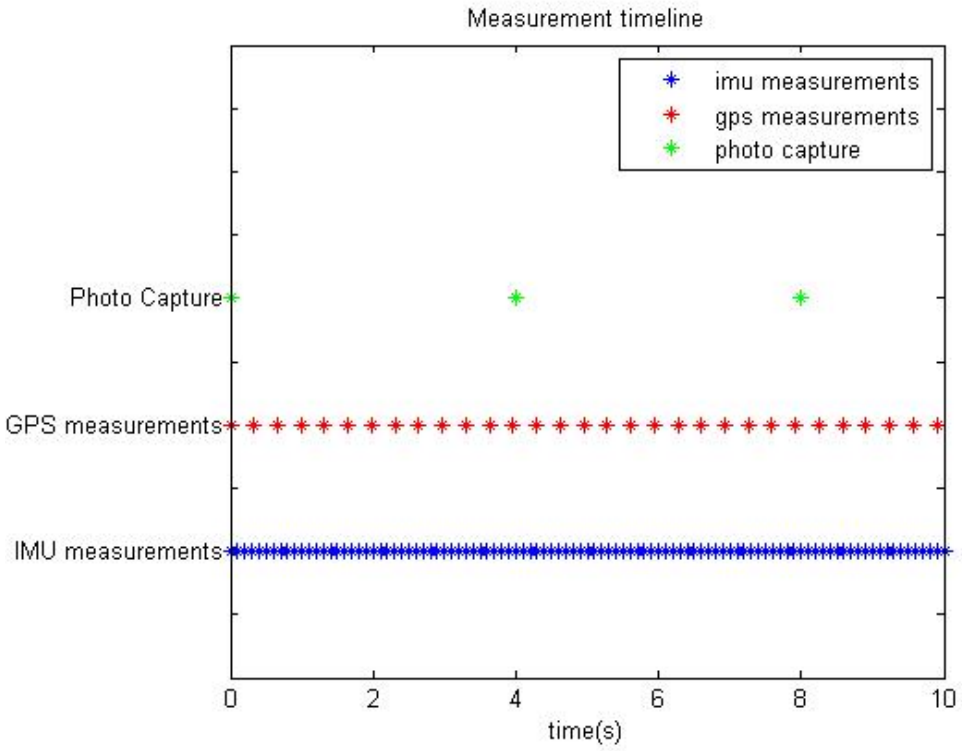

Figure 3.16: Measurements of the different sensors along a timeline

Combining the GPS and IMU measurements is pretty straightforward when

a Kalman Filter is used (see next section). This results in a combined data output wherein the location and attitude of the system is determined for each time epoch. However, this does not lead automatically to the exterior orientation parameters of the camera. Therefore the location and attitude of the system at the exact time the photograph is taken should be known. If the photographs are time-stamped, the location and attitude can be derived by interpolating the combined GPS and IMU output. The accuracy of this interpolation is dependent on the output rate of the system. If a navigation update is available every 0.1 seconds, the interpolation will be much more reliable than when a navigation update is available every 10 seconds.

3.4.2 Kalman Filtering

The GPS receiver and the IMU unit take measurements apart from each other. To combine the two measurements and update the state of the aircraft over time, usually Kalman filters are used. A Kalman filter is a mathematical model, derived by R.E. Kalman, which is used to estimate the solution x_k at time k to the linear stochastic difference equation $x_k = Ax_{k-1} + Bu_{k-1} + w_{k-1}$ with a measurement $z_k = Hx_k + v_k$ taken at time k. [Welsch 2006]
In these equations, the following symbols are used:

symbol	meaning
x_k	State of the system at time k
x_{k-1}	State of the system at time $k-1$
A	relates the state at time $k-1$ to the state at time k
u_{k-1}	(optional) control input at time $k-1$
B	relates the control input u_{k-1} to the state x
z_k	measurement at time k
H	relates the measurements z to the state x
w_k and v_k	represent respectively the process and measurement noise

Table 3.2: elements of Kalman Filter equations

The system process noise w_k and the measurement noise v_k are represented by the covariance matrices Q and R. The Kalman filter estimates the solution by using feedback control: First the estimates are predicted. These predictions are then checked by (noisy) measurements. Therefore, the Kalman Filter contains two steps, the *time update* and the *measurement update*. These steps are given in the table below:
This table contains a couple of variables not explained before. First of all, all elements with the - superscript are predictions of the values for the next

Time update	Measurement update
$\hat{x}_k^- = A\hat{x}_{k-1} + Bu_{k-1}$	$K_k = P_k^- H^T (HP_k^- H^T + R)^-1$
$P_k^- = AP_{k-1}A^T + Q$	$\hat{x}_k^- + K_k(z_k - H\hat{x_k^-})$
	$P_k = (I - K_k H)P_k^-$

Table 3.3: Kalman Filter steps

epoch. K_k is the so-called Kalman gain. P_k is the covariance matrix of the estimated state at time k.
A Kalman Filter can be a very powerful tool to reduce system noise. However, the goal of implementing a Kalman Filter in the GPS and IMU results is to link the two measurements together to get high accuracy estimations of the location of the aircraft and it's attitude angles. Models to combine GPS and Inertial measurements do exist, however these models assume that the output of the Inertial sensor is location, speed and acceleration in a 3D coordinate system, instead of the 3 rotations which are needed for the exterior orientation parameters [Grewal 2007]. For conventional aerial photogrammetry, complete systems are available which determines both the location and the attitute of the platform. These systems have a built in Kalman Filter that combines the GPS and IMU measurements, which gives a standard output of all 6 variables.

Chapter 4

Theoretical analysis of navigation errors

The main interest of this thesis is to determine the effects of errors in the navigational sensors on the accuracy of the final product. As descried in the previous chapters, the UAV contains a GPS receiver and an Internal Measurement Unit for it's own navigation. The output of these sensors are to be used as exterior orientation parameters for the photogrammetric process. Inaccuracies in these sensors influence the quality of the final product. To predict the behaviour of the final product under certain navigation errors, a simulation has been carried out using the standard mathematical background of the photogrammetric process: the collinearity equations. This simulation should give a theoretical answer two the question how the inaccuracies in the GPS and IMU sensors influence the outcoming terrain model. These theoretical results will then be verified using practical tests described in later chapters.

4.1 Theoretical GPS error influence on terrain points

The GPS receiver aboard the airplane is used to determine the coordinates of the camera centres when the photo's are taken. Errors in the GPS receiver therefore influence the errors in the camera centre coordinates.
In this section a theoretic assesment is made of the effects of errors in the coordinates of the camera centre on the terrain points. Assumed is that these coordinates are derived straight from the GPS measurements. The rotation parameters are set to zero and have an infinite accuracy (so the airplane flies constantly straight and level). This way, the results are not corrupted by

other error influences than just the coordinates. The used simulation consists of two photos taken with a camera with a focal length of 24 mm from a height of 80 meters. The flight line follows the X-axis and no rotations are assumed. The checkpoints are chosen at the so-called Von Gruber locations, which are situated at the edges and in the centre of the overlapping area. This way the influence over the whole overlapping area can be checked, because the influence is not the same everywhere in the area. The model without errors can be seen in Figure 4.1

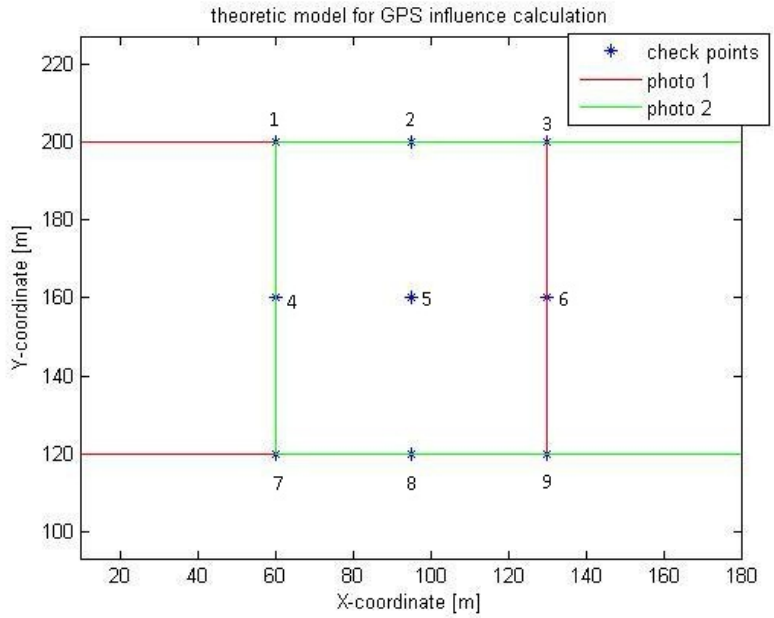

Figure 4.1: Theoretic simulation setup

To determine the terrain coordinates of a point on the ground from the image coordinates of that point in (at least) 2 photo's, we need the collinearity equations, given in equation 4.1

$$\begin{aligned} x_1 &= -f\frac{r_{11}^1\left(X-X_c^1\right)+r_{21}^1\left(Y-Y_c^1\right)r_{31}^1\left(Z-Z_c^1\right)}{r_{13}^1(X-X_c^1)+r_{23}^1(Y-Y_c^1)r_{33}^1(Z-Z_c^1)} \\ y_1 &= -f\frac{r_{12}^1\left(X-X_c^1\right)+r_{22}^1\left(Y-Y_c^1\right)r_{32}^1\left(Z-Z_c^1\right)}{r_{13}^1(X-X_c^1)+r_{23}^1(Y-Y_c^1)r_{33}^1(Z-Z_c^1)} \\ x_2 &= -f\frac{r_{11}^2\left(X-X_c^2\right)+r_{21}^2\left(Y-Y_c^2\right)r_{31}^2\left(Z-Z_c^2\right)}{r_{13}^1(X-X_c^2)+r_{23}^2(Y-Y_c^2)r_{33}^2(Z-Z_c^2)} \\ y_2 &= -f\frac{r_{12}^2\left(X-X_c^2\right)+r_{22}^2\left(Y-Y_c^2\right)r_{32}^2\left(Z-Z_c^2\right)}{r_{13}^2(X-X_c^2)+r_{23}^2(Y-Y_c^2)r_{33}^2(Z-Z_c^2)} \end{aligned} \tag{4.1}$$

The meanings of the variables of these equations are given in table 4.1

The effect of errors in the exterior orientation coordinates needs to be in-

variable	meaning
x_1, y_1	photo coordinates of terrain point in photo 1
x_2, y_2	photo coordinates of terrain point in photo 2
f	focal length of camera
r^1_{xy}	element in xth row and yth column of photo 1 rotation matrix
r^2_{xy}	element in xth row and yth column of photo 2 rotation matrix
X, Y, Z	terrain coordinates of terrain point
X^1_c, Y^1_c, Z^1_c	terrain coordinates of camera centre of photo 1
X^2_c, Y^2_c, Z^2_c	terrain coordinates of camera centre of photo 2

Table 4.1: variables of the collinearity equations

vestigated, so it is assumed that the rotation angles have an infinitely high accuracy. For this reason it makes sense to set them all to zero. This means that it is assumed the aircraft flies in X-direction (the Y-coordinate does not change) and the aircraft is flying straight and level. This gives the following rotation matrix: $R = \begin{bmatrix} 1 & 0 & 0 \\ 0 & 1 & 0 \\ 0 & 0 & 1 \end{bmatrix}$,which simplifies the collinearity equations to the equation 4.2.

$$x_1 = -f\left(\frac{X-X^1_c}{Z-Z^1_c}\right) \quad y_1 = -f\left(\frac{Y-Y^1_c}{Z-Z^1_c}\right) \quad x_2 = -f\left(\frac{X-X^2_c}{Z-Z^2_c}\right) \quad y_2 = -f\left(\frac{Y-Y^2_c}{Z-Z^2_c}\right) \tag{4.2}$$

These equations can now be rewritten as a set of linear equations in the form $c = Ad$, with d the unknowns and c the observations:

$$\begin{bmatrix} f & 0 & x_1 \\ 0 & f & y_1 \\ f & 0 & x_2 \\ 0 & f & y_2 \end{bmatrix} \begin{bmatrix} X \\ Y \\ Z \end{bmatrix} = \begin{bmatrix} fX_c1 + x_1Z_c1 \\ fY_c1 + y_1Z_c1 \\ fX_c2 + x_2Z_c2 \\ fY_c2 + y_2Z_c2 \end{bmatrix} \tag{4.3}$$

The unknowns in this equation are the unknown terrain coordinates (X, Y, Z) of a terrain point. The observations are now a linear combination of the observed photocoordinates (x, y), the focal length of the camera f and the exterior orientation parameters (X_c, Y_c, Z_c). Now a least squares estimation of the unknown terrain points can be determined, by

$$\hat{c} = (A'Q_d^{-1}A)^-1A'Q_d^{-1}d \tag{4.4}$$

The variances and covariances of the unknown terrain points can be found by determining the variance-covariance matrix of the unknowns:

$$Q_{\hat{c}} = (A'Q_d^{-1}A)^{-1} \tag{4.5}$$

In this equations $\hat{c}$ is the estimation of the unknown terrain coordinates X, Y, Z. d is the observation vector: $\begin{bmatrix} fX_c1 + x_1Z_c1 \\ fY_c1 + y_1Z_c1 \\ fX_c2 + x_2Z_c2 \\ fY_c2 + y_2Z_c2 \end{bmatrix}$, A is the design matrix: $\begin{bmatrix} f & 0 & x_1 \\ 0 & f & y_1 \\ f & 0 & x_2 \\ 0 & f & y_2 \end{bmatrix}$ and Q_d the covariance matrix of the observation vector d. The observation vector in it's turn is a linear combination of the form $d = By$ with y the exterior orientation parameters $(X_{c1}, Y_{c1}, Z_{c1}, X_{c2}, Y_{c2}, Z_{c2})$ and B the design matrix: $\begin{bmatrix} f & 0 & x_1 & 0 & 0 & 0 \\ 0 & f & y_1 & 0 & 0 & 0 \\ 0 & 0 & 0 & f & 0 & x_2 \\ 0 & 0 & 0 & 0 & f & y_2 \end{bmatrix}$ The covariance matrix Q_d can now be found with the propagation law:

$$Q_d = BQ_yB' \tag{4.6}$$

Using the equations given above it is now possible to determine a least squares estimation for the terrain coordinates of a group of check points. Given the model as given in Figure 4.xx, the effects of random errors can be determined by calculating the variance covariance matrix of the terrain coordinates of the 9 Von Gruber Points. First of all, the exterior orientation parameters must be filled in, for this simulation it is assumed that there is a terrain coordinate system with coordinates in meters. The aircraft is flying 80 m over the terrain. The terrain has an elevation of 1.5 meters, so the Z coordinates of the aircraft are 81.5 meters. The aircraft is flying in the X direction and takes two pictures, one at $X_c = 70, Y_c = 160$ and $Z_c = 81.5$ and one at $X_c = 130, Y_c = 160$ and $Z_c = 81.5$. Furthemore it is assumed that these photo centre coordinates have a standard deviation of 3 m in the terrain coordinates without correlation. This gives a variance of 9 meters, which gives us the following covariance matrix for the observation vectors y.

$$Q_y = \begin{bmatrix} 9 & 0 & 0 & 0 & 0 & 0 \\ 0 & 9 & 0 & 0 & 0 & 0 \\ 0 & 0 & 9 & 0 & 0 & 0 \\ 0 & 0 & 0 & 9 & 0 & 0 \\ 0 & 0 & 0 & 0 & 9 & 0 \\ 0 & 0 & 0 & 0 & 0 & 9 \end{bmatrix} \tag{4.7}$$

Furthermore the x_1, y_1 and x_2, y_2 photo coordinates of all the checkpoints are determined by measuring their coordinates in the simulation sketch. The

focal length of the camera f is assumed to be 24 mm. When these numbers are inserted in the equations 1.3 - 1.6, the estimation and the standard deviations of the terrain coordinates of the checkpoints can be determined.

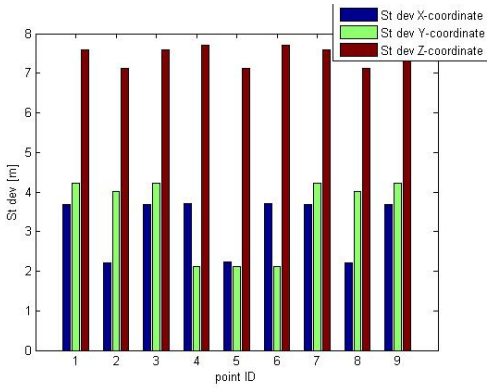

Figure 4.2: Standard deviations of Von Gruber points determined from standard deviation of camera centre coordinates

In Figure 4.2 the standard deviations for all three coordinates for each Von Gruber points are set out. From these results it follows that the Z-coordinate of the ground points is influenced most by errors in the camera centre coordinates, and are about twice the standard deviation of the camera centre coordinates itself.

Systematic errors

To asses the effect of a systematic error in any of the GPS coordinates, the simple theoretical model described above is revisited, but now the standard deviations will not be used. Instead a systematic measurement error of 3 m in each of the camera centre coordinates of the second picture is introduced. The estimated coordinates of the 9 Von Gruber points are calculated using the measurement error and the differences are analysed. The assumed errors are 3 meters in all directions. Then the horizontal and vertical difference vectors are plotted for all 9 Von Gruber points.
So the mathematical model is again based on the collinearity equations, but a systematic error of 3 m to one of the camera centre coordinates is introduced, therefore equation 4.3 changes into:

$$\begin{bmatrix} f & 0 & x_1 \\ 0 & f & y_1 \\ f & 0 & x_2 \\ 0 & f & y_2 \end{bmatrix} \begin{bmatrix} X \\ Y \\ Z \end{bmatrix} = \begin{bmatrix} fX_c1 + x_1Z_c1 \\ fY_c1 + y_1Z_c1 \\ f(X_c2 + 3) + x_2Z_c2 \\ fY_c2 + y_2Z_c2 \end{bmatrix} \tag{4.8}$$

This again gives a linear model in the form $d = Ac$. Now that no variances are considered, the least squares estimation is simplified to:

$$\hat{c} = (A'A)^{-}1A'd \tag{4.9}$$

This process is done three times with different observation vectors d, once with a systematic error of 3 m. to X_c, once to Y_c and once to Z_c. Equations 4.8 and 4.9 are now used to determine the unknown terrain coordinates X, Y, Z.The resulting difference vectors from the correct coordinates are shown in figure 4.3 Because the errors are relatively small with respect to the distances between points, we multiply the difference vectors with a factor 10 to get a better visualization.

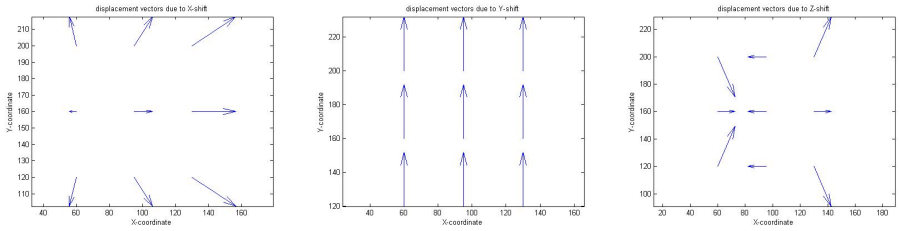

(a) X_c-error (b) Y_c-error (c) Z_c-error

Figure 4.3: Resulting difference vector fields due to error of 3 m in camera centre position

The bar diagrams in figure 4.4 show the amount of displacement due to the measurement errors. From figure 4.4 (a) it can be concluded that an error in the Xc coordinate influences the estimated Z-coordinate the most, the location does not seem to matter (the effect is the same everywhere). From figures 4.3 and 4.4 (a) it seem that the influence on the estimated Y-coordinate increases with the Y-distance from the flightline. The influence on the estimated X-coordinate increases with the X-distance from the (correctly measured) Xc coordinate of the first camera center.
Figure 4.4 (b) shows that an error in the Yc coordinate only influences the estimated Y-coordinate. The differences are the same everywhere (half the error). From figures 4.3 and 4.4 (c) it can be concluded that an error in the Zc coordinate influences the Z-coordinate, this increases with the X-distance from the second camera centre (the one with the error). The Y-coordinate increases with the Y-distance from the flightline. However, it is pointed inwards (towards the flightline) left of the centre of the overlapping area and outwards (from the flightline) right of the centre of the overlapping area. The direction of the shift in the X-coordinate is dependent on the X-location of the Von Gruber points.

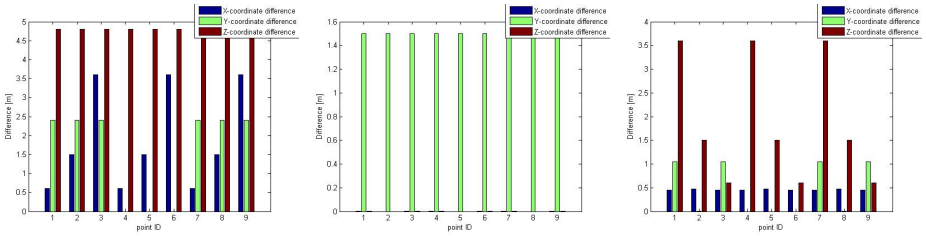

(a) X_c-error (b) Y_c-error (c) Z_c-error

Figure 4.4: Resulting errors due to error in camera centre position

4.2 Theoretic IMU error influence on terrain points

The IMU provides the system with rotation angles for the exterior orientation of the photos. Therefore, errors in the IMU measurements lead to errors in the rotation angles of the exterior orientations. To determine the influence of errors in the rotation angles on the outcoming terrain model, the collinearity equations are revisited.

$$\begin{aligned} x_1 &= -f\frac{r_{11}^1\left(X-X_c^1\right)+r_{21}^1\left(Y-Y_c^1\right)r_{31}^1\left(Z-Z_c^1\right)}{r_{13}^1(X-X_c^1)+r_{23}^1(Y-Y_c^1)r_{33}^1(Z-Z_c^1)} \\ y_1 &= -f\frac{r_{12}^1\left(X-X_c^1\right)+r_{22}^1\left(Y-Y_c^1\right)r_{32}^1\left(Z-Z_c^1\right)}{r_{13}^1(X-X_c^1)+r_{23}^1(Y-Y_c^1)r_{33}^1(Z-Z_c^1)} \\ x_2 &= -f\frac{r_{11}^2\left(X-X_c^2\right)+r_{21}^2\left(Y-Y_c^2\right)r_{31}^2\left(Z-Z_c^2\right)}{r_{13}^1(X-X_c^2)+r_{23}^2(Y-Y_c^2)r_{33}^2(Z-Z_c^2)} \\ y_2 &= -f\frac{r_{12}^2\left(X-X_c^2\right)+r_{22}^2\left(Y-Y_c^2\right)r_{32}^2\left(Z-Z_c^2\right)}{r_{13}^2(X-X_c^2)+r_{23}^2(Y-Y_c^2)r_{33}^2(Z-Z_c^2)} \end{aligned} \tag{4.10}$$

The same photo setup for determining the GPS errors (see section 4.1 and figure 4.1) is used. Because the errors in orientation angles are to be determined, the 3x3 identity matrix cannot be used as rotation matrix. Therefore the collinearity equations have to be rewritten in another way to be able to use a Best Linear Unbiased Estimator. The collinearity equations can be rewritten as in equation 4.11:

$$\begin{bmatrix} x_1r_{13}^1+fr_{11}^1 & x_1r_{23}^1+fr_{21}^1 & x_1r_{33}^1+fr_{31}^1 \\ y_1r_{13}^1+fr_{12}^1 & y_1r_{23}^1+fr_{22}^1 & y_1r_{33}^1+fr_{32}^1 \\ x_2r_{13}^2+fr_{11}^2 & x_2r_{23}^2+fr_{21}^2 & x_2r_{33}^2+fr_{31}^2 \\ y_2r_{13}^2+fr_{12}^2 & y_2r_{23}^2+fr_{22}^2 & y_2r_{33}^2+fr_{32}^2 \end{bmatrix} \begin{bmatrix} X \\ Y \\ Z \end{bmatrix} =$$

$$\begin{bmatrix} fX_{c1} & 0 & x_1X_{c1} & fY_{c1} & 0 & x_1Y_{c1} & fZ_{c1} & 0 & x_1Z_{c1} & \underline{0} \\ 0 & fX_{c1} & y_1X_{c1} & 0 & fY_{c1} & y_1Y_{c1} & 0 & fZ_{c1} & y_1Z_{c1} & \underline{0} \\ \underline{0} & fX_{c2} & 0 & x_2X_{c2} & fY_{c2} & 0 & x_2Y_{c2} & fZ_{c2} & 0 & x_2Z_{c2} \\ \underline{0} & 0 & fX_{c2} & y_2X_{c2} & 0 & fY_{c2} & y_2Y_{c2} & 0 & fZ_{c2} & y_2Z_{c2} \end{bmatrix} \begin{bmatrix} \underline{r^1} \\ \underline{r^2} \end{bmatrix} \tag{4.11}$$

$\underline{0}$ is a lying vector of nine zeroes and $\underline{r^x}$ is a vector with the nine elements of rotation matrix R defining the rotation of photo x.

Now the model is in the form $Ax = By$ and can be solved using a standard least squares estimation, as derived in section 4.1. However this model still has 2 problems. First the observations are now the elements of the rotation matrix R, while the real observations are the rotation angles ω, ϕ, κ. Of course the rotation angles lead easily to the rotation matrix but the effect of the standard deviation of the rotation angles on the rotation matrix elements is not trivial.
Furthermore we see the rotation matrix elements coming back in the first design matrix. Therefore we introduce an inaccuracy in this design matrix which further reduces the accuracy of the BLUE-estimation. This can be dealt with using a Total Least Squares estimation model. Such a model deals with uncertainties in the design matrix. An elaborate description and derivation of this model is given in Lucarini [2001]. In this case the uncertainties in the design matrix are ignored to get an approximation.
The standard deviations of the rotation matrix elements are calculated directly from the standard deviations of the rotation angles. A standard deviation of 1 degree is assumed. Then the rotation matrix elements are determined for an angle of 1 degree for all three rotation angles. The outcoming values are then regarderd as the standard deviation elements of the rotation matrix.
The least squares method is used to determine the estimation of the unknown coordinates and their standard deviations of the 9 Von Gruber points, the results are shown in Figure 4.5.

4.2.1 Systematic errors in IMU measurements

As earlier, to asses the effect of a systematic error in any of the 6 orientation parameters, we revisit the simple theoretical model described above, but now we will not use the standard deviations but instead we introduce a specific measurement error in the rotation parameters of the second picture, the first pictures stays fixed. We calculate the estimated coordinates of the 9 Von Gruber points using the measurement error and analyse the differences. The

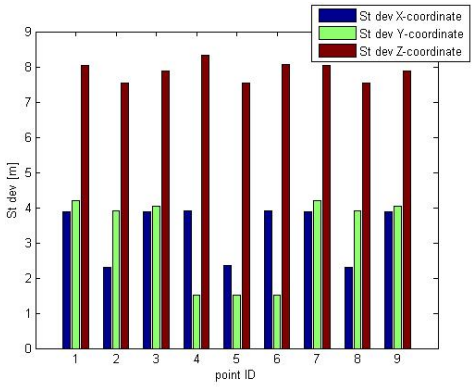

Figure 4.5: Standard deviations of Von Gruber Points due to standard deviations in rotation angles

errors we assume are 1 degree in rotation angles. Then we plot the horizontal and vertical difference vectors for all 9 plots. Because the errors are relatively small with respect to the distances between points, we multiply the difference vectors with a factor 10 to get a better visualization. This gives the results in Figure 4.6.

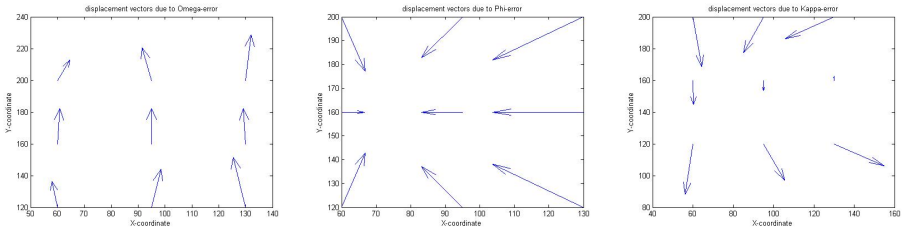

(a) ω-error = 1 degree (b) ϕ-error = 1 degree (c) κ-error = 1 degree

Figure 4.6: Terrain point error vectors resulted from an error in ω, ϕ and κ

From Figure 4.6 (a) it can be seen that an error in the ω angle has a very small effect on the X-coordinates of the Von Gruber points. The direction is dependant on the location of the terrain point. The error in the omega angle causes a positive (upward) shift of the Y-coordinates, the size is dependent on the X-distance from the error source, unless the points are lying on the flightline, in which case the error sizes don't change. An error in the ϕ angle causes a horizontal shift in direction of the correct camera centre (so both the X-coordinate shift and the Y-coordinate shift are pointing towards the correct camera centre. The size is dependant on the distance from the correct camera centre. An error in the kappa angle causes horizontal coordinate shifts

which seem to resemble a rotation of the x,y plane.

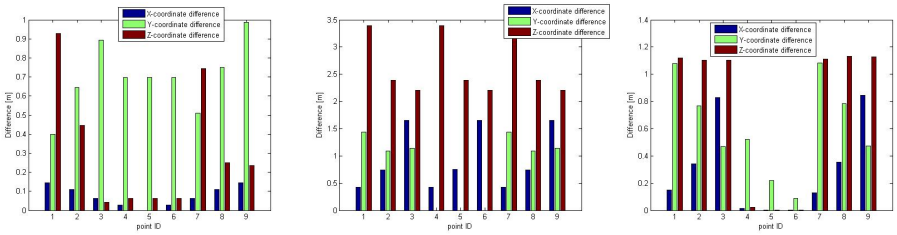

(a) ω-error = 1 degree (b) ϕ-error = 1 degree (c) κ-error = 1 degree

Figure 4.7: Quantitative terrain point errors resulted from an error in ω, ϕ and κ

Figure 4.7 shows the quantitative effects of errors in the IMU measurements on the Von Gruber points. From these figures it can be seen that the effects of 1 degree error in the rotation angles go up to several decimeters for errors in ω and κ and can go up to several meters for errors in ϕ. The graphs in figure 4.8 give an idea of the total error due to all 6 error sources. Do note however that the individual error values are absolute values. Therefore the total value presented in the figures below are pessimistic. It is very well possible that certain errors cancel each other out, which would improve the resulting outcome significantly.

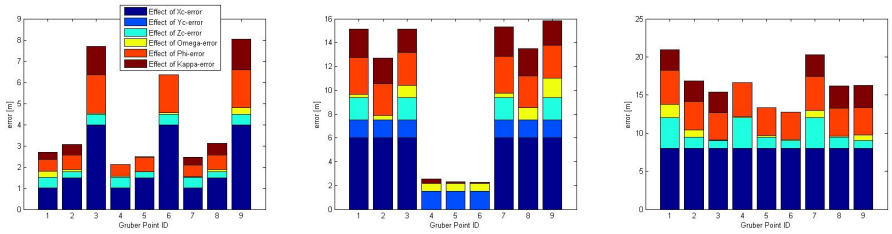

(a) errors in X coordinate (b) errors in Y coordinate (c) errors in Z coordinate

Figure 4.8: Quantitative error effects on Von Gruber point coordinates due to errors in all 6 Exterior orientation parameters

From these graphs we clearly see that the biggest contributors to errors are the Xc-coordinate and the phi-rotation angle. Improving the accuracy of these parameters would improve the results significantly. Note that the error-contribution of the X_c and Y_c coordinates are higher than that of Z_c. This is convenient because most GPS-receiver have a better accuracy in Planimetric coordinates (X,Y) than in height. The total error in terrain coordinates caused by 1 degree error in the rotation parameters and 3 m error in photo centre coordinates would exceed 20 meters in Z.

4.3 Overview of experiments

Up to this point, the error sources which influence the accuracy of the Digital Elevation Model, derived from the photographs taken from the UAV, have been identified. They are summed up and described in chapter 2. The error sources which are of interest for this thesis are errors in the navigational sensors and motion blur. The navigation sensors and their error sources are thoroughly described in chapter 3. The theoretical influence of errors in the navigation sensors has been simulated in this chapter.

To see how the UAV with the camera and navigation sensors behave in practice and to verify the results of the simulation described, a number of experiments have been carried out, which are described in detail in the next three chapters. First of all, the effect of motion blur is investigated in 2 experiments, described in detail in chapter 5. This is done using a block of 4 photos with known and fixed exterior orientation parameters. The first experiment introduces 5 checkpoints whose coordinates are determined by forward intersection from the photoblock, using different levels of blur. The second experiments has more or less the same setup, but instead of using checkpoints, a Digital Elevation Model is determined from the photoblock. The Digital Elevation Models of photoblocks with different blur levels are then compared with each other.
To see how the resulting DEM is influenced by errors in the navigation sensors in practice, a photoblock taken during a testflight at the unfinished A4 extension between Delft and Rotterdam have been processed, as described in chapter 6. The exterior orientation parameters of 7 photos are determined using 3 ground control points which are visible in these photos, using an aerial triangulation. The resulting exterior orientation parameters are then compared with the output of the navigation sensors aboard the UAV. In a second experiment using the same data, the outputs of the navigational sensors are fixed and used as exterior orientation parameters. The 3 ground control points are now used as checkpoints. Their coordinates are determined from the 7 photos by forward intersection.
With 7 photos and 3 ground control points, the experiments in chapter 6 gave some insight in the practical influence of errors in the navigation sensor outputs on the outcoming digital elevation model, but the outcoming data was not sufficient to verify the results found in the theoretical simulation as described above. Therefore experiments similar to those described in chapter 6 has been carried out using a block of 34 photos using 32 ground control points, as described in chapter 7. The photoblock was flown at the dyke along the Lek river near the village of Ammerstol.
The results of the experiments described in chapters 6 and 7 gave insight in the effects of errors in the navigation sensors on the outcoming digital elevation model. However, there was no "real" inertial measurement unit present during these test flights. The effects of errors in a real IMU on the resulting digital elevation model have thus not been tested. Therefore a final set of experiments are done using 5 photos of the parking lot of the Aerospace building taken from the roof, as described in chapter 8. These 5 photos are oriented using an aerial triangulation with 10 ground control points.
An overview of all experiments with their observed, unknown and fixed parameters is given in table 4.2:

experiment	photos	fixed parameters	observed parameters	unknown parameters
blur test 1	4	per photo 6 EO's	per photo (x, y) of 5 checkpoins	(X, Y, Z) of 5 checkpoints
blur test 2	4	per photo 6 EO's	per photo (x, y) of a terrain points	(X, Y, Z) of a terrain points
A4 test 1	7	(X, Y, Z) of 3 GCP's	per photo (x, y) of 3 GCP's	per photo 6 EO's
A4 test 2	7	per photo 6 EO's	per photo (x, y) of 3 checkpoins	(X, Y, Z) of 3 checkpoints
Ammerstol test 1	34	(X, Y, Z) of 32 GCP's	per photo (x, y) of b GCP's	per photo 6 EO's
Ammerstol test 2	34	per photo 6 EO's	per photo (x, y) of b checkpoins	(X, Y, Z) of 32 checkpoints
IMU roof test 1	5	(X, Y, Z) of 8 GCP's	per photo (x, y) of c GCP's	per photo 6 EO's
IMU roof test 2	5	per photo 6 EO's	per photo (x, y) of c checkpoins	(X, Y, Z) of 8 checkpoints

Table 4.2: overview of experiments

In this table the following symbols and abbreviations are used:
GCP = Ground control point
EO = Exterior orientation parameter
(x, y) = photocoordinates of a certain point in a certain photo
(X, Y, Z) = terrain coordinates of a certain point
In the Ammerstol test and the IMU roof test, the amount of visible ground points differed per picture, therefore the amount of visible ground points in an arbitrary photo in the Ammerstol test is called b and varies between 3 and 9. The amount of visible ground points in an arbitrary photo in the IMU roof test is called c and varies between 2 and 7.

Chapter 5

Forward Motion blur

In Aerial photogrammetry, forward motion blur is a factor which should be taken into account. During the opening time of the shutter of the camera, the aircraft continues flying. This causes the photo's to be unsharp, making it difficult to pinpoint terrain features in the photo's accurately. In full size aircrafts this can be mitigated with Forward Motion Compensation. This system makes the film move with the same speed of the aircraft in opposite direction. This system is much too large and heavy to be attached to a model airplane though, therefore the accuracy of the resulting height model can be compromised by forward motion blur. In digital aerial camera's TDI is used to prevent forward motion blur (see section 2.2), however TDI is not available in low cost off-the-shelf cameras.
For example, imagine that the aircraft flies with an average speed of 50 km/h = 13.9 m/s, with a shutter speed of 1/1000 second, the airplane flies 1.39 cm during the opening time of the camera lens. This may cause Motion blur. Theoretically we could say that with a chip size of 24 x 36 mm and 3744 x 5616 pixels 1 pixel corresponds to 1.89 x 1.89 cm on the ground. (with a flying height of 70 m and a focal length of 24 mm), if the airplane would be stationary at the moment the photo is taken. However, because the airplane flies 1.39 cm during the time the camera shutter is opened, the actual terrain covered by 1 pixel is 1.89 x (1.89 + 1.39) = (1.89 x 3.28). The adapted coverage per pixel in flying direction will cause blur in the photo's. This blur makes it more difficult to pinpoint terrain features in the photos. Since the accuracy of the outcoming terrain model is heavily dependent on this pinpointing, Forward Motion blur is a factor which can reduce the accuracy of the final product. To asses the influence of Forward Motion Blur on the final product, two tests have been performed. One test simulated automatic DEM generation and the other test simulated manual point measurements.

5.1 Experimental setup

With the camera of the faculty, a Canon EOS 5D mirror reflex camera with a focal length of 35 mm, 4 photographs were made of the parking lot from the roof of the Aerospace Building. These 4 photo's were loaded in Leica

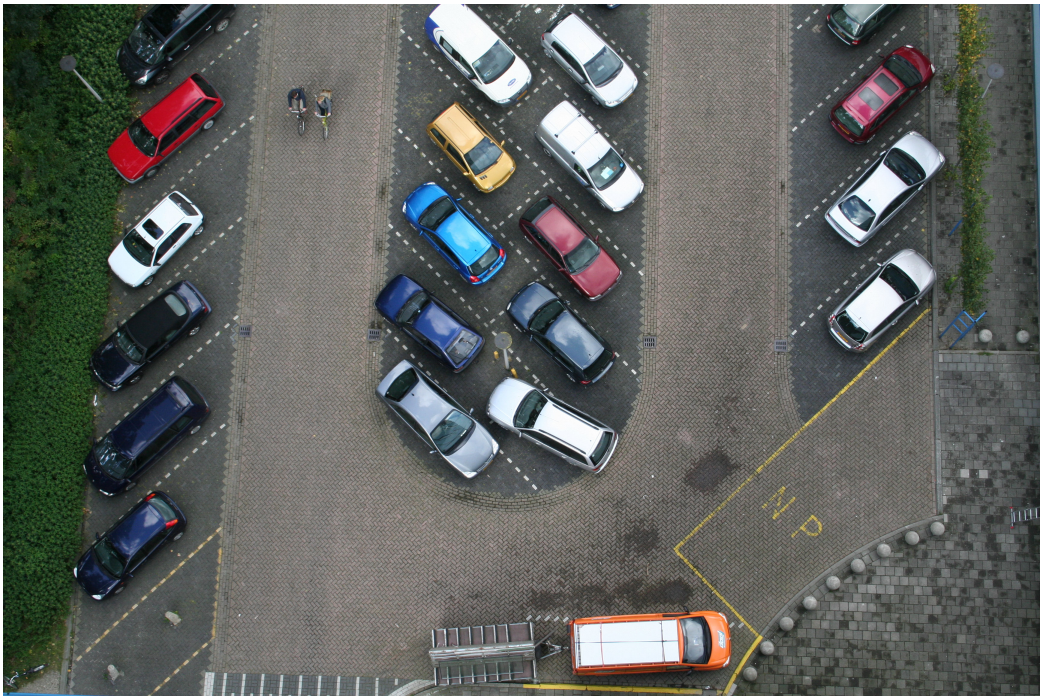

Figure 5.1: Example of photo of parking lot

Photogrammetry suite. Determining a bundle adjustment using a set of 5 given Ground Control Points failed in Leica Photogrammetric Suite. PhotoModeler was able to get results, but when the resulting exterior orientation parameters were inserted in LPS, the program still couldn't find a proper solution for the block. For a detailed description of PhotoModeler and LPS, see section 6.1.

5.1.1 Automatic DEM generation setup

In LPS, an earlier block was made of these 4 photos. When the orientation parameters of this block were loaded in LPS and used as fixed parameters, some results were achieved. When pinpointing the given ground control points in the photo's, using them as tiepoints and processing the block, the residuals were acceptable. When this was done a DEM was created in LPS in the form of an ascii file with per point the XYZ-values, so it could be

adapted in Matlab. To visualize the result and check if the result makes sense a scatterplot has been made, see Figure 5.2

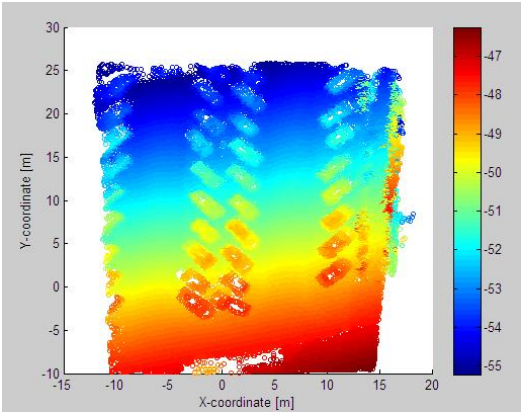

Figure 5.2: DEM scatterplot

In this result the parked cars can be seen sticking out. There is however also a clear trend in the z-values: they become lower if the Y-coordinate value increases. DEM pointclouds created by LPS can't easily be subtracted from each other, because the points are not lying on exactly the same location. Therefore a regular grid was created and the height values were interpolated on this regular grid. This also gave the opportunity to limit the DEM area to the center of the parking lot, where there are no unclear distortions; this gave the result shown in figure 5.3.

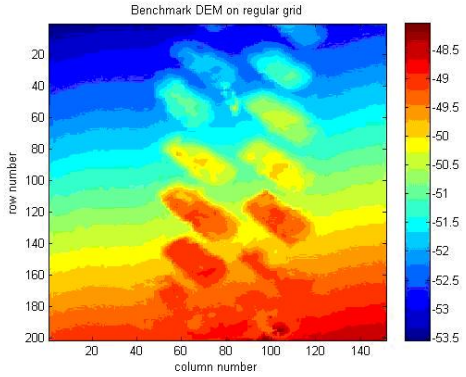

Figure 5.3: Benchmark DEM on regular grid

This gave a benchmark DEM. In a graphic editor (Corel Paint Shop Pro) the 4 pictures were given a blur of 1 to 15 pixels in row direction. The row direction follows the "flying" direction of the photos (i.e. the order in which they were taken). Blur in the flying direction has the most effect on the Z terrain-coordinates. These blurred pictures were used again to determine a DEM, which was interpolated on the same regular grid. These interpolated grids were then subtracted from each other, so that the differences between the benchmark DEM and the DEM created by the distorted pictures can be seen.

5.1.2 Manual point measurement setup

When the photo's of the parking lot were taken, a number of ground control points were determined by measuring a couple of corners of white stones with a theodolite. The coordinate system is arbitrary with the position of the theodolite as origin. As said earlier, using these ground control points to determine an exterior orientation failed. The given Ground Control Points were instead used as check points and pinpointed in the pictures, see figure 5.4.

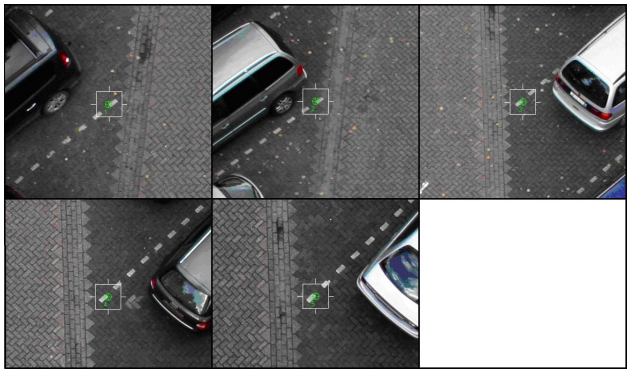

Figure 5.4: Pinpointed check points in the parking lot photos.

Because the origin of the coordinate system used in LPS is different than that used when the GCP's were measured, the coordinates of these checkpoints in the coordinate system used by LPS needed to be determined. This was done by pinpointing these points in the block determined by the sharp images. From this LPS calculated the coordinates. The checkpoint coordinates in the LPS coordinate system were then given to the checkpoints in the distorted blocks.
When these points are regarded as check points, LPS calculates the object coordinates from the interior and exterior orientation parameters and the image coordinates of the points. These are then checked with the given coordinates. The differences and their Root Mean Square values are displayed in the triangulation report. Also the residuals of the pixel coordinates of these points are given per point and as RMS value. This was done for the sharp images and all the distorted images.

5.2 Automatic DEM generation simulation

As described above, the simulation resulted in a grid with height differences between the heights estimated from the sharp images and those estimated from the blurry images, as shown in Figure 5.5.
In this figure it can be seen that the differences are highest at sudden height changes (i.e. parked cars), but are more or less constant (around zero) at flat terrain. As stated earlier DEMs were created for distortions from 1 up to 15 pixels. Every distortion DEM was then subtracted from the benchmark DEM, resulting in difference plots such as shown above. To be able to determine the behaviour of the DEM-differences, the mean and standard deviations for every difference plot, determined for every distortion, were

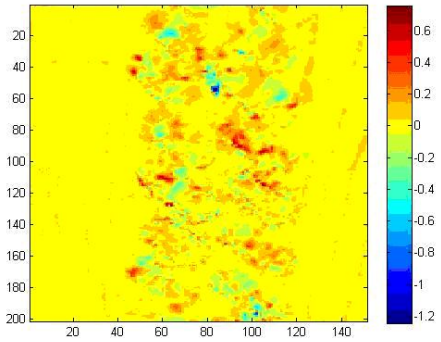

Figure 5.5: Differences between Benchmark DEM and DEM created from block of distorted images

determined.
From this it can be seen that the mean of differences of every photoblock is about 0.8 to 1 cm. (probably due to the outliers) and the standard deviation gets larger when the picture blur increases. However, it the maximum standard deviation is less than 0.3 meters for a ridiculously high blur value.

5.2.1 Analysis of the effects of Forward Motion Blur on DEM creation

First of all, the resulting DEM's all showed a clear trend going from high values in the lower part of the image to low values in the upper part of the image. Because all difference plots show no differences between the benchmark DEM and the DEM from distorted images on flat terrain, it can be concluded that this trend exists in the results of every distorted image block. This trend can be explained by the nature of the exterior orientation parameters. The used parameters were those determined in an earlier block which was acquired by my supervisor. These parameters were used as fixed parameters (so the triangulation process only calculated ground coordinates from measured image coordinates and didn't adapt the exterior orientation parameters). These exterior orientation parameters form a relative orientation. This means that the model coordinates are given in an arbitrary coordinate system, this was necessary because there was no information on terrain coordinates available.
The orientation of the photo's was therefore done relative to the first picture. Therefore all orientation parameters, including the rotation angles, of the first photo were set to zero. This means that it was assumed that the first

photo was taken straight down at the origin of the coordinate system. In reality however, the photo was taken from the roof of the Aerospace building (which has a height of about 50 meters). This explains why all DEM values are negative (around -50). Furthermore the pictures were taken at an angle of about 10 to 15 degrees. Therefore the area in the back of the parking lot is a bit "further" from the camera centre than the part in the front of the parking lot. Because LPS thinks the pictures are taken straight down, it therefore assumes that the area in the back of the parking lot is lying lower than the part in the front of the parking lot, hence the resulting trend.

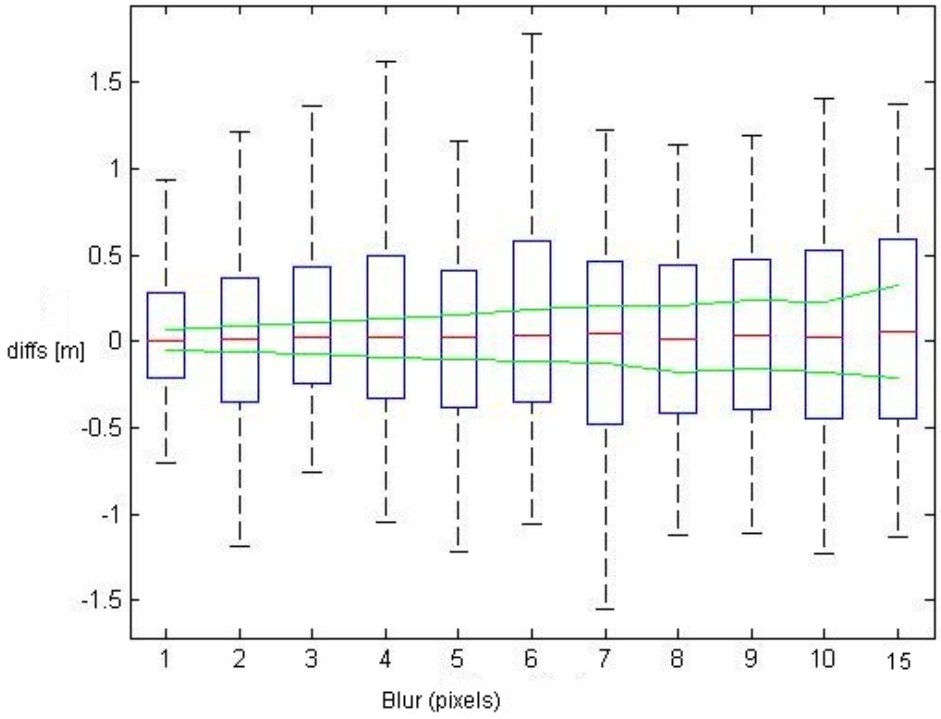

Figure 5.6: Mean and standard deviations of differences between Benchmark DEM and distorted DEMs

Of most interest is the influence of the blur on the accuracy of the model, this can be deducted from Figure 5.6 where for each pixel blur a boxplot is made showing the minimum and maximum differences, the mean differences and the upper and lower quartiles. For extra clarity, the upper and lower standard deviations are shown in green lines. From this figure it can be deducted that the influence of blur on the model accuracy is dependent on the scale of the photos. In this test-case the scale of this block is determined

by the focal length of the camera and the camera height. With a focal length of 35 mm and a camera height of about 50 meters (height of the roof of the Aerospace building), the scale is about 1:1500. For this scale the mean of the differences stay around 5 cm, while the standard deviations rise to up to about 25 to 30 cm for large blur values. This tells that the blur doesn't lead to systematic errors (as can be expected), but random errors increase if the blur increases. An increase in blur of 5 pixels causes an increase in the standard deviation of the differences of about 10 cm for a scale of 1:1500.

When a picture fragment with a distortion of 3 pixels is compared with one of the pictures taken during the test flight of September 2009, we see that the test flight pictures are a lot sharper, see figure 5.7, so the inaccuracies due to motion blur seem to be limited to about 1 decimeter.

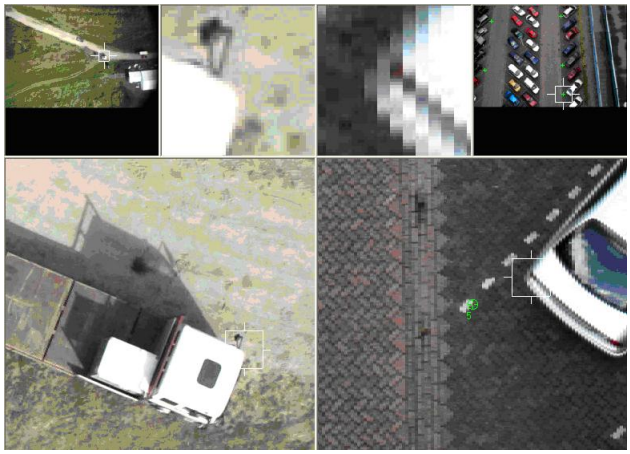

Figure 5.7: Comparison of blur between flight photo and test photo, left is an example of a flight photo, right is a test photo with a distortion of 3 pixels.

5.3 Manual point measurement simulation

To determine the effects of motion blur on the terrain coordinates of points measured in the photo's manually, 5 checkpoints were selected and pinpointed in the photographs. After LPS performs the triangulation of a photoblock containing checkpoints, the Root Mean Square values of the pixel residuals of the image coordinates of the checkpoints are given in the triangulation report. These RMS values are set out against the blur of the used photo's in figure 5.8. From this figure it can be seen that the X-RMS value rises if the blur gets larger. The Y-RMS value stays more or less constant. We do see some fluctuations though. Overall the RMS-value stays under 2 pixels.

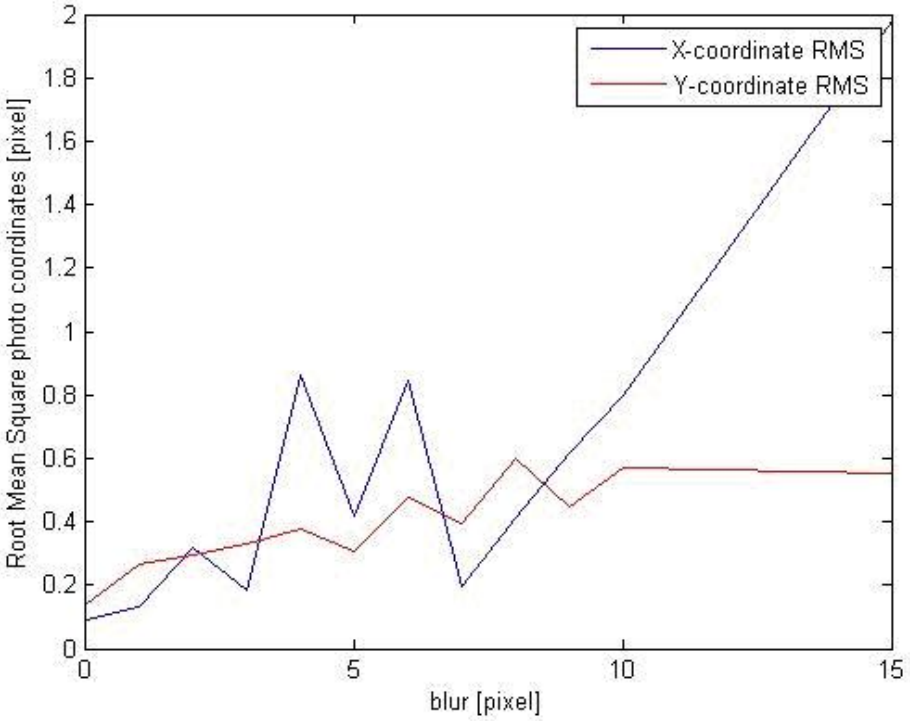

Figure 5.8: Root Mean Square values of the pixel residuals of the 5 check points

LPS also determines the differences between the calculated ground coordinates of the checkpoints and the observed ground coordinates. From this the Root Mean Square error (in Meters) is deducted. This is given in the triangulation report as well. The pixel values are determined by estimating the scale of the photo's (the terrain area corresponding to 1 pixel). Because we are dealing with flat terrain, the scale is the same over the whole terrain. Then the RMS errors in meters were divided by this scale, giving the RMS errors in pixels. The RMS values of the checkpoints in meters and pixels is plotted against the used blur in figure 5.9. From these graphs it can be seen that the X and Y errors stay roughly the same as the image blur, the Z errors are about 4 times as large. It also makes sense to compare the Z-RMS errors with the standard deviations of the DEM height differences. The Z-RMS errors follow more or less the same trend as the standard deviations, however we do see a sharp dip at around 8 pixels blur.

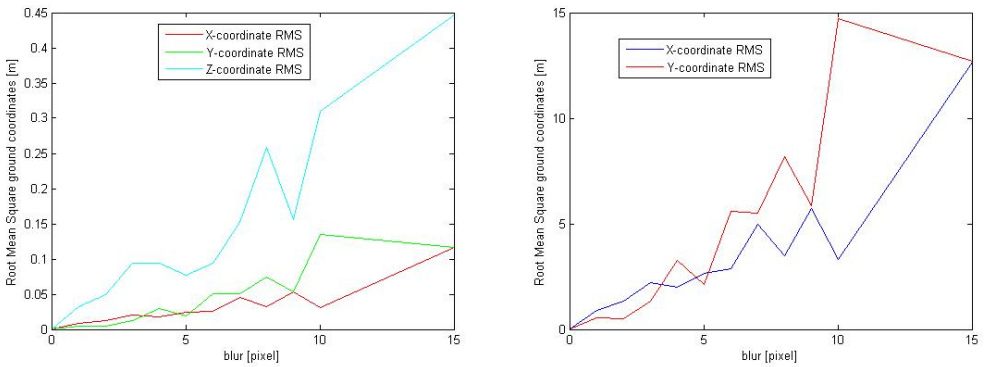

(a) RMS-error of terrain coordinates of check points in meters

(b) RMS-error of terrain coordinates of check points in pixels

Figure 5.9: RMS-errors

5.3.1 Analysis of the effects of Forward Motion Blur on point measurements

From the results shown above it can be seen that the accuracy of the terrain points is influenced by the motion blur. The RMS values of the Z-coordinates show more or less the same behaviour as the results from the automatic test described in section 5.2, so 5 pixels blur causes an inaccuracy of about 10 centimeters in Z-coordinates. The horizontal coordinates are influenced less however. This can be explained by the fact that the Z-coordinates are

more dependent on the baseline direction of the photos. In this test-case the blur was introduces in direction of the baseline, causing the determined Z-coordinates of the model to be less accurate.
Some fluctuations in the accuracy do occur. The RMS values are going up and down when the pixel blur increases. This is due to the fact that these results are achieved by manually pinpointing the check points. This pinpointing results in image coordinates of the checkpoints. When the picture blur is large, it is difficult to obtain the "right" image coordinates, because the object features can't be seen clearly, so one has to guess where exactly the terrain features are. When the RMS value decreases with increasing picture blur, it makes sense to assume that the user got lucky and either was able to see the searched object feature despite the picture blur or the user pinpointed near the "right" image coordinates by coincidence. As can be deducted from Figure 5.7, the expected blur from the flight photos is well within 5 pixels, so also from these results it is safe to say that the influence of Forward Motion Blur on the accuracy stays within 10 centimeters for a scale of approximately 1:1500.

Chapter 6

Delft A4 motorway test

In chapters 2 and 3 the influence of various factors on the accuracy of a Digital Terrain Model derived from photographs taken from the model airplane are described. In chapter 4 a theoretic simulation has been described which determines the theoretic effects of errors in the navigation sensors of the IMU on the resulting terrain model. To verify the error budgets derived in the previous chapters, a small block of photographs taken in a testflight in september 2009 is processed. This test was performed on the proposed extension of the A4-motorway just south of Delft. To be able to process the test photos a couple of ground control points were set up in the terrain and measured with GPS, see figure 6.1

Figure 6.1: Test area with Ground Control Points as tags, image taken from Google Earth

The Ground Control Points are signalled in the terrain in such a way that they are recognizable in the photos. Therefore the image coordinates of

the Ground Control Points can be measured and the exterior orientation parameters of the photo's can be determined using the collinearity equations. Normally 3 ground control points per picture are necessary to determine its exterior orientation parameters. This approach is the space resection and can be used to determine the exterior orientation of just 1 picture, or more pictures without overlap.
When enough tiepoints between the photo's are available, it is possible to determine an areal triangulation. This determines the orientation parameters of all the pictures in the block. This is done by calculating the pictures together using the tiepoints. These are points which are visible and recognizable in several photo's. The image coordinates of these tiepoints can therefore be determined in different photo's, but the ground control points are not known. The Ground Control Points are used to pin the resulting model to the terrain. For this in theory only a few ground control points are necessary if there are enough tiepoints available to calculate the photo's together.
The goal of this test was to get an idea of the accuracy of the direct sensor orientation. Using the ground control points as shown in figure 6.1, the photo's in the block are externally oriented using three different software packages. Unfortunately the 9 Ground Control Points were lying too far apart to be really useful, out of 170 taken photos, there are 99 photos which have at least 1 ground control point in them and only 35 with two or more ground control points on them. A block of 6 photo's could be created with the same 3 ground control points in them. This block was processed in two different ways:

1. The coordinates and rotation angles of the camera centre's using the known coordinates of the Ground control points as fixed values.

2. The coordinates of the Ground control points using the given coordinates and rotation angles of the camera centre's as fixed values.

6.1 Used photogrammetric platform

The photos were taken with a fixed-wing UAV developed by Heering UAS. The camera on board was a Kodak EOS 5D mirror reflex camera with a focal length of about 24 mm. The navigational system aboard the aircraft are described in the following subsections.

6.1.1 GPS receiver in current system

The GPS receiver currently installed in the aircraft is an m(u)-blox series 4 receiver. The technical specifications give a 3 meter Spherical Error Probability for Differential GPS or Space Based Augmentation System measurements, which is defined as a sphere with a diameter of (in this case) 3 meters, with the true location of the GPS - receiver in the centre of the sphere. Then 50 % of the measurements will fall within this 3 meter diametered sphere. This seems to be a low accuracy value, but the Spherical Error Probability value is a value which is seldom used in observation theory. To get an idea of the standard deviation of the GPS receiver two small tests with a loose module were performed. One test was static and one test was dynamic. These tests are described in Appendix B.

6.1.2 IMU error budget of current system

Due to the complexity of the used sensors, Inertial Measurement Units usually are large, heavy and expensive. Although continuing development have made Inertial Measurement Units smaller, lighter and cheaper, acquiring, installing and using a device still is a major investment. Therefore Heering UAS has tried to work around using an IMU by using different techniques for determining the rotation angles of the airplane. These different solutions have different error budgets.

Infrared sensors

On the current incarnation of the system, which was used for the test-flights described in the chapters 6 and 7, instead of an IMU, infrared sensors mounted on the wings are used. These sensors look in the flight direction and measure the surrounding heat. Based on the theory that the earth is warmer than the sky, a temperature plot is made and by thresholding the difference between earth and sky is determined. From this follows an artificial horizon, from which the roll and pitch angles of the airplane can be determined, see also figure 6.2. In this figure the blue area represents sky (and thus cold temperatures), the brown area is earth (and thus warm temperatures), the lines along the circle are used to read off the roll angle and the lines paralell to the horizon on the central vertical line of the gauge are used to determine the pitch angle. The technique is described in more detail in [Astheimer 1971]. Although this paper concentrates on using the technique for space vehicles, more or less the same principle holds for airborne vehicles.
This system has a major disadvantage though. The rotation angles are de-

Figure 6.2: Standard artificial horizon used in full sized aircraft, as represented in Microsoft Flight Simulator X

termined from the stance of the artificial horizon, which in it's turn is based on thresholding the temperature. Therefore an assumption must be made to distinguish between earth and sky, which can result in major errors. Furthermore, weather conditions can influence the temperature differences between the earth and the sky, causing a wrong threshold. On top of that, the heading angle is not determined this way, therefore this is determined directly from the GPS measurements.

6.2 Used software and processing methods

For comparison reasons three different software programs were used, being Leica Photogrammetry Suite (LPS), PhotoModeler and a Matlab script. The first two programs are aimed at deriving (geographic) models from photo's. Therefore these programs can process a bunch of photo's in one time. The Matlab scripts which were used were written to process just one or a few photo's. Therefore the approach of the Matlab script is different than that of the first two programs. Where LPS and PhotoModeler determine an areal triangulation, the Matlab script determines a space resection for every photo.

6.2.1 PhotoModeler

PhotoModeler is a photogrammetry software package created by EOS systems aimed at 3D modeling. Therefore the main focus of PhotoModeler is on close range photogrammetry. The idea behind the software is that the user takes photo's of the object to be modeled from all angles. These photo's are

then loaded into PhotoModeler. When the camera is calibrated, the user can pinpoint points of the model and using the reference tool quickly pinpoint one object point in several photo's. These points can even be connected with lines and surfaces. Therefore PhotoModeler is more of a 3D modeling software package supported by the theory of photogrammetry. It is possible though to calculate the orientation parameters of the photo's using control points. However, PhotoModeler is not capable of determining a model out of these photo's automatically. EOS systems created a more elaborate package, called PhotoModeler Scanner, which is aimed at this feature. However, this is a more advanced program and is therefore more expensive. In any case, it isn't available at the institute, so it couldn't be used.
Because of the nature of PhotoModeler is only used to determine the exterior orientation parameters of the photo's, which was enough for this test. The main advantages of PhotoModeler are as follows:

- It is user-friendly, all the main functions are easy to find and easy to use. Measuring and referencing points in photo's is done very quickly, because of the possibility to have several pictures open at once.
- Information on measured points and photo's is easily accessible from tables within the program.
- PhotoModeler doesn't need A-priori values for the exterior orientation parameters.

The main disadvantages are:

- Opening photo's in PhotoModeler costs a lot of memory. After opening a couple of photo's work memory runs out and the performance of the users machine starts to deteriorate.
- When the photo's are oriented, it is up to the user to create a 3D model from it. There is virtually no automatic processing after the orientation of the photo's.
- Because PhotoModeler is aimed at close range photogrammetry, the quality of the triangulation is not optimal when photo's are taken from more or less the same rotation angles. Therefore it is not really suitable for aerial photogrammetry.

6.2.2 Leica Photogrammetric Suite (LPS)

Leica Photogrammetry Suite is a professional software package aimed at processing photogrammetric project and remote sensing images. Contrary

to PhotoModeler, LPS is aimed at aerial photogrammetry. The program is capable of processing large photoblocks and gives detailed information on the accuracy of the determined orientations. Furthermore, when a photoblock is oriented, it is possible to derive a DEM from the photo's. This however takes a long time. For example, the DEMs generated from the photo's of the more elaborate test taken in Ammerstol (described in the next chapter) were created overnight.
The program is not very user friendly. A lot of important functions are hidden in subtools. It is possible to load data, such as a list of exterior orientation parameters for the photo's in the block from text files, but these import functions are hard to find and the data files to be imported need to be in a specific column format, otherwise LPS doesn't understand the file and does nothing with it. For smaller projects this causes that preparing the input files may cost as much time as adding everything manually in LPS.
Another disadvantage is that the program is not very robust. To be able to determine the orientation parameters of a photoblock, using Ground Control points and tiepoints, it still needs A-priori exterior orientation parameters with a reasonable accuracy. A triangulation of the complete fotoblock shot in September 2009 was attempted, but even with the GPS and IMU data and using the Ground Control Points as such in the triangulation, LPS couldn't achieve a decent convergence and therefore couldn't give a reasonable solution.
A good feature of LPS is the possibility to automatically generate Tiepoints. However, this process takes a long time though and the software crashed several times when an attempt of automatic tiepoint generation in bigger photoblocks was made. All in all the Leica Photogrammetry Suite is a good program aimed at aerial photogrammetry. It is hampered however by poor user interface and long processing times.

6.2.3 Matlab script

The used matlab scripts were home-made and designed to determine the exterior orientation parameters of 1 photo by space resection or determine the ground coordinates of an object, whose image coordinates are known in two photo's of which the exterior orientation parameters are also known. This information needs to be entered manually or loaded into matlab in separate input files. Therefore these scripts are totally unsuitable for processing bigger photoblocks or to determine a multitude of points. In this case they can be used to double check the outcomes however.

6.3 Results

As stated earlier, a block of 6 photo's with the same 3 Ground Control Points was created. First the exterior orientation parameters of the 6 photo's were determined and compared with the parameters from the direct sensor measurements. Then the direct sensor measurements were used as fixed exterior orientation parameters, the ground control points were now used as checkpoints, i.e. the coordinates of the ground control points were calculated using the fixed exterior orientation parameters. These are then compared with the known coordinates of the points. The resulting differences give an idea of the accuracy of the terrain model. The direct sensor data was as follows:

Used Photo's (ID)	X-coordinate [m]	Y-coordinate [m]	Z-coordinate [m]
2498	591474.09	5759704.6	79.06
2499	591469.12	5759713.8	80.36
2500	591464.65	5759723.1	80.03
2501	591461.34	5759732.8	81.1
2532	591443.36	5759685.5	78.9
2533	591440.59	5759692.4	78.34
2534	591434.06	5759697.8	77.98

Table 6.1: Photo ID's and GPS results.

Photo ID	ω angle [deg]	ϕ angle [deg]	κ angle [deg]
2498	5.5832	5.437	-61.5847
2499	0.6612	2.5312	-64.229
2500	2.2255	3.8828	-68.5319
2501	1.4733	-7.4014	-68.3049
2532	6.7404	-9.4033	-79.8351
2533	14.8513	-11.6377	-51.5207
2534	12.7702	-5.5613	-28.9685

Table 6.2: Photo ID's and rotation angles results

The used ground control points had the following characteristics:

GCP ID [m]	X-coordinate [m]	Y-coordinate [m]	Z-coordinate [m]
1	591477.664	5759758.579	42.768
2	591437.859	5759763.862	42.899
10	591507.345	5759674.209	42.978

Table 6.3: Point ID's and their coordinates

6.3.1 PhotoModeler test results

Coordinates and rotation angles of camera centre from ground control points

To determine the exterior orientation parameters of the photos they were loaded into the PhotoModeler project. The 3 Ground Control Points were marked in the Photos. The GCP's were given the terrain coordinates which were measured by a GPS receiver during the test. With only 3 GCP's PhotoModeler was not able to calculate the exterior orientation parameters of the photos, therefore a couple of tiepoints had to be addes. Luckily, there was a large party-tent present at the time of the test, therefore adding and referencing a couple of tiepoints in the photo's was quickly done, see also figure 6.2

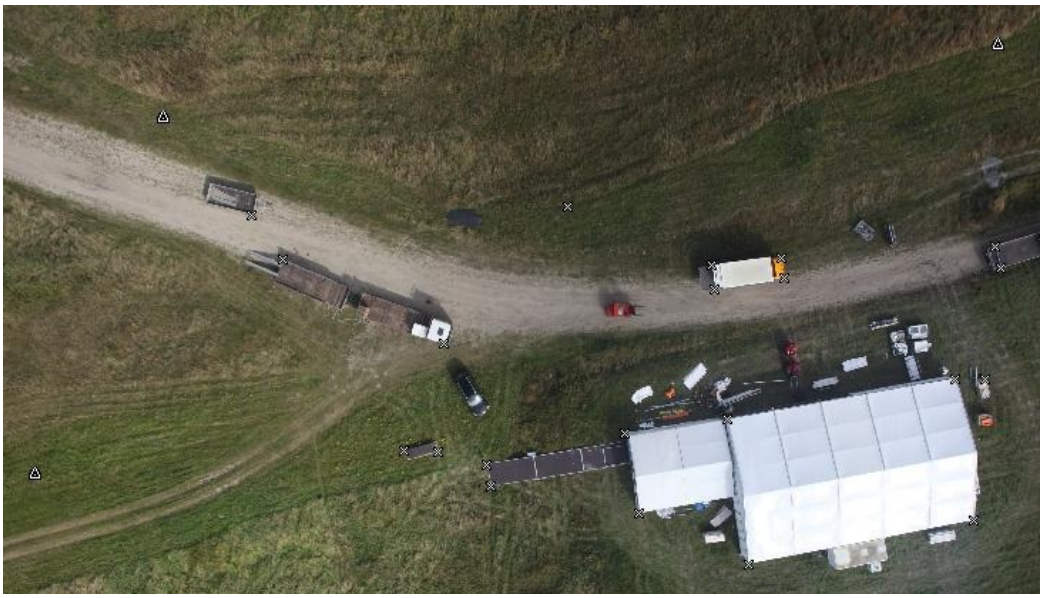

Figure 6.3: Example of GCP and tiepoint collection in PhotoModeler, the small triangles are GCP's marked in Photomodeler, the small crosses are extra tiepoints.

The exterior orientation parameters were now a result of an aerial triangulation performed by PhotoModeler. This gave the results shown in table 6.4 and 6.5. If these results are compared with the readings from the GPS and the IMU aboard the aircraft (so the direct sensor orientation parameters) the differences shown in table 6.6 are obtained.

Photo ID	X [m]	Y [m]	Z [m]
2498	591471,0098	5759705,6834	134,0478
2499	591466,3334	5759714,9063	133,6358
2500	591462,5938	5759723,3049	134,7122
2501	591456,2660	5759733,5189	133,0751
2532	591440,4454	5759685,9499	131,7419
2533	591436,0021	5759691,5110	131,0083
2534	591428,2972	5759696,2845	131,1837

Table 6.4: Camera centre coordinates out of triangulation by PhotoModeler

Photo ID	ω [deg]	ϕ [deg]	κ [deg]
2498	0,2179	2,3862	-74,0665
2499	-3,3491	2,5290	-76,2782
2500	-1,8858	1,6976	-78,5262
2501	-5,7587	-17,3368	-81,0680
2532	3,4269	-23,1424	-82,7735
2533	10,8327	-21,4916	-66,1357
2534	9,1341	-15,1245	-42,8047

Table 6.5: Rotation angles out of triangulation by PhotoModeler

There are differences of a couple of meters in X and Y directions, about 12 meters in height, about 3-5 degrees in omega angle, up to 10 degrees in phi angle and about 12 degrees in kappa angle.
The deviations in X and Y directions are more or less in line with what was expected due to the inaccuracy of the GPS-receiver. The difference in Z-direction is too big and too systematic to be due to measurement errors alone. A closer look at the data showed that there was a discrepancy between the flying height of the aircraft and the height of the ground control points. The flying height was measured as height above terrain, while the height of the ground control points was given as ellipsoidal height (in EGM96 reference frame). The actual NAP height of the test terrain is about 1.5 m below sea level. The difference between the EGM96 reference frame and the NAP level is 43.5 meters. The results in the table above are corrected for these offset,

Photo ID	X [m]	Y [m]	Z [m]	ω [deg]	ϕ [deg]	κ [deg]
2498	-3,0802	1,0834	11,4878	-5,3653	-3,0508	-12,4818
2499	-2,7866	1,1063	9,7758	-4,0103	-0,0022	-12,0492
2500	-2,0562	0,2049	11,1822	-4,1113	-2,1852	-9,9943
2501	-5,0740	0,7189	8,4751	-7,2318	-9,9354	-12,7631
2532	-2,9146	0,4499	9,3419	-3,3135	-13,7391	-2,9384
2533	-4,5879	-0,8890	9,1683	-4,0186	-9,8539	-14,6150
2534	-5,7628	-1,5155	9,7037	-3,6361	-9,5632	-13,8362

Table 6.6: Camera centre differences between PhotoModeler and Direct Sensor measurements

but there is a remaining deviation of about 10 meters. From the theoretic case we already saw that the height values are influenced the most by GPS-errors, furthermore, the pictures were taken rather close to each other, so the parallax angle was small. This further reduces the accuracy of the height value.
The angle differences are higher than expected, but the rotation angles in this test weren't measured by an actual IMU, but instead the omega and phi angles were measured by an infrared sensor which determined the position of the wings relative to the ground (see section 6.1.2) and the kappa angle was derived from the (already inaccurate) GPS data, therefore the given deviations in the rotation angles make sense.
What remains to be seen is how accurate the GCP's were measured during the test. The results from Matlab and photomodeler show a phi angle of about 20 degrees in some of the photos. This angle is the pitch angle of the aircraft. A pitch angle of 20 degrees would send a normal (full size) aircraft close to stalling.

Coordinates of ground control points from coordinates and rotation angles of camera centre

PhotoModeler allows the user to manually enter the exterior orientation parameters for the images loaded in the project. The terrain coordinates of terrain points can then be determined by marking a terrain point in a picture and referencing them in the other pictures. The corresponding terrain coordinates are then calculated automatically. Following this procedure the coordinates of the 3 ground control points visible in the block of photos were determined and compared with the coordinates measured during the test. This gave the results in table 6.7. The differences with the coordinates measured during the test are shown in table 6.8

Point ID	X [m]	Y [m]	Z [m]
1	591460,4700	5759784,8054	-32,3260
2	591411,5352	5759775,1588	-22,9714
10	591504,4112	5759693,2769	-15,8730

Table 6.7: Results of checkpoint calculation by PhotoModeler

Point ID	X [m]	Y [m]	Z [m]
1	-17,1940	26,2264	-31,5940
2	-26,3238	11,2968	-22,3704
10	-2,9338	19,0679	-15,3510

Table 6.8: Differences between observed and computed checkpoint coordinates

These differences seem rather high (about 10-25 meters in planimetric direction and more than 60 in height). The height difference can be partially explained by the datum shift as discussed above. The differences stay very large however. To determine if these differences make sense, it should be checked what kind of effect the estimated errors in the orientation parameters have on the estimated terrain coordinates. For this the theoretic case described in the previous chapter can be used. The most notable difference is those of the angles. From chapter 4 it can be seen that errors of 1 degree can lead to errors of 1 to 1.5 meters. Errors in the rotation angles of more than 10 degrees will therefore easily lead to terrain errors of more than 10 meters. Combined with GPS-inaccuracies and the fact that there are large inaccuracies in all 3 angles, the coordinate differences above make sense.

6.3.2 LPS test results

Leica Photogrammetry Suite is dependent on A-priori exterior orientation parameters to be able to get a solution. Using the GPS/IMU readouts from the aircraft caused the block to diverge, even with the ground control points measured in the photos and a number of tiepoints added (granted, by automatic tiepoint generation in LPS, which does not always give reliable results). To get an idea how LPS works, the resulting exterior orientation parameters from PhotoModeler have been used as A-priori exterior orientation parameters. This gave the results shown in table 6.9 and table 6.10.
These values are again compared with the GPS/IMU data. The differences are shown in table 6.11. The Z-difference is again corrected for the reference frame offset. More or less the same differences show up as in the PhotoMod-

Photo ID	X [m]	Y [m]	Z [m]
2498	591472.7780	5759705.9600	138.2720
2499	591467.9450	5759716.0330	137.9270
2500	591464.4920	5759725.6420	138.8710
2501	591458.0170	5759734.9770	137.1500
2532	591440.4500	5759685.9500	131.7420
2533	591436.2340	5759691.0340	135.7080
2534	591427.0700	5759696.7090	135.5510

Table 6.9: Camera centre coordinates out of triangulation by LPS

Photo ID	ω [deg]	ϕ [deg]	κ [deg]
2498	0.0044	3.3366	-74.0587
2499	-3.9182	3.3740	-76.1827
2500	-3.2492	2.7335	-78.4007
2501	-6.4944	-15.6854	-80.9233
2532	3.4269	-23.1424	-82.7700
2533	10.5540	-20.4753	-66.2405
2534	8.5317	-15.1682	-42.9654

Table 6.10: Rotation angles out of triangulation by LPS

Photo ID	X [m]	Y [m]	Z [m]	ω [deg]	ϕ [deg]	κ [deg]
2498	-1.3120	1.3600	15.7120	-5.5789	-2.1004	-12.4741
2499	-1.1750	2.2330	14.0670	-4.5794	0.8428	-11.9538
2500	-0.1580	2.5420	15.3410	-5.4747	-1.1494	-9.8689
2501	-3.3230	2.1770	12.5500	-7.9674	-8.2939	-12.6185
2532	-2.9150	0.4500	9.3420	-3.3135	-13.7391	-2.9384
2533	-4.3560	-1.3660	13.8680	-4.2974	-8.8376	-14.7197
2534	N/A	N/A	N/A	N/A	N/A	N/A

Table 6.11: differences between LPS exterior orientation parameters and direct sensor measurements

eler results.

6.3.3 Matlab test results

Coordinates and rotation angles of camera centre from ground control points.

With a relatively simple Matlab-script it is possible to calculate the coordinates and rotation angles of the camera centre of a photo from the coordinates of the ground control points visible in the photo. The Matlab script only allows to orientate 1 photo at a time however, so this method is a space-resection instead of an aerial triangulation as performed by PhotoModeler. The Matlab script uses a linearization of the collinearity equations with the exterior orientation parameters as unknowns. Therefore A-priori values needs to be found. The standard script estimates the A-priori values from the ground control point information and the focal length of the camera. This gave the results for the photo's in the block shown in table 6.12 and 6.13. These results can again be compared with the GPS and IMU data, giving the results shown in table 6.14. Do note that the exterior orientation parameters of photo 2532 are not determined. This is because this photo contained only two ground control points, which is not enough to determine an exterior orientation using the used Matlab script.

Photo ID	X [m]	Y [m]	Z [m]
2498	591472,5067	5759705,7158	138,0624
2499	591467,6040	5759715,6259	137,7215
2500	591464,0914	5759725,3186	138,6406
2501	591457,7377	5759734,6227	136,8547
2532	N/A	N/A	N/A
2533	591436,3099	5759690,9074	135,4351
2534	591427,3338	5759696,5005	135,3851

Table 6.12: Camera centre coordinates out of Matlab space resection

Again the expected deviations in the X and Y coordinates can be seen, furthermore there is a difference of about 50 meters in Z coordinates and there are rather large angle differences. These can of course be explained the same way as the deviations in the LPS and PhotoModeler results. Another way of performing the space-resection is using the GPS and IMU data from the aircraft as A-priori values for the space-resection, but the Matlab script failed to give reasonable orientation parameters this way.

Point ID	ω [deg]	ϕ [deg]	κ [deg]
2498	-0,0213	3,3495	-74,0543
2499	-3,8535	3,3421	-76,1870
2500	-3,2208	2,6802	-78,4082
2501	-6,4547	-15,7074	-80,9701
2532	N/A	N/A	N/A
2533	10,4512	-20,3413	-66,2763
2534	8,4225	-14,9994	-42,9897

Table 6.13: Rotation angles out of Matlab space resection

Photo ID	X [m]	Y [m]	Z [m]	ω [deg]	ϕ [deg]	κ [deg]
2498	-1.5833	1.1158	15.5024	-5.6045	-2.0875	-12.4697
2499	-1.5160	1.8259	13.8615	-4.5147	0.8109	-11.9581
2500	-0.5586	2.2186	15.1106	-5.4463	-1.2026	-9.8764
2501	-3.6023	1.8227	12.2547	-7.9278	-8.3060	-12.6653
2532	N/A	N/A	N/A	N/A	N/A	N/A
2533	-4.2801	-1.4926	13.5951	-4.4001	-8.7036	-14.7555
2534	-6.7262	-1.2995	13.9051	-4.3477	-9.4381	-14.0212

Table 6.14: Differences between Matlab results and direct sensor measurements

Using the exterior orientation parameters of the block photos, a second Matlab script performed a forward intersection to determine the ground coordinates of the ground control points visible in the photos. This gave the results shown in table 6.15 and 6.16.

Point ID	X	Y	Z
1	591462,4717	5759776,2801	-25,7935
2	591415,7449	5759773,2918	-25,1283
10	591508,6503	5759693,6100	-18,7323

Table 6.15: Results of forward intersection in Matlab.

Point ID	X	Y	Z
1	-15,19	17,7	-15,19
2	-22,11	9,43	-22,11
10	1,31	19,4	1,31

Table 6.16: Differences between Matlab forward intersection of checkpoints and GPS measurements

The deviations between the computed coordinates and the measured coordinates are quite large due to the GPS/IMU inaccuracies as discussed before, but we also see some differences between the coordinates calculated by PhotoModeler and those calculated by Matlab. Because it is not clear how PhotoModeler calculates the ground coordinates of a specific point, It can't be said where these differences come from.

6.3.4 Comparison of results

To check if there are no systematic errors in the processing results, the exterior orientation parameters which rolled out of the different software packages are also compared with each other, giving the results in tables 6.17 - 6.19:

The differences between the LPS outcomes and the GPS/IMU data look similar to the previous differences. When comparing the outcomes with those of PhotoModeler and Matlab, we see that the differences with the Matlab coordinates is very small. Because Photo 2532 only has two ground control points, that photo couldn't be processed in Matlab. We see that the differences between LPS and Photomodeler for this photograph is neglectable. From this it seems that LPS needs accurate A-priori values for its calculation

Photo ID	X	Y	Z	Omega	Phi	Kappa
2498	1,7682	0,2766	4,2242	-0,2135	0,9504	0,0077
2499	1,6116	1,1267	4,2912	-0,5691	0,8450	0,0955
2500	1,8982	2,3371	4,1588	-1,3634	1,0359	0,1254
2501	1,7510	1,4581	4,0749	-0,7357	1,6515	0,1446
2532	-0,0004	0,0001	0,0001	0,0000	0,0000	0,0000
2533	0,2319	-0,4770	4,6997	-0,2787	1,0163	-0,1048
2534	-1,2272	0,4245	4,3673	-0,6024	-0,0437	-0,1607

Table 6.17: Differences between LPS and PhotoModeler

Photo ID	X	Y	Z	Omega	Phi	Kappa
2498	0,2713	0,2442	0,2096	0,0257	-0,0129	-0,0044
2499	0,3410	0,4071	0,2055	-0,0647	0,0319	0,0043
2500	0,4006	0,3234	0,2304	-0,0284	0,0533	0,0075
2501	0,2793	0,3543	0,2953	-0,0397	0,0221	0,0468
2533	-0,0759	0,1266	0,2729	0,1028	-0,1340	0,0358
2534	-0,2638	0,2085	0,1659	0,1092	-0,1688	0,0243

Table 6.18: Differences between LPS and Matlab

Photo ID	X	Y	Z	Omega	Phi	Kappa
2498	1,4969	0,0324	4,0146	-0,2392	0,9633	0,0122
2499	1,2706	0,7196	4,0857	-0,5044	0,8131	0,0912
2500	1,4976	2,0137	3,9284	-1,3350	0,9826	0,1180
2501	1,4717	1,1038	3,7796	-0,6960	1,6294	0,0979
2533	0,3078	-0,6036	4,4268	-0,3815	1,1503	-0,1406
2534	-0,9634	0,2160	4,2014	-0,7116	0,1251	-0,1850

Table 6.19: Differences between PhotoModeler and Matlab

and calculates the exterior orientation parameters on a photo by photo basis. Therefore it needs at least 3 ground control points to determine the exterior orientation parameters of a certain photo. That's why the outcome of 2532 is the same as that of PhotoModeler, the program just keeps the A-priori value.

Chapter 7

Ammerstol Test

The previous chapter described the processing of a small block flown in september 2009. Although the result gave some insight in the accuracy that can be achieved using the aircraft as it is, there was not enough data to verify the results of the theoretic approach described in chapter 4. Therefore a more elaborate test is needed. For this test the following aspects are important:

- Testing of directional differences between computed and real coordinates requires several checkpoints evenly distributed in each image pair.
- Checkpoints should be measured with high accuracy (accuracy of 2 3 cm would be optimal).
- The distance between photos should give 60% overlap and 30% sidelap, so that overlap is guaranteed over the whole area to be photographed, but the amount of photos to be taken does not become too large.
- For optimal test results, the photo's should be taken in strips of approximately equal length. This requires the aircraft to fly straight strips and return at the end of a strip.
- For optimal test results, flat terrain without big objects would be ideal. A large grassland or the beach would be optimal.
- Better IMU instrument would be preferred.

The requirements given above can be fulfilled if the test setup is something like shown in figure 7.1:
In this picture, the small crosses are ground points, which can either be used as control points to determine the exterior orientation parameters of the photos through aerial triangulation, or as check points, which are used to check

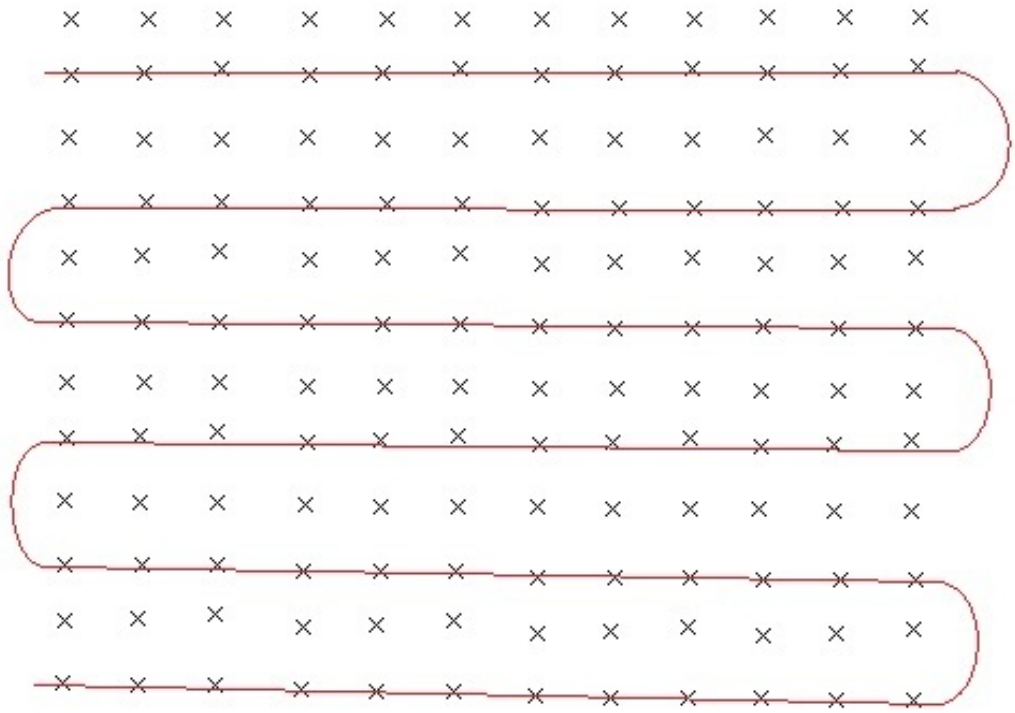

Figure 7.1: Preferred test setup

the exterior orientation parameters, by determining the check point coordinates from the photos and comparing them with the coordinates as measured on the ground. The distance between the ground points is important. The idea is that in one photo pair a block of 3 x 3 check points are visible. In the theoretic case we saw that the distance between points then needs to be about 30 meters. This way the checkpoints will lie more or less on the location of the Von Gruber Points in the photo's. The results shown in figures 4.3 and 4.6 show that the size and direction of an error in the terrain coordinates is dependent on the location of the feature point in the photos. To check these resutls, the ground points should be spread evenly over the photos.
From the figure it follows that the aircraft follows the orientation of the check point grid. This would make it easy to transform the coordinate system to a local system, wherein the X-coordinate corresponds with the flight direction and the Y-coordinate is perpendicular to the flight direction. This would immediately result in derivations parallel and perpendicular to the flight direction, as determined in the theoretic case, making comparison easier. Another important aspect is the distance between the camera centres of two consecutive photos in the flying line, this should be defined such that there is alway 60% overlap between two photos. This would require setting the time interval between pictures so that the distance between two consecutive pictures is the "right" distance for 60% overlap, which requires accurate knowledge of the flying speed. However, if more photo's are taken than necessary, it is possible to select photos at the correct distance afterwards.
From the results of the A4 site test, it can be concluded that measuring rotation angles, using infrared sensors to determine a temperature difference (and thus an artificial horizon) is frankly useless. The high errors in rotation angles causes differences in terrain coordinates of up to 20 meters. Furthermore, because the aerial triangulation is a linearized least squares problem, a-priori values for the rotation angles. While processing the results of the A4 test, it became clear that if these a-priori values differ from the real rotation angles too much, the linearized least squares problem will not converge. However, this might not be a problem if there are enough ground control points available for the aerial triangulation. All in all, a better way of measuring the rotation angles should be found. Installing a low-end IMU on the aircraft for the purpose of the test might improve the results considerably.
On the 29th of june an elaborate test flight was undertaken at the village of Ammerstol, which is located along the dyke of the river Lek. This location should make it possible to see some height differences in the picture, because the dyke is several meters higher than the surrounding land. The engineering company GeoDelta assisted this test by placing and measuring Ground

Control Points. The placement of Ground Control Points was much denser than during the september 2009 test. Therefore, in most pictures, several Ground Control Points could be seen. The test area can be seen in figure 7.2

Figure 7.2: Test area with Ground Control Points as tags, image taken from Google Earth

The test setup in Ammerstol didn't meet all requirements mentioned above. Especially the position of the photo's (60% overlap and 30 % sidelap) is not met. In conventional photogrammetry an operator flies along who takes care of a good geometry between the photo's. This is not possible in UAV photogrammetry. Furthermore it is hard to let the airplane fly in straight lines parallel to the Ground Control Point orientation. The Ground Points itself could not easily be laid in a regular grid as shown in figure 7.1 due to all kinds of objects.
As can be seen most ground control points were lying on the dyke itself or in the area between the dyke and the river (known as the outer area, because it lies "outside" the area protected by the dyke).

7.1 Data description

During the flight, the location and rotation angles were measured by the Ublox GPS-receiver and the infrared sensors on the wings, the same way as during the test flight at the A4 site. The photos were signalized with ground control points, which were measured with the help of GPS with an accuracy of about 1 to 2 cm. This high accuracy was achieved by using the 06-GPS service, which downloads error corrections from a network of reference

stations in the country. Therefore it is possible to obtain Differential GPS accuracy using only one receiver. For more information on GPS techniques, see paragraph 3.1

The delivered data after the test flight were:

- Two rows of photos.
- Per photo the coordinates of the camera centre in both UTM and WGS-84 coordinates.
- Per photo the 3 rotation angles
- A list of coordinates of the ground control points with their standard deviation (in RD/NAP).
- A list of correspondences. (pixel coordinates of locations which can be seen in two or more photos).

The delivered pictures mostly showed the dyke itself, while the upper row of pictures also showed the inner area bordering the dyke, an area where almost no ground control points were visible. Therefore the pictures were lying more or less on the edge of the block. This means that, although most photo's contained plenty of Ground Control Points they weren't evenly distributed over the photo's. This can influence the accuracy of the processing results.
The goal is to describe the accuracy of the process and the resulting model. To do this the photos were processed in 3 different ways.

- Using the coordinates of the ground control points, I calculated the exterior orientation parameters of the photos in the block
- Using the data from the aircraft as (fixed) exterior orientation parameters, I calculated the coordinates of the ground control points by measuring them in the photos.
- Using Leica Photogrammetric Suite I determined Digital Elevation Models using both the exterior orientation parameters calculated from the GCPs and the direct sensor measurements.

First of all though, the delivered coordinates were not in the same reference system, so first of all the coordinates needed to be transformed into the same system. The ground control points were measured in the Dutch RD/NAP system. Because the coordinates in this system are given in meters, it is easy to compare coordinates with each other and get an idea of the overall accuracy. Therefore the coordinates of the camera centres needed to be

converted to RD/NAP. For this I used the program PCTrans developed by the Dutch Navy. This program can not cope with NAP-heights however. The heights accompanying the UTM coordinates of the camera centres are relative to the Geoid while the heights accompanying the WGS-84 coordinates are relative to the Ellipsoid. The Geoid heights should more or less correspond with sea level. Therefore the difference between Geoid heights and NAP-heights is the smallest, but there is still a small offset.

7.2 Processing

Determining the exterior orientation parameters from the Ground Control Points means pinpointing all the ground control points in every picture. Furthermore the coordinates of the ground control points must be given. GeoDelta provided us with an exterior orientation. These exterior orientation parameters were loaded into Leica Photogrammetry Suite. To check the exterior orientation results, the Ground Control Points are regarded as check points. Their coordinates are determined via a forward intersection in LPS. The resulting coordinates are then compared with the results of the terrestrial GPS measurements carried out by GeoDelta.
Leica Photogrammetric Suite and PhotoModeler depend on manual pinpointing of the ground control points. Overall the photos were well signalized, but there were a few problems with the Ground Control Points. First of all, the centres of the used targets were a bit too large. On the photos the centre of a Ground Control Points were a couple of pixels. This made it very difficult to pinpoint a Ground Control Point with sub-pixel accuracy

Figure 7.3: Pinpointed Ground Control Point in LPS

Furthermore, some ground control points in some photos were poorly visible due to the sun shining on them. The targets itself were visible, but the black and white structure was blinded by sunlight. This could be mitigated by thresholding the histogram of the photo in the LPS point measurement tool. If the minimal histogram value is set about 5 pixel values under the maximal value which occurs, the structure was found back. See figure 7.4

Figure 7.4: GCP blinded by sunlight (left) and result of histogram adaptation (right)

Leica Photogrammetric Suite needs reasonable A-priori data to be able to let the block converge and come with a solution. PhotoModeler does not need these a-priori data, so I first performed the Areal triangulation in PhotoModeler. The resulting exterior orientation parameters were compared with the output of the test flight. This resulted in a difference of each parameter for each picture. The resulting exterior orientation parameters were used as a-priori parameters in Leica Photogrammetric Suite. After pinpointing all the ground control points and (manually) inserting the coordinates of the GCPs the block could be triangulated, which again resulted in calculated exterior orientation parameters. These were again compared with the flight data. Also, a space resection using a Matlab script was performed. For this the image coordinates of the ground control points needed to be inserted as well. For these I used the measured image coordinates from LPS, which are shown in the LPS measurement tool. It later turned out that the orientation parameters from the flight data were good enough for LPS to determine a triangulation with the Ground Control Points as such. The difference results are almost the same as when the results from PhotoModeler are used.

7.3 Results

7.3.1 Exterior Orientation parameters from Aerial Triangulation using GCPs

As stated in the previous paragraph, a comparison between the outcome of the processing of GeoDelta and the flight data is made by taking the difference between the exterior orientation parameters from both sources. To summarize the results, in the table 7.1 the mean difference and its standard deviation is given for each parameter.
From these results it follows that there are systematic differences in both the camera centre coordinates and the rotation angles. There is an offset of 6 meters in X-direction, about 2 meters in Y-direction and about 12 meters

Parameter	Mean	Standard Deviation
X-difference [m]	6.6650	0.4579
Y-difference [m]	2.0169	0.5099
Z-difference [m]	-7.3197	0.5443
Roll-difference [degrees]	-4.2983	2.3540
Pitch-difference [degrees]	6.7551	2.1495
Heading-difference [degrees]	1.7463	2.2795
X-coordinate Checkpoint differences	-0.0923	0.4051
Y-coordinate Checkpoint differences	0.1293	0.4251
Z-coordinate Checkpoint differences	-3.2462	1.1657

Table 7.1: GeoDelta block results

in Z-direction determined by the 3 software programs which were used and about 7 meters as determined by GeoDelta. The difference in rotation angles are -4 degrees for the omega angle, about 7 degrees for the Phi angle and about 1.5 degrees for the Kappa angle

7.3.2 Checkpoint coordinates from direct sensor measurement results

To see how the inaccuracies of the on-board sensors influence the accuracy of the object coordinates determined from the photos, the exterior orientation parameters where fixed to the values determined during the flight and used the ground control points as check points. Again the three software packages were used. PhotoModeler couldnt give a solution. LPS regarded the GCP's as checkpoints. LPS doesnt update the ground point coordinates during the triangulation but instead calculates the differences, this gave the results in table 7.2. The Matlab script results are shown in table 7.3.

Coordinate	Mean	Standard deviation
X-coordinate	-0.9434	2.2664
Y-coordinate	-3.3382	1.5965
Z-coordinate	-14.5593	8.5688

Table 7.2: LPS observed - computed checkpoint differences

The most apparent differences are those of the height Z-coordinates of the points, which makes sense, because the Z-coordinates of the camera centres also showed the largest errors (see tables 7.1 7.4). There are small systematic shifts in X (about 1 meter) and Y (about 3 meters). They can be a result

Coordinate	Mean	Standard deviation
X-coordinate	-1.0320	2.4260
Y-coordinate	-3.0367	1.6258
Z-coordinate	-12.5621	8.4568

Table 7.3: Matlab observed - computed checkpoint differences

of the systematic deviations in X and phi found in the exterior orientation results, described above.
As can be seen from the differences between the computed exterior orientation parameters and the flight data, there are some systematic differences, mainly in X and Z directions and in the Phi rotation angle. If the flight data are adapted according to these differences and the coordinates of the Ground Control Points are calculated again from the photos in Leica Photogrammetric Suite (so using the GCPs as checkpoints), the results in table 7.4 show up. If the same thing is done in Matlab, the results in table 7.5 are achieved.

Coordinate	Mean	Standard deviation
X-coordinate	0.5062	2.1093
Y-coordinate	-3.1417	1.1841
Z-coordinate	-3.2516	5.4879

Table 7.4: LPS observed - computed checkpoint differences after adapting exterior orientation parameters

Coordinate	Mean	Standard deviation
X-coordinate	0.2104	2.0971
Y-coordinate	-2.8401	1.1926
Z-coordinate	-1.4013	5.3540

Table 7.5: Matlab observed - computed checkpoint differences after adapting exterior orientation parameters

Especially the Z-coordinate values profit from the adaptation of the flight data, which makes sense, because the Z-coordinates of the camera centres showed the largest errors. Futhermore, from the theoretic assesment of the influence of the GPS measurements on the resulting terrain model from chapter 4.3, it follows that the Z-coordinates of the terrain points is influences most by GPS errors. It can be seen that the standard deviation of the Z

coordinates is much larger than that of the X and Y coordinates, which can also be expected on the basis of the results of the theoretical tests.

7.3.3 Determination of DTMs

LPS is able to determine a Digital Terrain Model from a triangulated block of photos. These Digital Terrain Models are saved in the form of point clouds with xyz coordinates, which can be visualized in a scatterplot. To get an idea of the results, DTMs of the three blocks which were processed in LPS were made:

1. The block with A-priori values from PhotoModeler and ground points as GCPs, shown in figure 7.5a
2. The block with the flight data as fixed exterior orientation parameters and ground points as check points, which is shown in figure 7.5b
3. The block with the flight data as A-priori values and ground points as GCPs, shown in figure 7.6a
4. The block with the GeoDelta exteriors as fixed values and the ground points as check points, shown in figure 7.6b

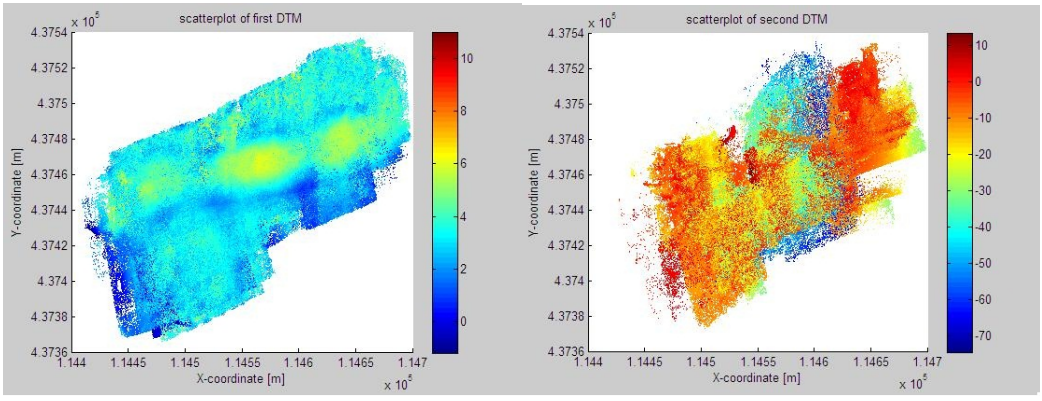

(a) A-priori Photomodeler;GCPs (b) flight data fixed; checkpoints

Figure 7.5: DEM scatterplots 1

From these figures we see that the DTMs determined with the ground points as GCPs are reasonable. We see the dyke of the Lek river running through the models. The model derived from the flight data with the ground points as check points is not good enough. We see big height fluctuations (going

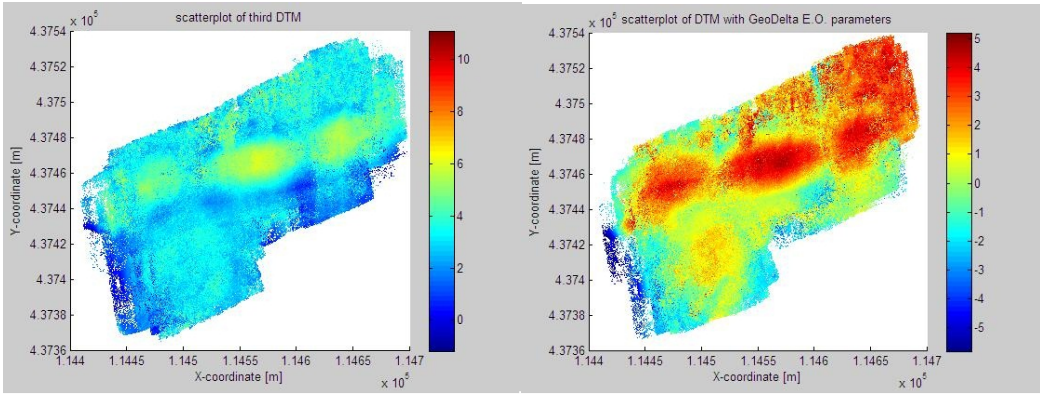

(a) A-priori flight data; GCPs (b) Geodelta fixed; Checkpoints

Figure 7.6: DEM scatterplots 2

from -70 to + 10). The dyke itself should be a about 6 meters above sea level, because the area around the river is at about 1.5 to 2 meters above sea level and the dyke is obviously higher. From this we can conclude that only the flight data is not good enough to determine a height model from the photos.

To check the resulting height models, we need to compare it with existing data. Therefore the above models are compared with the AHN-data (Actueel Hoogtemodel Nederland) determined by the Dutch Cadastre. The AHN-data was delivered in the form of loose xyz coordinates. To be able to compare the AHN-data with the model created by LPS, the AHN pointcloud is interpolated on a regular grid. Then the pointcloud created by LPS is interpolated on the same regular grid. These two interpolations are then subtracted from each other.
The interpolated AHN data is shown in figure 7.7. We can clearly see the river dike and the height difference between the land areas on both side of the dyke (the land behind the dyke is obviously lying lower, because the dyke protects this land from the river). The result of the interpolation of the LPS model is shown in figure 7.8a.
We do see the dyke back, but the height difference between the areas on both sides of the dyke are not clear. The area behind the dyke (and thus protected by the dyke) seems to be higher than the outer area. Figure 7.8b shows the difference between the AHN data and the LPS data, where we see that the area protected by the dyke is much higher in the LPS data then in the AHN data. This may be due to terrain objects (trees and houses) visible in the LPS data, which are removed from the AHN data. On the

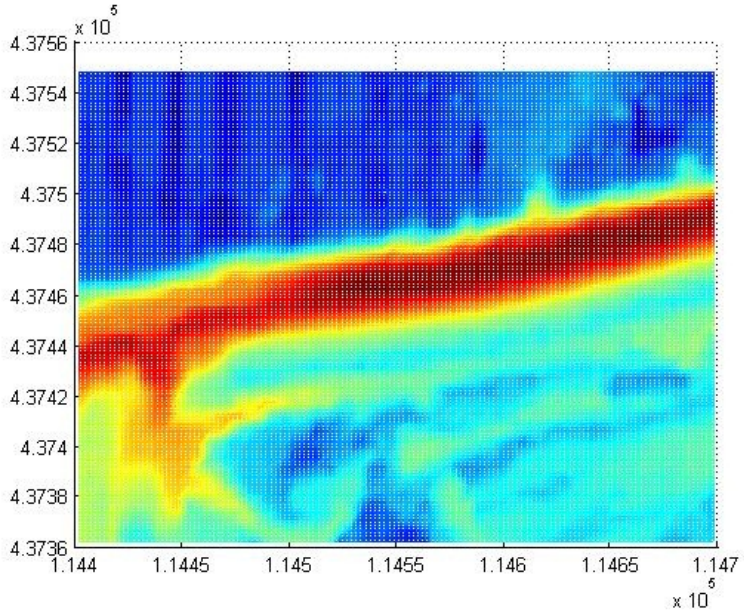

Figure 7.7: Interpolated AHN data

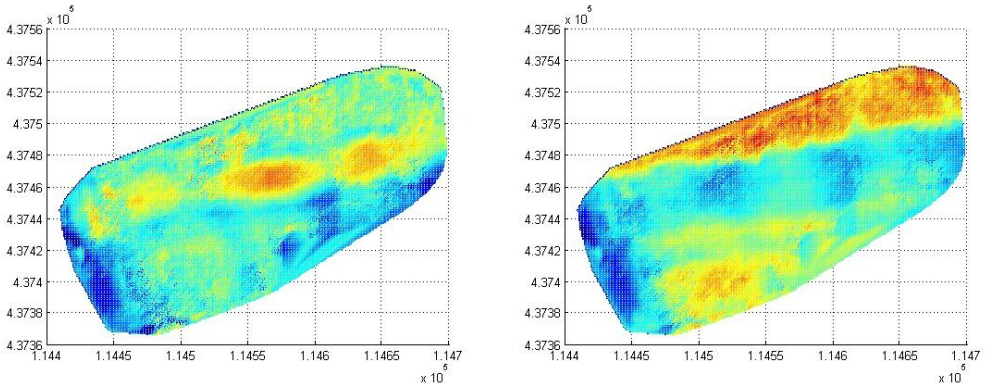

(a) Interpolation of LPS pointcloud

(b) LPS - AHN difference

Figure 7.8: Interpolated LPS data

dyke itself the differences are quite small, while in the outer area the differences become larger again, which again may be due to the presence of trees. During the test, the engineering company GeoDelta helped acquiring data, mainly by measuring the Ground Control Points. They also evaluated the resulting photos and came up with a height model of their own. Unlike the model described above GeoDelta only used points directly on the terrain (so no trees, bushes, buildings, etc.) This can be clearly seen in the resulting pointcloud, shown in figure 7.9a.

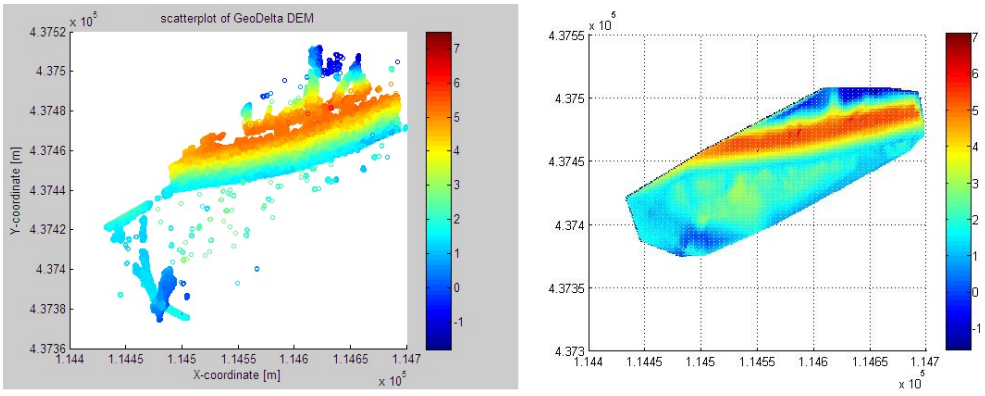

(a) GeoDelta DTM pointcloud

(b) GeoDelta DTM interpolation on a regular grid

Figure 7.9: Results of processing by GeoDelta

When this pointcloud is interpolated on the same regular grid as used to determine the difference between the LPS elevation model and the AHN model, the result shown in figure 7.9b is achieved. The river dyke is clearly seen in the upper part of the picture. However, there seem to be some elevated regions in the area not protected by the dyke. This region is only very sparsely visible in the original pointcloud, therefore the interpolation in this area is not as reliable as in other areas (such as on the dyke itself). When we compare the DEM above with the AHN data we can see this back, the largest differences occur in the area not protected by the dyke. The other differences are close to zero, see figure 7.10

As described above, the GeoDelta orientation parameters were also used in LPS to determine an extra block. The resulting DEM pointcloud is shown above in figure 7.6b. Figure 7.11 shows the interpolation on the same regular grid on the left. On the right the differences between this interpolation and the AHN-model is shown. The differences are especially high at the inner side of the dyke, but there are also some high lying areas at the outer side of the dyke. These probably are (again) terrain features such as trees and

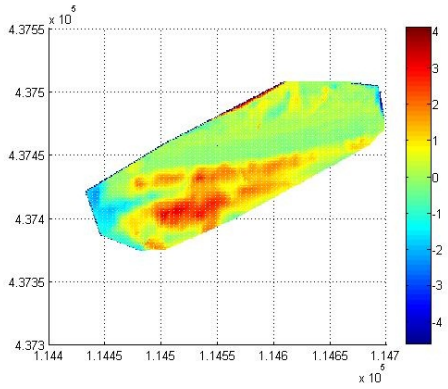

Figure 7.10: Differences between interpolated Geodelta DEM and AHN data

houses), which are not visible in the AHN data. Notable in all LPS results is the very low lying area on the left of the images, which are not easily explainable. Overall it can be said that the DEM creation is a nice tool in LPS, but it is not accurate enough to give a final product.

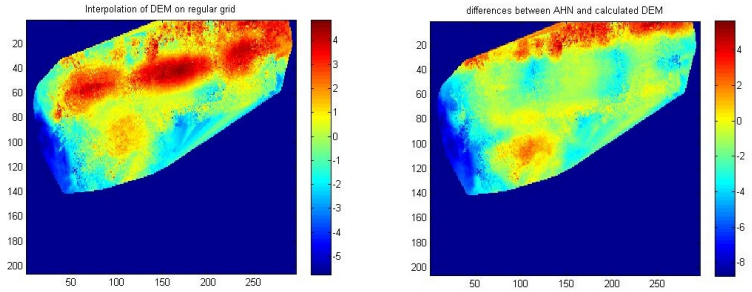

Figure 7.11: Interpolation of DTM determined by LPS using GeoDelta exterior orientation parameters

7.4 Result Analysis

There are systematic differences for the coordinates of the camera centres in all three coordinates. As explained earlier, there should be a small offset in height, because of the different height datum (Geoid height and NAP height). This difference should be about 40 cm. The results show a difference of about 12 meter in height. Therefore it is assumed that there are systematic errors in the measurements from the GPS receiver aboard the airplane. This would also explain the errors in X and Y directions. This makes sense, because

the used GPS receiver is a low end receiver and single point positioning is used, therefore all kinds of errors are not mitigated and therefore corrupt the result. See also chapter 2
As explained in paragraph 6.1, the rotation angles are determined by infrared sensors on the wings of the aircraft. These infrared sensors measures the surrounding temperature and construct an artificial horizon from these temperature measurements. This artificial horizon is than used to determine the roll and pitch angles. The accuracy of the rotation angles when determined this way is amongst others dependent on weather conditions. Especially the temperature difference between air and terrain should be noticable. The systematic differences of 4 degrees in roll and 6 degrees in pitch show that the system apparently had trouble finding this difference (perhaps a wrong threshold is used).
The κ (heading) angle is determined from the GPS measurements. The angle between the X and Y measurement can easily be calculated. The Kappa angle is therefore directly dependent on the accuracy of the GPS receiver. Systematic errors in the GPS receiver shouldn't influence the heading angle, because if at different locations the GPS-errors in all directions are the same, the resulting movement doesn't change, only the locations are shifted. This would explain why the heading angle is reasonably accurate in comparison with the other rotation angles.
The standard deviations of the differences for the three used software programs (Matlab, LPS and PhotoModeler) show values which would comply with the specifications of the GPS receiver and the estimated accuracy of the infrared system in favourable weather conditions. However, the standard deviations of the differences between the flight data and the results of GeoDelta are smaller, especially for the camera centre coordinates. This further confirms the assumption that these differences are due to systematic errors in the GPS measurements. Apparently there are also inaccuracies in the processing done by the used software programs. Because the used software is not open-source, it can't be determined how the software performs the triangulation, but the resulting reports should give an idea of the accuracy. Both in PhotoModeler and in Leica Photogrammetric Suite, there were some large residuals in the image coordinates after the triangulation process. Especially in PhotoModeler the residuals would suggest that one or more points were mismatched. However after manually checking and double checking the blocks no blunders were found in the process of pinpointing the GCPs. Therefore these large residuals are either the result of a blunder in the GPS coordinates of the GCPs or due to overall unstable pinpointing. The difficulties with pinpointing the GCPs discussed above might have something to do with this, but in PhotoModeler ridiculously high residuals (about

100 pixels or even more) showed up, so that cant be the sole reason for the residuals. These high residuals are a logical explanation for the fact that the processing results of PhotoModeler, LPS and Matlab (because Matlab uses image coordinates derived from LPS) are not as accurate as the GeoDelta results.

7.4.1 Validation of theoretic analysis

To visualize the individual checkpoint offsets vector fields are created of the differences between the observed checkpoints and the calculated checkpoints by both LPS and the Matlab script, see figure 7.12.

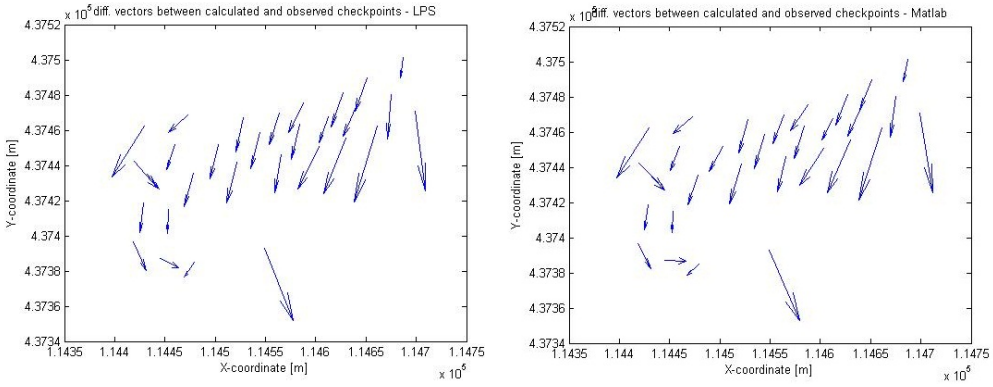

Figure 7.12: Difference vectors between observed checkpoints and calculated in LPS (left) and by Matlab script (right)

Matlab and LPS give more or less the same result, as can be expected. The vector fields show a clear trend to the south and most checkpoints are shifted a bit to the east as well. To check if this difference pattern can be expected, the differences occuring in a single photopair are compared with a theoretic case using the GPS/IMU errors as calculated above. Figure 7.13 shows the offset vectors of the checkpoints occuring in the photo's 6 and 7 calculated in LPS and Matlab.
Then a theoretic setups was made, with 2 photo's lying in an arbitrary coordinate system, relative to each other the same way as photo's 6 and 7. Checkpoints were placed on a regular grid, see figure 7.14. Their image coordinates were determined by measuring them from the center lines of the photo layouts. To keep the setup simple, the following simplifications were made:

- The focal length was set to exactly 24 mm

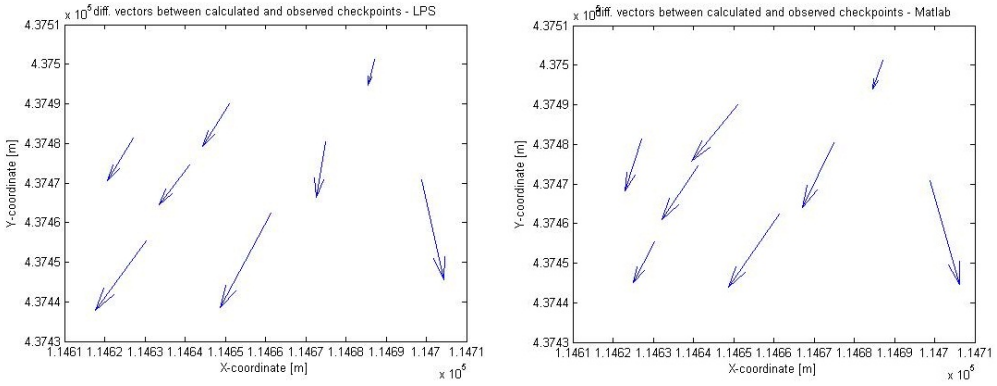

Figure 7.13: Difference vectors between observed checkpoints and calculated in LPS (left and by Matlab script (right) for photo's 6 and 7

- The flying height for both pictures was the same at exactly 80 meters
- The aircraft was flying straight and level, so the omega and phi rotation angles were set to zero

To determine if the same pattern as in figure 7.13 shows up, the exterior orientation parameters of the two images in the theoretic case are given the same errors as found for the photo's 6 and 7. Figure 7.15 shows the theoretic offsets from the described theoretic case.
The shift downward wich was also found in the data from Ammerstol can be seen back. The shift to the left tends to become larger more to the left of the terrain. This more or less follows the result obtaines from only photo's 6 and 7 but can't be found back in the overall results shown in figure 7.12. This is because the overall results uses the whole block. The more pictures are used, the more difference effects will disappear.

After the exterior orientation parameters determined from the flight data was adapted to the found systematical errors, the individual checkpoint offsets vector fields are determined to see if there is a specific pattern in the differences after adapting the flight data for the found systematic errors, see figure 7.16, and a comparison with the theoretic case is made. Figure 7.17 shows the offset vectors of the checkpoints occuring in the photo's 6 and 7 calculated in LPS and Matlab. The errors given to both pictures in the theoretic case are adapted with respect to the found systematic errors in the flight data. Figure 7.11 shows the resulting theoretic offsets from the above case.

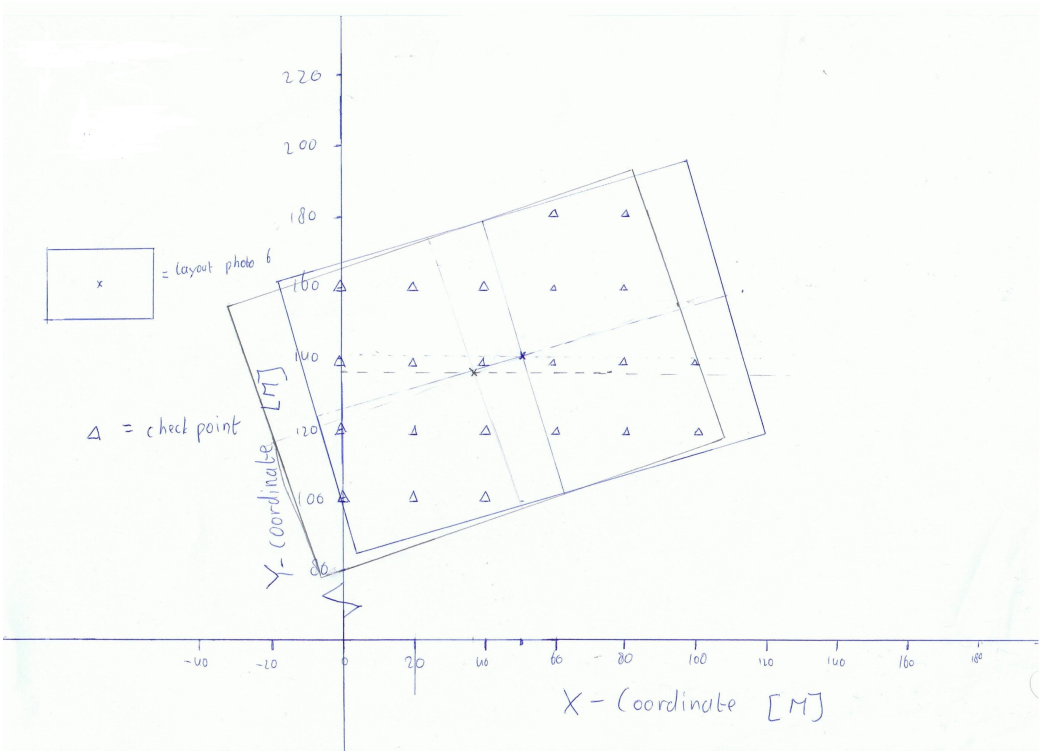

Figure 7.14: Theoretic case setup

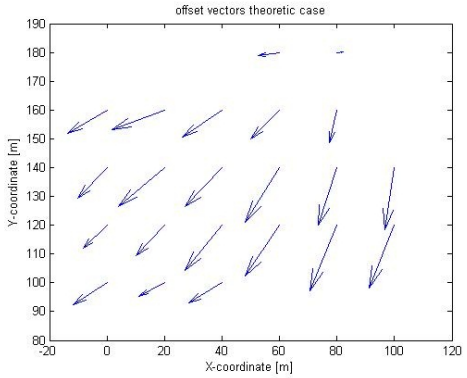

Figure 7.15: Difference vector of the theoretic case

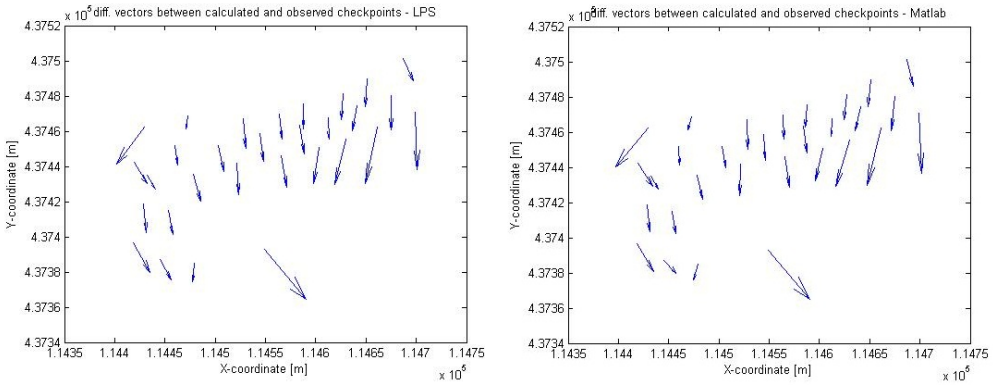

Figure 7.16: Difference vectors between observed checkpoints and calculated in LPS (left and by Matlab script (right) for photo's 6 and 7 after eliminating systematic E.O. errors

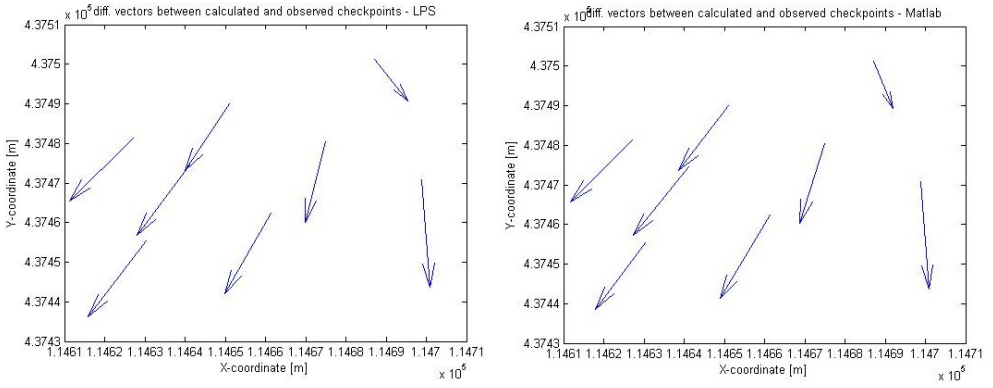

Figure 7.17: Difference vectors between observed checkpoints and calculated in LPS (left and by Matlab script (right) for photo's 6 and 7 after eliminating systematic E.O. errors

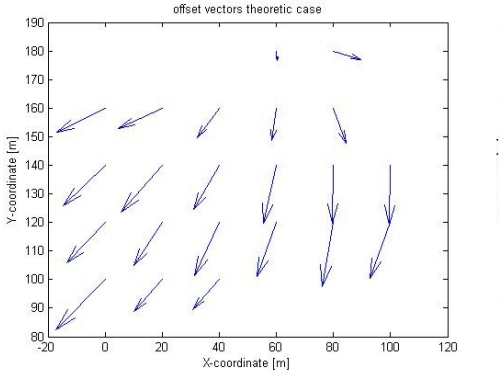

Figure 7.18: Difference vector of the theoretic case after eliminating systematic E.O. errors

7.4.2 Comparison with A4 site test data.

Because the setup of the test was more or less the same as the A4 site test described earlier a comparison between the two tests can be made. First of all, when processing the results of the A4 site test, a block of only 7 photos were made with only 3 GCPs visible in 2 or more of these photos. Therefore the Ammerstol test is much more elaborate with 34 photos and 32 GCPs of which only 2 are visible in just one photo. Also, most photos contain 6 or more GCPs, which is considerably more than during the A4 site test. Therefore the Ammerstol data contains much more redundancy.
The differences between the computed and observed camera centre coordinates are more or less comparable for the two tests; however, the A4 site test doesnt show the described X-offset of 7 meters. The rotation angles in the A4 site test show more fluctuations than in the Ammerstol test. However, we do see a structural difference in the Φ angle of -9 degrees in the A4 site test. If we flip the κ angle observations, these observations are notably better than found from the A4 site test, when deviations of more than 10 degrees were observed. This makes the suspicion that the *phi*-angle measurement is influenced by one factor or the other even larger.
When comparing the results of the check point calculation (using the flight data to calculate the coordinates of the ground control points and comparing them with the observed coordinates), we see that the Ammerstol results are much better than the results of A4 site test. This is probably due to the fact that the Kappa angles are determined much better. Furthermore, there are much more photos in the block; therefore we have more observation per point. This would strengthen the mean of the coordinates and therefore make it a bit more accurate. However systematical errors remain visible.

From the results of the test in Ammerstol, it can be concluded that with the current aircraft setup it is possible to determine an accurate terrain model, however extensive signalization with Ground Control Points is necessary. The direct sensor measurements are not accurate enough to produce reliable results, as can be seen especially from table 7.1-5 and figure 7.5b. The test results seem to follow the trends detected in the theoretical analysis of chapter 4. This can be concluded from the determination of the standard deviations of the differences between the observed and calculated terrain points, when the Ground Control Points are used as check points and the flight data is used as fixed exterior orientation parameters. Furthermore, when the theoretic approach is adapted to the used photo layout , the theoretic offset pattern follows that of the actual data, as can be seen in figures 7.15 and 7.18.

Chapter 8

IMU roof test

The tests described in the previous two chapters give detailed results for the Ublox GPS receiver. The results show that the actual errors in the resulting ground coordinates due to GPS errors follow the results of the theoretical analysis. However, because the infrared system, which determines the rotational angles, is inadequate to produce reliable results, the theoretical analysis for the errors in the rotation angles couldn't be verified. Therefore an off-the-shelf IMU needed to be tested. To be sure that the test results are not corrupted by errors in the GPS results, a contraption with two dual frequency GPS receivers is used. The GPS readings were post-processed by 06-GPS after the test.
The device which has been tested is the MTi-G created by the company xsens. It consists of a GPS-receiver, which measures the C/A code on the L1 band (for details see section 2.1). Furthermore it contains an IMU consisting of MEMS-based gyroscopes and accelerometers. On top of that, according to the specification leaflet, "the sensor contains Xsens sensor fusion algorithm to estimate the most accurate orientation and position possible". Although this sounds more like a marketing statement than a real specification of the product, it would suggest that the GPS and IMU results are combined and filtered using some kind of Kalman filter (see paragraph 3.4). Table 8.1 displays the accuracy specifications according to the product leaflet. The GPS

Factor	Accuracy value
Static angular Accuracy (Roll/Pitch)	$\leq$ 0.5 deg
Static angular Accuracy (Heading)	$\leq$ 1 deg
Dynamic angular Accuracy	1 deg RMS
Position Accuracy	2.5 m CEP (see paragraph 2.x)

Table 8.1: Accuracy budget of MTi-G

errors are too large to be used as exterior orientation parameters. However, the angular accuracy of about 1 degree is promising. The MTi-G has been tested, which is described in Appendix C.

8.1 Test description

The GPS contraption consists of a beam with a length of 1 meter with an antenna on both sides of the beam. These antennas are connected to a central receiver unit which determines and stores the location of both antennas. The antenna on the nose is the main antenna and the antenna at the tail of the aircraft is the auxilliary antenna. With this GPS contraption mounted on a hull and a low cost IMU to determine the rotation angles, five photographs of the parking lot were taken from the roof of the aerospace engineering building. The hull was mounted on a large plank which was placed on a chair and the roof railing for stability (see figure 8.1). The raw GPS measurements were sent to the 06-GPS service for post-processing, which should result in position estimates with an accuracy of about 2 to 3 centimeters.

Figure 8.1: Setup of roof test

The idea for the processing of the photos was the same as for the tests at the A4 motorway and Ammerstol. Thus, the measured camera centre coor-

dinates and rotation angles would be compared with the resulting exterior orientation parameters after an aerial triangulation with the help of ground control points.
Due to the proximity of the Aerospace building and some high trees on the other side of the parking lot, the accuracy of GPS measurements suffer from multipath effects. To be able to obtain high accuracy GPS results, a differential GPS measurement of the points was needed. This could either be achieved by using a GPS service like 06-GPS or setting up a reference unit manually. Due to difficulties in the availability of GPS receivers and radio permits at the faculty, neither approach could be performed easily. Therefore, a more elaborate approach of determining the Ground Control Points was chosen. A selection of 10 points which were clearly recognisable in the photo's was chosen. These points were measured terrestrially using a TotalStation. This instrument measures the distance and azimuth of each point from the position of the instrument. From this the location of the points is determined in a local coordinate system with the position of the TotalStation as origin.

8.2 Processing

The processing of the five photographs is done in LPS and in the Inpho Photogrammetric software package developed by Trimble. The first step was to load the captured photographs with the exterior orientation parameters as measured by the GPS contraption. The measured rotational angles needed to be transformed from Roll, pitch, heading angles to ω, ϕ and κ angles. This transformation is done automatically by Inpho if the rotation angles are set to roll, pitch and heading.
A triangulation was also performed in Match-AT, the aerial triangulation software of Inpho. Inpho didn't need any parameters to be fixed to give a solution. However, it does need estimates for the accuracy of the GPS and IMU values. 06-GPS uses a network of GPS-receivers set up on locations known in coordinates. Therefore these act as reference stations which can determine all kinds of signal propagation delays, and are therefore acting as reference stations in a Differential GPS measurement setup. The expected signal propagation delays at the location of the GPS receiver is determined by interpolation. The accuracy of the GPS results after post-processing therefore increases to centimeter level. To check this, for every photo measurement, the distance between the main and auxilliary GPS receiver is measured. This distance is 1 meter by design. The distances derived from the GPS measurements only vary about 2 cm. To be on the safe site, a standard deviation of

3 cm. is adopted. The standard deviation of the resulting rotation angles is harder to derive. An estimation is made using figure 8.2 (taken from paragraph 3.2.3), depicting the possible theoretical orientation errors due to GPS measurement errors of 3 centimeters.

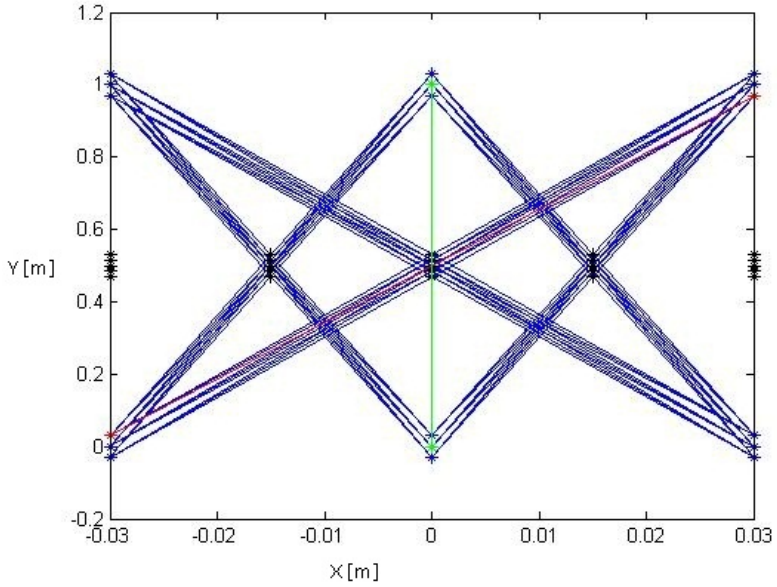

Figure 8.2: Possible orientation solutions due to GPS inaccuracies

From this figure it follows that the maximum possible error is about 3.7 degrees, when a position error of 3 cm occurs. This is the angle between the red and the green line in the figure Therefore a raw estimation of a standard deviation of 2 degrees is used.
The resulting exterior orientation parameters were used to determine the ground coordinates of three ground control points. This was done by fixing the found exterior orientation parameters, selecting three ground control points and pinpointing them in photogrammetric software, so that their ground coordinates were determined. This was done both in PhotoModeler and LPS, the results were comparable. Using the ground coordinates of the three ground control points and the local TotalStation coordinates of the same three points, the parameters for the coordinate transformation between the Ground coordinate system and the local TotalStation system are determined using a Matlab script based on Horn [1987]. The found transformation parameters were then used to transform all TotalStation coordinates to the ground coordinate system, giving the ground coordinates of all the Ground Control Points. These were then used in LPS for a second triangula-

tion determining the exterior orientation parameters from the ground control points.

8.3 Results

A total of five photos were taken from the roof, together with a measurement of the camera position and attitude, using the dual GPS receiver, as described in the previous section. These measurements are used as a-priori estimates in the aerial triangulation. These photos were loaded with the measured position and attitude parameters in the Inpho software. The Inpho software did not need fixing of parameters to give a solution. After loading the photos and the measured orientation parameters, the tiepoints needed to be measured and the triangulation could be calculated. The point measurement tool in Inpho gives an estimation of a certain point in all photographs in the block once it is measured in one photograph. During the process of measuring the tiepoints, several estimations were quite inaccurate. A pattern of offsets was recognizable however. These patterns hinted in the direction of inaccuracies in the rotation angles. The estimates in the second photo were too far off however. Furthermore, this second photo didn't "fit" in the OrthoPhoto creation. Therefore the measured orientation parameters of this second photo are considered suspicious and this photo is left out of the block, therefore 4 photo's remained. An orthomosaic of these 4 photo's is given in figure 8.4. In this figure it can be seen that the photos does not fit exactly, the errors seem to come from errors in the heading angles of the figures.
The results of the measurements by the GPS receives and the IMU unit are given in the tables 8.2 and 8.3. The rotation angles given in the table are ω, ϕ, κ angles. These are automatically transformed from roll, pitch and yaw angles by Inpho.

Photo ID	X [m]	Y [m]	Z [m]
P9011618	85501.590	445074.110	53.060
P9011621	85498.867	445080.780	53.143
P9011624	85496.748	445086.000	53.070
P9011625	85492.968	445095.005	53.130
P9011629	85489.460	445103.280	53.086

Table 8.2: Measured exterior orientation parameters, photo centre coordinates

Table 8.4 show the resulting rotation angles after the triangulation by Inpho, using fixed GPS measurements of the camera and tiepoints between the

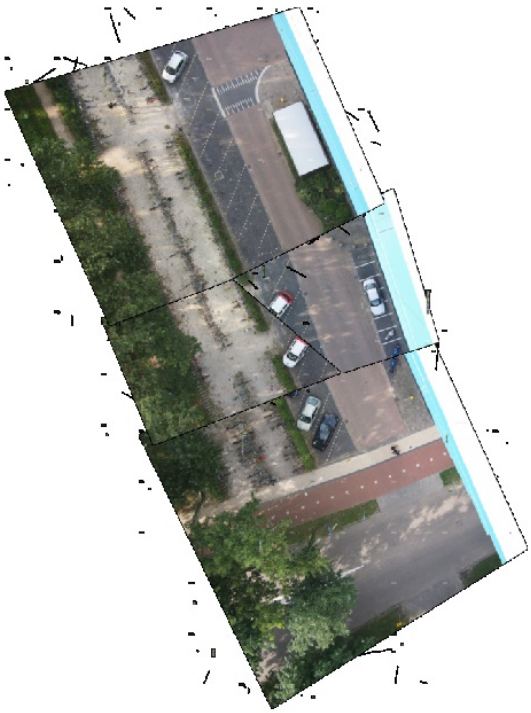

Figure 8.3: Orthomosaic of 4 used photo's using measured EO parameters

Photo ID	ω [degrees]	ϕ [degrees]	κ [degrees]
P9011618	-18.0285	6.3317	-13.5100
P9011621	-17.0369	8.5663	-19.4650
P9011624	-17.1652	6.4910	-22.6482
P9011625	-18.6838	3.5883	-21.2860
P9011629	-17.9719	3.5310	-9.4770

Table 8.3: Measured exterior orientation parameters, IMU output

photos.

Photo ID	ω [degrees]	ϕ [degrees]	κ [degrees]
P9011618	-5.1072	17.6076	114.2636
P9011621	N/A	N/A	N/A
P9011624	-3.0140	18.4501	111.0994
P9011625	-7.9846	17.3633	112.7971
P9011629	-6.5944	17.5255	114.3083

Table 8.4: Estimated exterior orientation parameters from Inpho Triangulation, photo centre rotation angles

Figure 8.4 shows the orthomosaic when the found exterior orientation parameters are used. This figure shows that the photo's line up nicely but that there is too much overlap.
Using these exterior orientation parameters, the ground coordinates of 3 ground control points are determined, which are used to determine the transormation between the ground coordinate system and the local TotalStation. From this transformation the ground coordinates of all the ground control points are determined. These are then used to determine a second triangulation in LPS, with the results of the GPS contraption as A-priori values. This resulted in the exterior orientation parameters given in tables 8.5 and 8.6

Photo ID	X [m]	Y [m]	Z [m]
P9011618	85501.3504	445075.1000	49.0811
P9011621	85500.1295	445079.0969	50.1325
P9011624	85498.2813	445081.9678	51.0102
P9011625	85494.9383	445088.2565	53.2546
P9011629	85490.6800	445099/3836	56.0915

Table 8.5: LPS triangulation results, camera centre coordinates

Photo ID	ω [degrees]	ϕ [degrees]	κ [degrees]
P9011618	-6.2126	18.3989	114.1938
P9011621	-0.0925	21.9176	111.6333
P9011624	1.3375	20.3263	110.6249
P9011625	-0.5129	19.3712	111.3655
P9011629	-2.1134	18.5305	113.1976

Table 8.6: LPS triangulation results, camera rotation angles

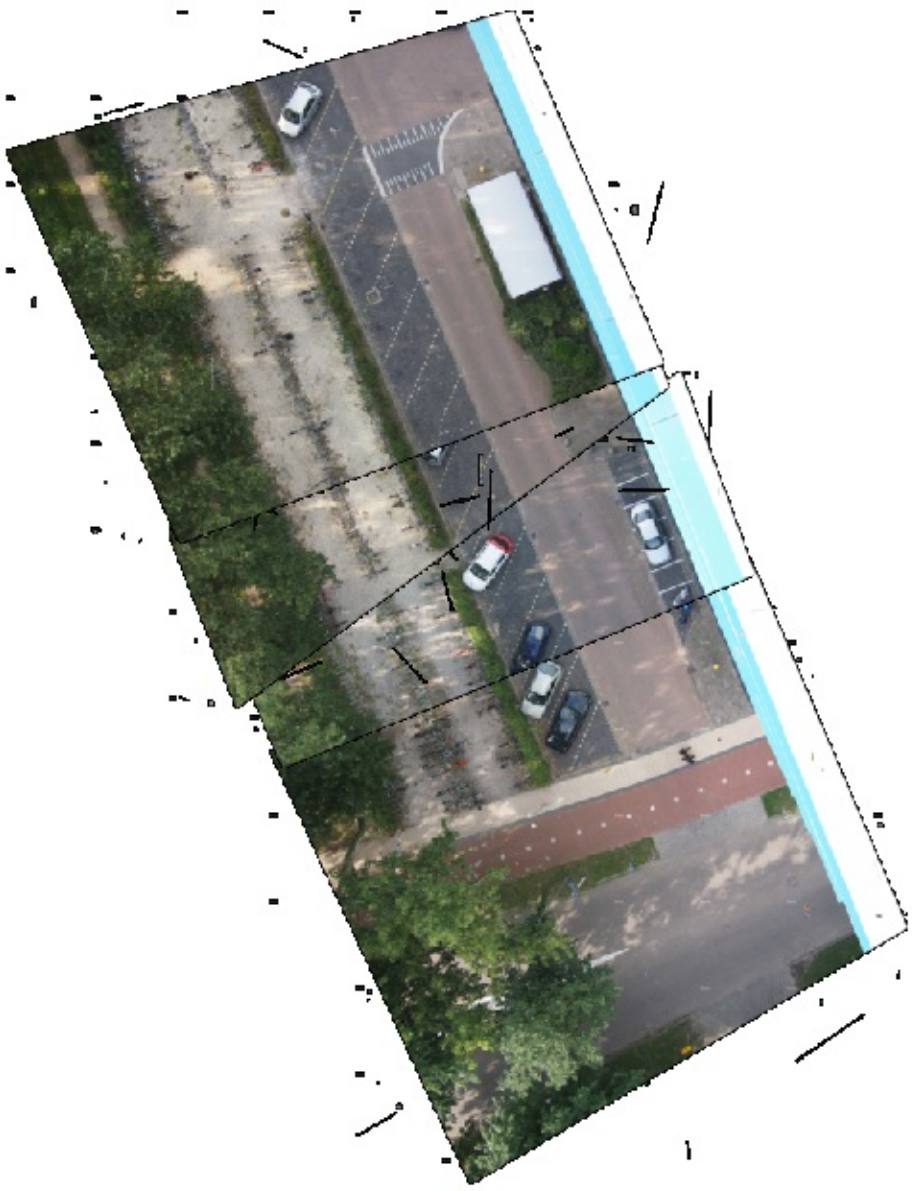

Figure 8.4: Orthomosaic of 4 used photo's using EO parameter results from Inpho triangulation

Now the IMU readouts can be compared with the triangulated rotation angles. The differences between the two outcomes are not only the result of inaccuracies of the IMU but also due to misalignment of the axes of the IMU frame and the camera frame. To correct for these misalignments, the mean difference of each rotation angle is calculated. The mean differences are then used to correct the IMU outcomes. The differences between the IMU output and the LPS triangulation results are given in table 8.7. The resulting corrected IMU outcomes are given in table 8.8

Photo ID	Ω [degrees]	ϕ [degrees]	κ [degrees]
P9011618	11.8159	12.0672	127.7038
P9011621	16.9445	13.3543	131.0983
P9011624	18.5027	13.8353	133.2731
P9011625	18.1709	15.7829	132.6515
P9011629	15.8585	14.9995	122.6746
mean	16.2585	14.0078	129.4803

Table 8.7: differences between IMU outcomes and resulting rotations of LPS triangulation

Photo ID	ω [degrees]	ϕ [degrees]	κ [degrees]
P9011618	-1.7700	20.3395	115.9703
P9011621	-0.7784	22.5711	110.0153
P9011624	-0.9067	20.4988	106.8321
P9011625	-2.4253	17.5961	108.1943
P9011629	-1.7134	17.5388	120.0033

Table 8.8: corrected IMU outcomes

The differences between the corrected IMU outcomes and the triangulation results are given in table 8.9
The standard deviations of the differences between the IMU outcomes and the triangulated results give an idea of the accuracy of the IMU itself. These are given in table 8.10

8.3.1 ground point coordinates from direct sensor measurement results

Now that the errors in the IMU are determined, the effects of these IMU errors on the ground coordinates of the points determined from the photos

Photo ID	ω [degrees]	ϕ [degrees]	κ [degrees]
P9011618	-4.4426	-1.9406	-1.7765
P9011621	0.6860	-0.6535	1.6180
P9011624	2.2442	-0.1725	3.7928
P9011625	1.9124	1.7751	3.1712
P9011629	-0.4000	0.9917	-6.8057

Table 8.9: differences between IMU outcomes and results of LPS triangulation

σ ω	2.6954
σ ϕ	1.4454
σ κ	4.3742

Table 8.10: standard deviations of differences between IMU outcomes and triangulated results

needs to be found. To do this, the output of the IMU is again used as fixed exterior orientation parameters. The ground points are used as check points. Their coordinates are determined by a forward intersection from the 5 photos. The outcoming coordinates are then compared with the transformed results of the totalstation measurements of the ground points. Table 8.11 shows the outcoming differences.

Point ID	X difference [m]	Y difference [m]	Z difference [m]
3	-0.0866	-4.6634	1.7479
4	1.8307	-4.2077	5.6302
5	1.5313	-3.8586	0.7663
6	1.9657	-1.5272	0.0808
8	1.8935	-3.9741	6.4177
9	1.9132	-5.8614	9.1509

Table 8.11: differences between measured ground control point coordinates and forward intersection results

To see if there is a pattern in the differences between the ground coordinates, which are estimated using the IMU output as exterior orientation parameters and the ground coordinates estimated using the results of the triangulation in Inpho, the ground coordinates of a group of tiepoints are determined using both the IMU outcomes and the Inpho triangulation results as exterior orientation parameters. The resulting difference vectors for the X and Y coordinates have been plotted in figure 8.5.

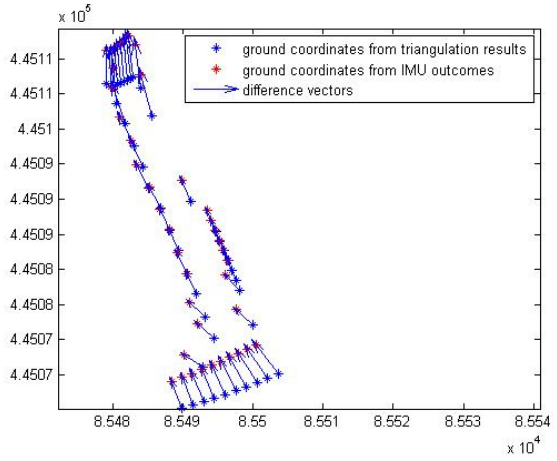

Figure 8.5: Tiepoint coordinates from forward intersection using triangulation results and IMU outcomes

8.4 Result analysis

The IMU output as given in table 8.3 has notable differences with the resulting rotation angles after the aerial triangulation using ground control points. The resulting rotation angles after the aerial triangulation are given in table 8.6 and the differences between those are given in table 8.7. In table 8.7 it can be seen that there are systematic differences of about 15 degrees in the ω and ϕ angles and about 130 degrees in the κ angle. These systematic differences are regarded as misalignments between the axes of the IMU coordinate frame and the camra coordinate frame. Misalignments of 15 degrees in the ω and ϕ angles are reasonable if the gyroscope axes of the IMU are not lined up exactly to the camera frame. Since the IMU unit (which is a closed box) and the camera were attached to the aircraft hull without accurately lining out the coordinate frames, the found misalignments are very reasonable. The systematic difference in the κ angle of 130 degrees seems large, but this can be a result of different definitions for the zero direction of the κ angle.

The IMU output is corrected for the found misalignments in table 8.7 and these corrected rotation angles are again compared with the resulting rotation angles after the aerial triangulation using the ground control points. The resulting differences are shown in table 8.9 and their standard deviations are shown in table 8.10. These tables show that the IMU has errors of about 1 - 2 degrees in the ω and ϕ angels after misalignment correction and about 4 degrees in the κ angle. These values are higher than given in the specifications for the IMU, which assumes that errors stay within 1 degree.

However, with only 5 photos in the block, the effects of a possible outlier are quite large. Furthermore, because the ground control points were measured using a TotalStation, whose coordinates were later transformed to the RD coordinate system, errors could have slipped in the ground coordinates of these ground control points. Errors in these coordinates obviously influences the outcome of the second aerial triangulation based on these ground control points. Therefore, the found differences between the IMU output and the rotation angles as determined by the aerial triangulation can be pessimistic values for the used IMU.

The effect of the found errors in the IMU output on the digital elevation model is investigated by using the ground points as checkpoints. The differences between the found coordinates using the IMU output as fixed exterior orientation parameters and the results of the totalstation measurements are given in table 8.11. In this table we see differences of about 2 - 4 metres for the planimetric coordinates and about 5 - 6 metres in height. The planimetric differences more or less folow the results of the theoretic simulation as described in chapter 4. The height differences are larger though.
From these results it can be concluded that the output of the used IMU is not accurate enough to be used in a direct sensor orientation setup. Even if the found angular differences would correspond with the specifications of the IMU (about 1 degree for each angle), the effects of these errors on the resulting terrain model would still be too large. However, the IMU output could be used in a GPS-photogrammetry setup, wherein the location of the camera centre, as determined by the GPS receiver of the aircraft is fixed and the rotation angles as determined by the IMU output are used as a-priori values in an aerial triangulation using only tiepoints between the photos.

Chapter 9

Conclusions and Recommendations

With the results of the tests described in the previous chapters, the research questions can be answered. First, let's revisit the research objectives and research questions. The main objective of this research is to evaluate the accuracy of digital terrain models, derived from aerial imagery taken from an unmanned aerial vehicle without using ground control points, but instead using low-cost GPS and IMU sensors aboard the UAV. This leads to the following questions:

- Main Question: What is the accuracy of object measurements using low cost GPS and IMU sensors and cheap off-the-shelf cameras for exterior orientation on an unmanned aerial vehicle?

To answer this main question, the following sub-question needs to be answered:

- Which factors limit the accuracy of the terrain model?
- What is the effect of these factors on the accuracy of the terrain model?
- Will it be possible to create a stereomodel using direct sensor orientation?
- How does the resulting terrain model compare with accurate models?
- How should the used techniques be enhanced to obtain the desired accuracy for the DTM?

9.1 Answers to research questions

Which factors limit the accuracy of the terrain model?

Factors which limit the accuracy of the terrain model include but are not limited to errors in the GPS and IMU sensors, camera interior errors and GPS/IMU integration errors. This research concentrated on the accuracy of the aerial system during the photogrammetric flight. This includes the navigational sensors (GPS and IMU), the coupling between the navigational sensors and the camera and the influence of flight movements on the camera. Factors influencing the accuracy during the flight are the accuracy of the sensors providing data on location and rotation angles of the camera. Furthermore, although the taken photographs are time-stamped, so that the time of photo capture is known, to determine the location and attitute of the camera centre, the GPS and IMU data have to be combined and interpolated to determine the location and attitute of the camera centre at the exact time a photograph is taken.
The movement of the aircraft causes the captured photos to be unsharp. This is called motion blur. This motion blur makes it more difficult to pinpoint terrain features in the photographs, limiting the accuracy of the final product.

What is the effect of these factors on the accuracy of the terrain model?

The effects of inaccuracies in the navigational sensors on the accuracy of the final product have been theoretically analyzed using the collinearity equations in chapter 4. The results of this theoretical analysis have been verified using the results of the Ammerstol test, as described in chapter 7. The results of the theoretical analysis shows that inaccuracies in the camera centre location causes inaccuracies in the data at a rate of 1 to 1 in planimetric coordinates and 1 to 1.5 in height coordinates, i.e. an error of 1 meter in the location of the camera centre causes an error of 1 meter in planimetric coordinates and 1.5 meters in height coordinates. This analysis has been verified by the determined deviations of the checkpoint coordinates in chapter 6 and 7.
Inaccuracies in the rotation angles of the camera centres causes inaccuracies of several meters in the terrain coordinates for every degree error, so an error of 1 degree causes errors of 3 to 4 metres planimetrically and double that in height. The planimetrical differences were verified in the test described in chapter 8, however even larger height differences were found in this test.
Due to the fact that the coupling between camera and navigational system is not finalized on the system created by Heering UAS, the influence of timing errors on the accuracy of the final product could not be tested. However,

this timing error will cause extra errors in location and rotation angles of the camera centre, which influence can be estimated by the theoretical models discussed in chapter 4.
The influence of motion blur on the final product has been researched in chapter 5. The results show that motion blur of up to 15 pixels causes inaccuracies of 2 to 3 decimeters in the terrain model. The actual motion blur occuring in the taken photographs was limited to two, maybe three pixels, in which case the inaccuracies in the terrain model stay below 5 centimeters.

Will it be possible to create a Digital Elevation Model using direct sensor orientation?

The used software (Photomodeler, LPS and Inpho) are able to determine a Digital Elevation Model from the used photographs as an equivalent for a stereomodel. The strict question "Will it be possible to create a stereomodel using direct sensor orientation?" can be answered with "yes". It has been achieved in chapter 7 using the Ammerstol test results (figure 7.5 b). However, the outcoming result is not nearly good enough to use as a final product. To get a better model, an aerial triangulation should be performed. In chapter 7 this has been done using ground control points, giving better results (figure 7.5 a and 7.6 a). An aerial triangulation is also possible when only tiepoints are used. The coordinates of the camera centre then act as control points. However, these should then be very accurate.

How does the resulting terrain model compare with accurate models?

To see if the resulting terrain model derived from the Ammerstol test data makes sense, it has been compared with a Digital Terrain Model from the AHN (Actueel Hoogtebestand Nederland). The comparison result show that the resulting terrain model more or less follow the terrain as it is, but that there are some major inaccuracies. These are due to the inaccuracies in the navigational data of the aircraft.

How should the used techniques be enhanced to obtain the desired accuracy for the DTM?

As can be seen in the answers of the previous research questions, it is possible to get an accurate terrain model using direct sensor measurements of the exterior orientation parameters. The accuracy demands on the navigational sensors (the GPS receiver and IMU) are very high though. These accuracy demands can not be obtained using low cost "off-the-shelf" sensors on an

unmanned aerial vehicle. Furthermore, the limitations of an unmanned platform as discussed in chapter 2, limit the ability to create neat photoblocks, further reducing the accuracy. This can not be mended, therefore the exterior orientation parameters have to be very accurace to be able to produce reliable results.
To be able to achieve a final product with a good enough accuracy, the idea of direct sensor measurement has to be left. This does not mean however that it is necessary to use Ground Control Points for a classical aerial triangulation. Instead, if the GPS measurements of the receiver aboard the aircraft are accurate enough (about cm. level), an aerial triangulation using the coordinates of the camera centres as control points, IMU measurements as initial values and tiepoints defining the internal geometry between the photos in the block can result in an accurate terrain model.

With the subquestions answered, the main question can now be answered.

What is the accuracy of object measurements using low cost GPS and IMU sensors and standard cameras for exterior orientation on an unmanned aerial vehicle?

This research shows that the accuracy of object measurements is dependent on several factors, but relies mostly on the accuracy of the GPS and IMU sensors. Errors in these sensors have a significant effect on the accuracy of the terrain model. Errors in the results of the GPS measurements causes errors in the terrain model of about the same magnitude. Errors in the IMU measurements causes errors in the terrain model of several meters per degree error. Motion blur in the pictures also causes errors in the terrain model, but on a much smaller scale. The effects of motion blur on the terrain model is limited to a couple of centimeters per pixel of blur.
Heering UAS is still developing the platform which is going to be used to determine terrain models. The sensors used on the platform which was used for the A4 motorway and Ammerstol tests is not nearly accurate enough. The GPS receiver has a standard error of a couple of meters. The rotation angles are determined by infrared sensors, resulting in high inaccuracies. The accuracy of this system is absolutely not good enough for the purposes of Heering UAS. A better platform is developed, using two dual frequency GPS antenna's, which gives estimates for the location of the camera centre which accuracy is good enough. However, the accuracy of the rotation angles derived from these GPS readings are not accurate enough for direct sensor measurements.

9.2 Recommendations for further research

Because Heering UAS is still developing the final platform, not all factors influencing the accuracy of the terrain model are properly dealt with yet and therefore could not be tested. First of all, the coupling between the GPS/IMU system and the camera is not clear. The taken photographs during the flight are time-stamped so that the time when a photograph is taken is known. From this, the GPS/IMU measurements can be coupled to the photographs, so that the right coordinates and rotation angles are coupled to the right photos. The way this coupling is done is very important, because if a photograph is taken at not the exact moment of a GPS/IMU reading, there will be errors in the location data, causing errors in the final terrain model. Therefore, the coupling between GPS/IMU and methods of interpolating the GPS/IMU data to the exact time a photograph is taken has to be investigated.

It has been concluded that the Xsens MTI-G inertial measurement unit is not accurate enough for direct sensor orientation. Therefore a more accurate way of measuring the rotation angles of the aircraft should be found. Using two different (dual frequency) GPS receivers to determine the rotation angles is an ingenious way two prevent the use of an (expensive) IMU. However, not only is the accuracy of the outcoming rotation angles not very good, also the integrity of the system is at stake when this method is used. In full-scale photogrammetric projects an IMU is used next to the GPS to determine the location of the aircraft. The GPS results and the IMU results are combined using a Kalman Filter to get a highly accurate position result. If for whatever reason the GPS signal is lost, the IMU still records data from which the location of the aircraft can be determined. When a system with two GPS antenna's is used to determine both the locations and the rotation angles, there is no backup if the GPS signal is lost for whatever reason. Therefore looking further for a solution to determine the rotation angles apart from the GPS measurements is recommended.

One limiting factor for the navigational sensors aboard the UAV is the payload of the aircraft. The GPS and IMU sensors can not be too big and heavy. Small off-the-shelf navigation sensors which are small and light enough to be taken aboard a model aircraft have limited accuracy as can be seen throughout this thesis. So, for the navigation sensors an optimum has to be found between accuracy of the navigation sensors, their price and their size and weight.

During the research a lot has been said about accuracy. However, the subject of reliability has sparsely been dealt with. Where accuracy tells us what the quality of the measurements is, i.e. what the expected errors in the data are, reliability tells us something about the ability to detect non-random errors such as blunders or systematic errors. In normal photogrammetry projects, the results are checked using check points. These are recognizable points in the terrain which are known in terrain coordinates, just as ground control points are. However, these check points are not used in the triangulation. The terrain coordinates of the check points are determined from the photos after the triangulation and compared with the coordinates measured on the ground. Differences higher than the expected standard deviation would suggest some kind of error. If Heering UAS is going to fly without the use of points measured on the ground, a way of checking and validating the results has to be found. Either some information on the location of terrain features has to be obtained from other sources, or Heering UAS has to use at least some check points in the measurements.

Appendix A

References

Berthold K.P. Horn, Closed-form solution of absolute orientation using unit quaternions, University of Hawaii, Honolulu, 1987

George Vosselman, Fotogrammetrie, dictaat behorende bij het college Fotogrammetrie aan de TU Delft (in Dutch), TU Delft 1999

Michael Cramer, Dirk Stallmann, Norbert Haala; Direct georeferencing using GPS/inertial exterior orientations for photogrammetric applications, IAPRS 2000

Husti, Global Positioning System - een inleiding (in Dutch), Delft University Press 2000

Peter Teunissen, Adjustment theory, Delft University Press 2000

Valerio Lucarini, Total Least Squares, University of Reading, 2001

Guenther Seeber, Satellite Geodesy, 2002

Christian Heipke, Karsten Jacobsen, Helge Weggman; Integrated Sensor Orientation, Test reports and workshop proceedings, OEEPE 2002

Klaus Peter Schwarz, Naser El-Sheimy, Mobile Mapping Systems - State of the art and future trends, University of Calgary 2004

UAS. Roadmap 2005, Unmanned Aircraft Systems roadmap 2005-2030, The Offic of the Secretary of Defence, Washington DC, USA

Greg Welsch, Gary Bishop, An introduction to the Kalman Filter, University of North Carolina 2006

Chalermchon Satirapod, Phakphong Homnian, GPS precise point positioning software for Ground Control Point Establishment in Remote Sensing Applications, in: Journal of Surveying Engineering, February 2006

Oliver J. Woodman, An introduction to inertial navigation, University of Cambridge 2007

Mohinder S. Grewal et al., Global postioning systems, inertial navigation and integration, Wiley 2007

P. Van Blyenburgh, UAS Unmanned Aircraft Systems, The Global Perspective 2007/2008, UVS 2007

Jurgen Everaerts, Unmanned aerial vehicles for photogrammetry and remote sensing, Chapter 9 from Advances in Photogrammetry, Remote Sensing and Spatial Information Sciences, 2008 ISPRS Congress Book.

R.B. Haarbrink, Accurate DSM Production from unmanned helicopter systems, Commission I,SS-4, 2008

Henri Eisenbeiss, UAV Photogrammetry - doctoral thesis, Technical University of Zurich 2009

Hans van der Marel, Lecture slides for the course of Satellite Navigation, TU Delft 2009

I. Colomina, E. Aigner, A. Agea et al., The uVISION project for helicopter-UAV photogrammetry and remote sensing, Institut de Geomatica Castelldefels, Spain, 2009

A. Gruen, H. Eisenbeiss, M. Blaha et al., UAV Photogrammetry Project Drapham Dzong, Bhutan, Swiss-Liechtenstein Foundation for Archaeological Research Abroad, 2009

P. Patias, G. Olga, G. Charalampos, et al. Photogrammetric documentation and digital representation of excavations at Keros island in the Cyclades, CIPA symposium, 2009

F. Chiabrando, F. NEx, D. Piatti, F. Rinaudo, UAV and RPV systems for Photogrammetric surveys in Archaelogical Areas: Two tests in the Piedmont region (Italy), Journal of Archaelogical science, 2010

Encyclopedia Britannica entry on Photogrammetry

Appendix B

Practical tests of Ublox GPS receiver

The GPS receiver currently installed in the aircraft is an m(u)-blox series 4 receiver. The technical specifications give a 3 meter Spherical Error Probability for Differential GPS or Space Based Augmentation System measurements, which is defined as a sphere with a diameter of (in this case) 3 meters, with the true location of the GPS - receiver in the centre of the sphere. Then 50 % of the measurements will fall within this 3 meter diametered sphere. This seems to be a low accuracy value, but the Spherical Error Probability value is a value which is seldom used in observation theory. To get an idea of the standard deviation of the GPS receiver two small tests with a loose module were performed. One test was static and one test was dynamic.

Static test

To determine the accuracy of the GPS receiver, it is placed on a point known in coordinates. The measurements are then compared with the known coordinates, the differences give an idea of the accuracy of the receiver. The chosen point for this test was a RD-surveying benchmark placed in a water pump along the Schie canal just south of Delft. There the receiver was placed on the benchmark, where it measured it's coordinates for about half an hour. A half an hour seems short, but the receiver was nothing more than a chip with an antenna mounted on it. This chip had to be connected to a computer with GPS evaluation software on it. The software which was used (U-center) creates measurement databases where every measurement epoch is stored in, with a default maximum of 1800 epochs. Because the U-blox gives a solution every second, the measurement time is limited to 1800 seconds, which is 30 minutes. The epoch maximum of the database can be adjusted, but because

in the open terrain a laptop needs to be used with a limited power supply, also reducing the measurement time.
The GPS-solutions where compared with the known coordinates from het Kadaster. This gave the results shown in figure 4.1. The PDOP (Precision Dilution of Precision) is a value describing the effect of the satellite configuration on the solution accuracy (see paragaph 3.2.5), it can be seen that the amount of used satellites and the PDOP value are strongly related to each other. A high PDOP value means a less suitable satellite configuration. From the image follows that the greatest fluctuations between the GPS solution and the actual coordinates occur at high PDOP values. Overall it can be seen that the differences are a couple of meters.

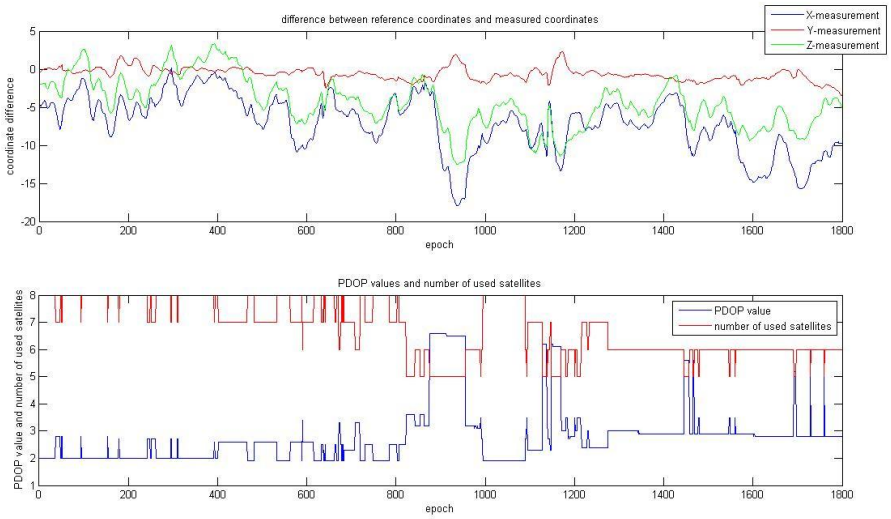

Figure B.1: Differences between Ublox GPS measurements of the benchmark, the PDOP value and number of used satellites during the measurement.

Dynamic test

A GPS-receiver in motion usually gives less accurate solutions than a static GPS receiver. Because the GPS receiver in the aircraft will be in motion, a dynamic test of the accuracy needs to be taken. With a loose U-blox unit this was very difficult however. Normally a dynamic test consists of moving the receiver in a straight line between two known points. The results are then compared with the vector between the points. Because the loose unit must be connected to a computer with specific software, this is very difficult to achieve. Furthermore, there were no two points known in coordinates

in a straight line available. To get a first idea of the dynamic accuracy of the receiver a different, simple test was performed: The Ublox GPS receiver measured it's position during a train ride between Schiedam and Hoek van Holland. The outcomes could then be compared with the location of the railway line. Because vector information of the railway line is not easily available, another way of comparing was needed. The U-center software is able to create a KML file of the GPS-solutions which can be loaded in Google earth. Figure 4.2 shows a zoomed in sample of the results of the return leg from Hoek van Holland back to Schiedam.

Figure B.2: Ublox measurements taken from the train at Maassluis Railway station

In this figure the measurements during a stopping procedure at the railway station of Maassluis are shown. The train comes from the northwest, slows down and stops along the platform to let passengers in and out. After the stop it pulls up again and drives away in southwestern direction. Rail traffic in the Netherlands is done on the right track in case of double track. Therefore, the line of GPS-measurements should follow the railway track just south of the platform. It can be seen that in the northwestern area of the picture, the line runs over the platform area, then it has some fluctuations in all directions (the train was standing still here) and in the southwestern area the GPS-measurements are lying a bit too much to the south. The rail profile in the Netherlands has a width of about 2.5 to 3 meters. The GPS-measurements seem to be just outside of the rail profile of the track it should follow. From this it can be concluded that the planimetric accuracy is 4 to 5 meters, but

this is a very raw estimation.
Although the outcoming estimations do seem to follow the the specs given by the manufacturer of the Ublox, the test described here is not scientifically reliable. Measuring with GPS from inside a train introduces a lot of factors reducing the accuracy. First of all, the GPS receiver is inside the train, therefore the already weak signals need to penetrate through the wall of the train, which is made of metal and thus acts as a Faraday cage. Furthermore, the are 1500 Volts of electricity running through the overhead wires powering the trains, which further influences the received signal. Along the railway track there are more cables used for signalization and safety measures for the railway operation. The electric currents running through these cables further influence the GPS measurements. Therefore the test described here must not be taken into high value.

Appendix C

Xsens MTI-g Inertial Measurement Unit

For the next incarnation of the aircraft, Heering UAS purchased a small device which combines GPS measurements and Inertial measurements to get a total navigation solution from just one device. The device in question is the MTi-G created by the company xsens. It consists of a GPS-receiver, which can measure the C/A code on the L1 band (for details see paragraph 2.1). Furthermore it contains an IMU consisting of MEMS-based gyroscopes and accelerometers. On top of that, according to the specification leaflet, "the sensor contains Xsens sensor fusion algorithm to estimate the most accurate orientation and position possible". Although this sounds more like a marketing statement than a real specification of the product, it would suggest that the GPS and IMU results are combined and filtered using some kind of Kalman filter (see paragraph 3.4). Table C.1 displays the accuracy specifications according to the product leaflet. The GPS errors are too large

Factor	Accuracy value
Static angular Accuracy (Roll/Pitch)	$\leq$ 0.5 deg
Static angular Accuracy (Heading)	$\leq$ 1 deg
Dynamic angular Accuracy	1 deg RMS
Position Accuracy	2.5 m CEP (see paragraph 2.x)

Table C.1: accuracy budget of MTi-G

to be used as exterior orientation parameters. However, the angular accuracy of about 1 degree is promising.

A test has been performed to check these accuracy vectors. A group of pictures of the parking lot have been taken from the roof of the aerospace

building. The photocamera and the MTi-G sensor were mounted to the hull of the unfinished airplane, which was held and aimed at the parking lot manually. While taking the pictures, the sensor was set to measure. Because there is no automatic timer, the sensor needed to be started and stopped manually. Therefore the photo's and measurements were taken as follows: Start sensor take picture stop sensor walk to next location start sensor take picture stop sensor, etc.

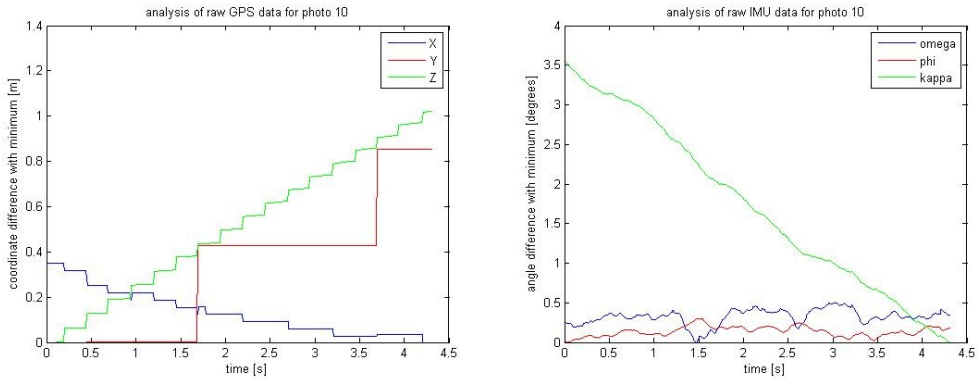

(a) GPS diffs

(b) IMU diffs

Figure C.1: GPS and IMU output differences for photo 10

An example of how the output behaves is shown in figure C.1. To clearly see the differences in the output values, all output values are substracted from the minimum value, so that the behaviour of the outout becomes clear.
The differences of the GPS measurements stay within a meter, but there is a clear trend visible in the height measurement. There is also a clear trend in the kappa (heading) angle of the IMU measurements, but further they stay neatly within half a degree difference. The results for the other photos are similar with the exception of photo 12, where big differences in the IMU measurements were found. See figure C.2
In this case, the GPS measurement are quite stable and stay within 4 decimeters difference. However, there are differences of more than 10 degrees in the rotation angles. The behaviour of the IMU data is similar to that of the other photos until about 4 seconds in the measurements when there are sudden changes of about 10 degrees. This suggests that the platform moved a bit during the measurements. This might very well be possible, because the hull was holded in someones hands and was hanging over the railing of the roof while taking the pictures. Therefore the orientation of the hull was not very stable. Therefore this test is not very reliable, but it does show that

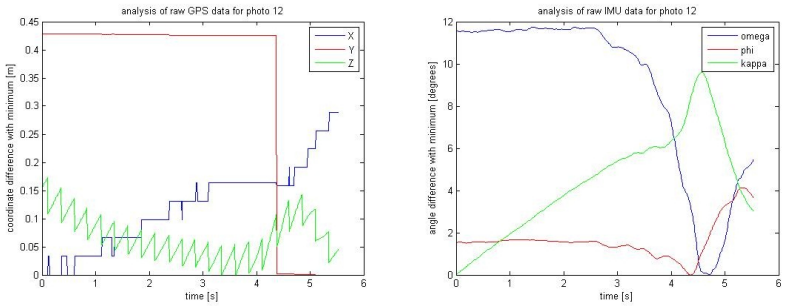

(a) GPS diffs (b) IMU diffs

Figure C.2: GPS and IMU output differences for photo 12

the accuracy of the MTi-G is about 1 to 1.5 degrees, which is not enough for direct sensor measurements.